Lsz
9 000004 122341

OF 1915

ANALELE UNIVERSITATII BUCURESTI

fizica

Theoretical Physics • Plasma Physics •
Liquid State Physics • Solid State Physics
• Polymer Physics • Earth Physics

ANUL XXXIV — 1985

FIZICĂ

COMITETUL DE REDACȚIE

Redactor responsabil : Prof. dr. *C. N. Plăvițu*
Redactor responsabil adj. : Conf. dr. *I. Licea*
Membri : Prof. dr. *I. Dima*
Prof. dr. *V. Gheorghe*
Prof. dr. *V. Grecu*
Prof. dr. *I. Iova*
Conf. dr. *C. Vrejoiu*
Secretar de redacție : Conf. dr. *L. Georgescu*

REDACȚIA
TIPOGRAFIA UNIVERSITĂȚII BUCUREȘTI
Șos. Panduri, nr. 90
Telefon 13.40.00/122

OF 1915

ANALELE UNIVERSITĂȚII BUCUREȘTI

1989

FIZICĂ

1985

BUDAPESTI MŰSZAKI ÉS GAZDASÁGTUDOMÁNYI EGYETEM
Országos Műszaki Információs Központ és Könyvtár
2001

SUMAR ● CONTENTS ● SOMMAIRE

THEORETICAL PHYSICS pag.

S. TURBATU : Ein Umkehrungsproblem in der Instationären Schallnahen Strömung 3

D. ȘTEFĂNESCU : On the Landau Curve of the Open Envelope Diagram . . 9

T. POPESCU ,M. N. ȚUGULEA : New Tools for an Efficient Use of the Felix C-32 Computer 15

PLASMA PHYSICS

I. IOVA, I. CHERA, GH. ILIE : On the Radiative Properties of a Wall-Stabilized Arc Discharge 19

LIQUID STATE PHYSICS

L. GEORGESCU, V. POPA-NIȚĂ and M. CHIPARĂ : A Statistical Theory of Surface Tension in Nematic Liquid Crystals 29

SOLID STATE PHYSICS

ATH. TRUȚIA, FLORIANA IOVA and MIRELLA MANDA : Electron Transfer Bands of Fe^{3+} in Tetrahedral Complexes 37

I. LICEA, B. LOGOFĂTU, MICHAELA LOGOFĂTU, I. MUNTEANU, I. DIMA, M. F. LĂZĂRESCU : On the Electron Mobility in n-Type InAs . . . 41

S. I. SPÂNULESCU and I. SPÂNULESCU : Increasing the Analog-Digital Converters Performances by Numerically Correcting the Components' Errors 47

A. DAFINEI, I. LICEA : On the Evaluation of the Short Circuit Current in the Thin Film Cu_2S—CdS Electron-Voltaic Cells 53

C. CIUCU, R. P. LUNGU : Relaxation Times Associated with 2-Phonons Proceses in Metalic Crystals 57

POLYMER PHYSICS

LIVIA MARIA IONESCU, MARIANA CIOAREC : Study of Rumanian Rubber Carom in Working Conditions of Bearing Packings Type RS . . . 69

pag.

M. COJOCARU, LIVIA MARIA IONESCU : Sur la flexibilité des chaines macromoléculaires dans les copolymeres methacryliques avec des groupes lateraux longs 75

E. BARNA, LIVIA MARIA IONESCU : Influence de la masse moléculaire sur la cinetique de cristallisation isotherme du polyethylene . . . 81

EARTH PHYSICS

ELENA DECU, ȘT. LASCU, SAEED BAFAYAD : Correlations between the Indoor and the Outdoor Particle Concentration 87

SABINA ȘTEFAN, D. BORȘAN, IOLANDA OSVATH : Numerical Simulation Scheme of the Cloud Coalescence Process 95

*

L'académicien ȘERBAN ȚIȚEICA (1908—1985) 101

BME KÖZPONTI KÖNYVTÁRA
F
8482
FOLYÓIRATOSZTÁLY

Budapesti Műszaki Egyetem
Központi Könyvtára
Folyóiratleltár
P 04/1988

BUDAPESTI MŰSZAKI EGYETEM KÖNYVTÁRA
1848

ANALELE UNIVERSITĂŢII BUCUREŞTI, FIZICĂ, XXXIV, 1985, PAG. 3—7

EIN UMKEHRUNGSPROBLEM IN DER INSTATIONÄREN SCHALLNAHEN STRÖMUNG

S. TURBATU
Fakultät für Physik — Universität Bukarest

Zusammenfassung. Wir suchen in der instationären schallnahen Strömung die Körperkontur, die mit der parabolischen Methode zu einer bekannten Geschwindigkeitsverteilung auf dem Körper führt.

1. **Einleitung**

In der vorliegenden Arbeit wird die parabolische Methode für das instationäre Strömungsfeld benutzt, um nicht das Potential zu einem vorgegebenen Profil zu bestimmen, sondern — wie J. ZIEREP [1] — wir kehren die Fragestellung um. Wir suchen die Körperkontur, die mit der parabolischen Methode zu einer bekannten Geschwindigkeitsverteilung auf dem Körper führt. Es sei hier lediglich der Fall der instationären, ebenen schallnahen Strömung um ein Profil betrachtet. Besonders bevorzugt ist in diesem Zusammenhang die lineare Verteilung, weil einerseits hierbei auf dem Körper die Voraussetzung der parabolischen Methode — $\Psi_{xx}(x, 0) = \text{Konst.}$ — erfüllt ist, und andererseits in diesem Fall eine Losung des Umkehrungsproblems in der stationären Strömung vorliegt [1].

2. **Grundgleichungen**

Unter der Voraussetzung, dass Reibung und Wärmeleitung vernachlässigt werden und dass keine starken Verdichtungsstösse auftreten, kann die Strömung durch ein Geschwindigkeitspotential beschrieben werden. Die Theorie kleiner Störungen liefert dann in Schallnähe eine nichtlineare Potentialgleichung :

$$[1-M_\infty^2 - (\gamma+1)M_\infty^2\Phi_x - (\gamma-1)M_\infty^2\Phi_t]\Phi_{xx} + \Phi_{yy} - 2M_\infty^2\Phi_{xt} - M_\infty^2\Phi_{tt} = 0 \qquad (1)$$

Hierin bedeuten : M_∞ die MACH—Zahl der Anströmung ; $\gamma = c_p/c_v$ das konstante Werhältnis der spezifischen Wärmen ; x-Koordinate in Strömungslängsrichtung, y-Querkoordinate, die durch die Körperlänge L dimensionslos gemacht sind ; t die Zeit, die durch L/u_∞ dimensionslos gemacht ist ; Φ (x, y, t) das Störpotential definiert durch die Ableitungen

$$\Phi_x = \frac{u-u_\infty}{u_\infty}, \quad \Phi_y = \frac{v}{u_\infty},$$

die die bezogenen Geschwindigkeitsstörungen in Längs — und in Querrichtung darstellen.

Bezüglich der genauen Ableitung der Gleichung (1) sei auf die Arbeit von G. D. SEWOSTIANOW [2] hingewisen.

In dieser Arbeit wollen wir nur Strömungen mit $M_\infty = 1$ behandeln, d.h. es gilt :

$$[-(\gamma+1)\Phi_x-(\gamma-1)\Phi_t]\Phi_{xx}+\Phi_{yy}-2\Phi_{xt}-\Phi_{tt}=0 \qquad (2)$$

Die Randbedingungen in der Theorie erster Ordnung können auf der Profilachse erfüllt werden. Das Profil wird als symmetrisch zur x-Achse gelegen betrachtet. Daher braucht man nur das Feld $y \geqslant o$ zu berechnen. Damit lauten die Randbedingungen :

$$\Phi_y(x,+0;t)=\frac{\sigma h}{\sigma x}(x,t)+\frac{\sigma h}{\sigma t}(x,t), \qquad t>0 \qquad (3)$$

$y = h(x,t)$ ist hierin die fur $0 \leqslant x \leqslant 1$ gegebene — durch die Körperlänge dimensionslos gemachte — Profilkontur. Der Flügel erstrecke sich dabei auf die Nachbarschaft von $y=0$. Da nur strömungen ohne Verdichtungsstösse betrachtet werden sollen, sind keine zusätzlichen Randbedingungen an Stossfronten zu erfullen.

Zur Lösung von Gleichung (2) sei ein Störungsansatz gewählt, der die stationäre Strömung exakt und die instationäre Strömung in erster Ordnung berücksichtigt. Es soll eine Nachbarlösung zum stationären Problem gesucht werden [3] :

$$\Phi(x,y;t)=\Psi(x,y)+\varphi(x,y)e^{ikt}. \qquad (4)$$

Darin bedeutet k die reduzierte Frequenz.

Setzt man den Ansatz (4) in die Gleichung (2) ein und vernachlässigt die Glieder zweiter und höherer Ordnung in der Amplitudenfunktion, so ergibt sich

$$-(\gamma+1)\Psi_x\Psi_{xx}+\Psi_{yy}=0, \qquad (5)$$

$$[-(\gamma+1)\Psi_x]\varphi_{xx}+\varphi_{yy}-(2ik+(\gamma+1)\Psi_{xx})\varphi_x+(k^2-(\gamma-1)ik\Psi_{xx})\varphi=0 \qquad (6)$$

Mit der Gleichung (5) ist die Berechnung des stationären Strömungsfeldes abgespalten worden.

In der Randbedingung kann analog zum Ansatz (4) vorgegangen werden. Die Bewegung des Profils sei gegeben durch

$$h(x,t)=h_0(x)+h_1(x)e^{ikt}, \qquad (7)$$

wo h_0 die Dickenverteilung bedeutet und $h_1(x)e^{ikt}$ sich auf die instationäre Verschiebung bezieht. Man erhält sodann als Randbedingung für (5) bzw. für (6) :

$$\Psi_y(x,+0)=h_0'(x), \qquad (8)$$

$$\varphi_y(x,+0)=h_1'(x)+ikh_1(x). \qquad (9)$$

3. Das Randwertproblem

Die für schallnahe Strömungen geläufige Nichtlinearität tritt also auch im instationären auf. Wir wenden nun die für stationäre Strömungen widerholt angewandte Idee der parabolischen Methode von K. OSWATITSCH auch hier an, d. h. wir setzen voraus, dass gilt

$$(\gamma+1)\Psi_{xx} = \text{Konstante} = \lambda > 0. \tag{10}$$

Mit (10) lautet Gleichung (6)

$$-(\gamma+1)\Psi_x\varphi_{xx} + \varphi_{yy} - A\varphi_x + B\varphi = 0 \tag{11}$$

mit

$$A = 2ik + \lambda, \qquad B = k^2 - \frac{\gamma-1}{\gamma+1} ik\lambda. \tag{12}$$

Als ersten Versuch für eine parabolische Näherungstheorie soll das Glied $(\gamma+1)\Psi_x\varphi_{xx}$ vernachlässigt werden [3]. Man hat damit folgendes Randwertproblem :

„Gesucht ist eine zweimaligstetig differenzierbare Funktion φ die die Differentialgleichung

$$\varphi_{yy} - A\varphi_x + B\varphi = 0 \tag{13}$$

genügt und die Randbedingungen

$$\varphi(x,+0) = 0, \qquad x \leqslant 0 \tag{14}$$

$$\varphi_y(x,+0) = h_1(x) + ikh_1(x), \qquad 0 < x < 1, \tag{15}$$

erfüllt".

Die Lösung dieses Randwertproblems kann nach [3], [4], und [5] unter der Form

$$\varphi(x,y) = -\frac{1}{\sqrt{\pi A}}\int_0^x (h_1'(\xi) + ikh_1(\xi)).\ \exp\left(\frac{B}{A}(x-\xi) - \frac{Ay^2}{4(x-\xi)}\right)\frac{d\xi}{\sqrt{x-\xi}}, \tag{16}$$

geschrieben werden.

Beschränkt man sich auf $y = +0$, so findet man

$$\varphi(x,+0) = -\frac{1}{\sqrt{\pi A}}\int_0^x (h_1'(\xi) + ikh_1(\xi)).\ \exp\frac{B}{A}(x-\xi))\frac{d\xi}{\sqrt{x-\xi}}, \quad 0 \leqslant x \leqslant 1 \tag{17}$$

Damit ist eine allgemeine Formel gegeben, die die Berechnung aller gewünschten Grössen erlaubt,

4. Das Umkehrungsproblem

Nun bestimmen wir nicht das Potential φ zu einem vorgegebenen Profil, sondern — wie J. ZIEREP [1] — wir kehren die Fragestellung um. Wir suchen die Körperkontur, die mit der parabolischen Methode zu einer bekannten linearen Geschwindigkeitsverteilung auf dem Körper führt. Die lineare Geschwindigkeit lautet :

$$\varphi_x(x,+0) = ax + b, \qquad b \geqslant 0 \tag{18}$$

Aus (18) folgt nun

$$\varphi(x,+0) = \frac{a}{2}x^2 + bx + c \tag{19}$$

Dabei wird vorausgesetzt, dass $\varphi(0,0)=0$ ist. In diesem Fall $c=o$ ist, so dass aus (19) erhält man

$$\varphi(x,+0) = \frac{a}{2}x^2+bx \tag{20}$$

Setzt man die Beziehung (20) in die Formel (17) ein, so ergibt sich eine singuläre Integralgleichung :

$$f(x) = \int_0^x \frac{h_1'(\xi) + ikh_1(\xi)}{\sqrt{x-\xi}} \exp(\sigma(x-\xi))d\xi \tag{21}$$

mit

$$f(x) = -\sqrt{\pi A}\left(\frac{a}{2}x^2 + bx\right), \qquad \sigma = \frac{B}{A}. \tag{22}$$

Zur Lösung von solchen Integralgleichungen vom Faltungstypus mit den endlichen Grenzen 0 und x, lassen sich die Operatorenrechnung von MIKUSINSKI und die Distributionen Theorie mit Erfolg anwenden [7]. Die Lösung der singulären Integralgleichung (21) ist

$$h_1'(x) + ikh_1(x) = -\frac{1}{2\pi}\int_0^x \xi^{-3/2} e^{\sigma x} f(x-\xi)d\xi. \tag{23}$$

Unter Beachtung der Beziehung (22) und nach einiger Zwischenrechnung, lässt sich (23) auch in der Form

$$h_1'(x)+ikh_1(x) = -\frac{1}{2}\sqrt{\frac{A}{\pi}}\Big[ax^{3/2}e^{\sigma x} + 2bx^{4/2}e^{\sigma x} - (2ax^{3/2}(\sigma x-1) +$$

$$+ 2bx^{1/2}(2\sigma x-1))\,{}_1F_1\left(\frac{1}{2}, \frac{3}{2}; \sigma x\right) - \frac{a}{3}x^{3/2}\,{}_1F_1\left(\frac{3}{2}, \frac{5}{2}; \sigma x\right)\Big] \tag{24}$$

schreiben, wobei ${}_1F_1(\alpha, \beta ; \zeta)$ die KUMMERsche Funktion ist. Das ist eine Differentialgleichung erster Ordnung. Nach dem Existenz- und Eindeutingkeitssatz der Lösung, suchen wir eine analytische Funktion h_1 von x zu bestimmen, welche fur $x=0$ den Wert $h_1(0)=0$ annimmt und der Differentialgleichung (24) genügt. Diese Lösung hat die form [6]:

$$h_1(x) = -\frac{4}{3}b\sqrt{\frac{A}{\pi}}x^{3/2} + \sqrt{\frac{A}{\pi}}\left(\frac{8}{30}b\sigma + \frac{16}{17}\frac{ikb}{2} - \frac{16}{30}a\right)x^{5/2} +$$

$$+ \left[\frac{4}{3}\sqrt{\frac{A}{\pi}}\left\{\left(\frac{2}{35}\sigma + \frac{4}{35}ik\right)a + \left(\frac{\sigma^2}{7} - \frac{2}{35}ik\sigma + \frac{8}{35}k^2\right)b\right\}\right]x^{7/2} + \ldots,$$

$$0 < x \leqslant 1 \tag{25}$$

Für dieses Profil liefert also die parabolische Methode eine lineare Geschwindigkeit auf dem Körper.

Um den Anschluss an bekannte Formel von J. ZIEREP [1] der stationären Theorie zu haben, seien in (25) $k=0$ und $a=\psi_{xx}(x,+0)$ — also $\lambda=(\gamma+1)a$ — gesetzt. In diesem Fall, findet man die Formel (2.3) von J. ZIEREP [1]:

$$h_{st}(x) = -\sqrt{\frac{a(\gamma+1)}{\pi}} \cdot \frac{4}{3} x^{3/2} \left(\frac{2}{5} ax + b \right).$$

LITERATUR

1. ZIEREP, J., Zeitsch. für Angew. Math. und Mech. 43, 182 (1963).
2. SEWOSTIANOW, D. G., Mehanika Jidkosti i Gasa, 1, 105 (1977).
3. TEIPEL, I., Zeitsch. für Flügwissenschaften, 12, 1, 6 (1964).
4. IWANOW, W. A. — SEWOSTIANOW, D. G., Aerodynamika, Saratow-Universität, 6 (9), 41 (1978).
5. TURBATU, S., Topics in Physics, IX, 136 (1980).
6. TURBATU, S., An. Univ. Buc. Mat.-Mec. XVIII, 2, 137 (1969).
7. ZEMANIAN, A. H., *Distribution Theory and Transform Analysis*, *McGraw-*Hill (1965).

ANALELE UNIVERSITĂŢII BUCUREŞTI, FIZICĂ, XXXIV, 1985, PAG. 9—13

ON THE LANDAU CURVE OF THE OPEN ENVELOPE DIAGRAM

D. ŞTEFĂNESCU
University of Bucharest, Faculty of Physics *

Abstract. We study the singularities of the Landau curve of the open envelope diagram. We obtain a criterion of nonsingularity for such a Landau curve. We also give a characterization of a class of nonsingular algebraic rational plane curves.

1. Introduction

A Feynman graph is a graph such that each line represents a propagation of a free elementary particle and each vertext represents an interaction of elementary particles. L. D. Landau has given in [4] a criterion for determining the position of certain singularities of the amplitude corresponding to an arbitrary Feynman graph.

Let's recall that a Feynman integral is the scattering amplitude A (s, t) corresponding to a Feynman diagram with n internal directions and p loops of integration

$$A(s,t) = \int \frac{\prod_{l=j}^{p} d^4k_j}{\prod_{k=1}^{n} (q_k^2 - m_k^2 + i\varepsilon)} = \int \frac{\prod_{k=1}^{n} d\alpha_k\, \delta(-1 + \sum_{k=1}^{n} \alpha_k)[C(\alpha)]^{m-2p-2}}{[D(\alpha,s,t) + i\varepsilon C(\alpha)]^{m-2p}}, \tag{1}$$

where C, D are polynomials in $\alpha_1,\dots,\alpha_n$, s, t. There is a complex domain R on which D (α, st) is analytic in s, t, continous in $\alpha_1,\dots,\alpha_n$ and A (s, t) is single valued except for a subset $K \subset R$ of actual singuarities. From the Landau rules it follows that the set K is contained in a plane complex curve $C = V(F(s, t))$.

We mention that analytical, topological and homological properties of the Feynman integrals and of the Landau curves are studied in [1], [3], [5], [6], [7]. In this paper we study the Landau curve of the open envelope diagram from the point of view of algebraic geometry. This allows us to establish in what cases such a Landau curve is singular and to evaluate its genus. We also give a characterization of a family of nonsingular algebraic rational plane curves.

2. The Landau curve of the open envelope diagram

The Lndau curve of the open envelope diagram is a rational plane algebraic curve. Its parametric equations are :

$$s = 4 + 4y + 4v + 2y_{24} + 2y_{56} \tag{2}$$
$$t = 4 + 4x + 4u + 2y_{13} - 2y_{56},$$

---

* National Center ol Physics, Bucharest-Măgurele, P.O. 5211, Romania.

where

$$y_{56} = \frac{1}{1-z^2}\,[y(y+uz) - x(u+yz)],$$

$$y_{24} = \frac{1}{1-u^2}\,[v(y+uz) - w(z+uy)],$$

$$y_{13} = \frac{1}{1-y^2}\,[x(u+yz) - z(z+uy)],$$

and

$$y = A(x) \pm B(x, u),\ z = A(x) \mp B(x, u),$$

$$v = A(u) \pm B(u, x),\ w = A(u) \mp B(u, x),$$

$$A(x) = \frac{1}{2}(b - x),$$

$$B(x, u) = \frac{1}{2}\left[(1+u)\left(2 - \frac{(b-x)^2}{1-u}\right)\right]^{1/2}, \tag{3}$$

$$b = \frac{1}{2}(M^2 - 3),$$

the internal masses are unity, m, M represent the external masses.

From (2) and (3) it follows that

$$(s-t)^2 = (u-u_1)\,(u-u_2)\,\frac{u - 4(M^2-1)}{u - m^2(M^2-1)} \tag{4}$$

where

$$u_{1,\,2} = \frac{m^2}{2}\,[M^2 + 3 \pm (M^2-1)^{1/2}\ (M^2-9)^{1/2}]. \tag{5}$$

It follows that (4) represents a plane cubic C which is on the unphysical sheet.

Let $z = s - t$. Therefore C is given by

$$z^2[u - m^2(M^2-1)] = (u-u_1)\,(u-u_2)\,[u - 4(M^2-1)]. \tag{6}$$

Since $u_1 + u_2 = m^2(M^2+3)$ and $u_1u_2 = 4m^4M^2$ from (6) we deduce that $C = V(F)$, where

$$\begin{aligned} F(u,z) &= u^3 - uz^2 + m^2(M^2-1)z^2 - [(m^2+4)M^2 + 3m^2 - 4]u^2 \\ &\quad + 4m^2[m^2M^2 + (M^2-1)(M^2+3)]u - 16m^4M^2(M^2-1). \end{aligned} \tag{7}$$

The curve $C = V(F)$ can have at most one singular point because it is a cubic. If (u_0, z_0) is such a point the following relations must be fulfilled :

$$F(u_0,z_0) = \frac{\partial F}{\partial u}(u_0,z_0) = \frac{\partial F}{\partial z}(u_0,z_0) = 0.$$

We have

$$\begin{aligned} \frac{\partial F}{\partial u} &= 3u^2 - z^2 - 2[(m^2+4)M^2 + 3m^2 - 4]u + \\ &\quad + 4m^2\,[m^2M^2 + (M^2-1)(M^2+3)], \end{aligned}$$

$$\frac{\partial F}{\partial z} = 2[m^2(M^2-1) - u]z = 0. \tag{9}$$

If $u_0 = m^2(M^2 - 1)$ then from (9) it follows that

$$z_0^2 = 3u_0^2 - 2[(m^2 + 4)M^2 + 3m^2 - 4]u_0 + 4m^2[m^2M^2 + (M^2 - 1)(M^2 + 3)] = 3[m^2(M^2 - 1)]^2 - 2[(m^2 + 4)M^2 + 3m^2 - 4]m^2(M^2 - 1) + 4m^2[m^2M^2 + (M^2 - 1)(M^2 + 3)]. \tag{10}$$

Let's remark that we must choose a single value for z_0 because a cubic cannot contain two distinct singular points. The point (u_0,z_0), where $u_0 = m^2(M^2 - 1)$ and z_0 is given by (10) is on the curve C if and only if

$$[m^2(M^2 - 1)]^3 + [m^2(M^2 - 1)]^2[4 - 3m^2 - (m^2 + 4)M^2] + 4m^4(M^2 - 1)[m^2M^2 + (M^2 - 1)(M^2 + 3)]\,16m^4M^2(M^2 - 1) = 0, \tag{11}$$

If $z_0 = 0$ then u_0 is a solution of the following two equations :

$$u^3 - [(m^2 + 4)M^2 + 3m^2 - 4]u^2 + 4m^2[m^2M^2 + (M^2 - 1)(M^2 + 3)]u - 16m^4M^2(M^2 - 1) = 0 \tag{12}$$

$$3u^2 - 2[(m^2 + 4)M^2 + 3m^2 - 4]u + 4m^2[m^2M^2 + (M^2 - 1)(M^2 + 3)] = 0$$

It follows that

$$u_0 = \frac{80m^2M^2(M^2 - 1)}{11[m^2M^2 + (M^2 - 1)(M^2 + 3)]}$$

The point $\left(\dfrac{80m^2(M^2 - 1)}{11[m^2M^2 + (M^2 - 1)(M^2 + 3)]}, 0\right)$ must satisfy tht conditions $F(u_0,0) = 0$ and $\dfrac{\partial F}{\partial u}(u_0,0) = 0$.

From $F(u_0,0) = 0$ it follows that (m, M) must be on the curve $C_1 = V(F_1)$, where

$$F_1(z_1,z_2) = 80^3 z_1^6 z_2^6 (z_2^2 - 1)^3 - 11\cdot 80^2 z_1^4 z_2^4 (z_2^2 - 1)^2 [(z_1^2 + 4)z_2^2 + 3z_1^2 - 4]\cdot [z_1^2 z_2^2 +)z_1^2 - 1)(z_2^2 + 3)] + 4\cdot 11^2 z_1^4 z_2^2 (z_2^2 - 1)[z_1^2 z_2^2 + (z_2^2 - 1)(z_2^2 + 3)]^3 - 16\cdot 11^3 z_1^4 z_2^2 (z_2^2 - 1)[z_1^2 z_2^2 + (z_2^2 - 1)(z_2^2 + 3)]^3 \tag{13}$$

From $\dfrac{\partial F}{\partial u} u_0,0) = 0$ it follows that (m, M) must also be on the curve $C_2 = V(F_2)$, where

$$F_2(z_1,z_2) = 3 \cdot 80^2 z_1^4 z_2^4 (z_2^2 - 1)^2 - 2\cdot 11\cdot 80 z_1^2 z_2^2 (z_2^2 - 1)[(z_1^2 + 4)z_2^2 + 3z_1^2 - 4]\cdot [z_1^2 z_2^2 + (z_2^2 - 1)(z_2^2 + 3)]4\cdot 11^2 z_1^2 [z_1^2 z_2^2 + (z_2^2 - 1)(z_2^2 + 3)]^3 \tag{14}$$

Since deg $F_1 = 20$ and deg $F_2 = 14$ it follows from the Bézout intersection theorem that the point $\left(\dfrac{80m^2M^2(M^2 - 1)}{11[m^2M^2 + (M^2 - 1)(M^2 + 3)}, 0\right)$ is a singular point of the Landau curve $C = V(F)$ in at most 280 cases.

We can now obtain the following criterion.

1. *PROPOSITION. The Landau curve* $C = V(F)$, *where F is griven by* (7) *is a plane rational cubic and one of the conditions* A), B) *is satisfied :*

A) C *is nonsingular of genus* $g = 1$.

B) C *has one singular point and* $g = 0$.

The curve C satisfies B) if and only if the point (m, M) *is on the curve defined by* (11) *or is one of the possible* 280 *intersection points of the curves* $C_1 = P(F_1)$, $C_2 = V(F_2)$, *where* F_1 *and* F_2 *are defined by (13) and (14) respectively.*

Proof.

From the analysis before we deduce that the Landau curve $C = V(F)$ is singular if and only if the point (m, M) satisfies the relation (11) or it is an intersection point of the curves $C_1 = V(F_1)$ and $C_2 = V(F_2)$.

For establishing the genus g of the curve C let's recall the Plücker formula ([8])

$$g = \frac{(n-1)(n-2)}{2} - d - c \tag{15}$$

where g is the genus of the curve C, n is the degree of the curve, d is the number of the double points and c is the number of the cusp points. Since $n = 3$ it follows that

$$g = 1 - d - c. \tag{16}$$

But the cubic $C = V(F)$ can have only one singular point. Therefore $d = c = 0$ or $(d = 1,\ c = 0)$ or $(d = 0,\ c = 1)$. If C is nonsingular then $d = c = 0$, hence $g = 1$ and we obtain A). If the curve C is singular then $d + c = 1$, hence $g = 1 - 1 = 0$ and we obtain B).

Remark If the curve $C = V(F)$ is singular then the singularity can be resolved by a finite number of quadratic transformations.

3. A class of nonsingular plane curves

The criterion we present below can be applied to the study of the rational plane curves which can be parametrized by polynomials.

2. *PROPOSITION. Let k be a commutative field of characteristic zero and let C be an algebraic k-rational plane curve which is parametrized by*

$$\begin{aligned} u &= a_0 + a_1 Z + \dots + a_n Z^n \\ v &= b_0 + b_1 Z + \dots + b_m Z^m \end{aligned} \tag{17}$$

Let's suppose that $a_{n-1} = \dots = a_{n-i+1} = 0, \quad a_{n-i} \neq 0$

$b_{m-1} = \dots = b_{m-j+1} = 0, \quad b_{m-j} \neq 0.$

If the curve C doesn't satisfy to one of the conditions :

I) $n = m$,

II) $n \neq m$ *and* $i = j$,

III) $n = 1$ *or* $m = 1$

then it is a singular curve.

Proof.

We first remark that the curve C is nonsingular if and only if $k[u,v] = k[Z]$. For a proof of this see [9].

If C is nonsingular then there are $a_{ij} \in k$ such that

$$\sum a_{ij} u^i v^j = z \tag{18}$$

If $n = 1$ or $m = 1$ the condition III) is satisfied. Therefore we may suppose that $n, m > 1$. Hence there are (i, j), (s, t) such that $(i,j) \neq (s, t)$ but

$$u^i v^j = u^s v^t \tag{19}$$

Let's suppose that $i < s$. Then $t < j$. Hence $u^i v^t (v^{j-t} - u^{s-i}) = 0$. Therefore there are $q, r \varepsilon N^*$ such that

$$u^q = v^r. \tag{20}$$

Therefore

$$\begin{aligned}(a_0 + a_1 Z + \ldots + a_{n-i} Z^{n-i} + a_n Z^n)^q &= \\ (b_0 + b_1 Z + \ldots + b_{m-j} Z^{m-j} + b_m Z^m)^r &\end{aligned} \tag{21}$$

From (21) it follows that $nq = mr$.

We now consider the terms from the both sides of (21) which have the greatest degree strictly less than nq. We must consider the following four cases :

i) $q = r = 1$. Then $n = m$, hence the condition I) is satisfied.

ii) $q = 1$, $r \geqslant 2$. Then $n = mr$ and $n\text{-}i = m(r-1) + m\text{-}j$. Therefore $n\text{-}i = mr\text{-}j = nq\text{-}j = n\text{-}j$. It follows that $i = j$ and $n \neq m$, hence the condition II) is satisfied.

iii) If $q \geqslant 2$, $r = 1$ then we deduce like in the former case that the condition II) is satisfied.

iv) If $q \geqq 2$, $r \geqslant 2$ then $n(q-1) + n-1 = m(r-1) + m-j$, hence $nq-i = mr-j$. Therefore $i = j$. If $q = r$ then $n = m$ and the condition I) is satisfied. If $q \neq r$ then we have $n \neq m$ and $i = j$, hence the condition II) is satisfied.

REFERENCES

1. R. E. CUTKOVSKY, *J. Math. Phys. 1*, 429 (1960).
2. R. P. FEYNMAN, Phys. Rev., 76, 769 (1949).
3. R. C. HWA, V. L. TEPLITZ, *Homology and Feynman Integrals*, W. A. Benjamin, New York/Amsterdam (1966).
4. L. D. LANDAU, Nucl. Phys. *13*, 181 (1959).
5. N. NAKANISHI, *Graph Theory and Feynman Integrals*, Gordon and Breach, New York/London/Paris (1971).
6. F. PHAM, *Introduction à l'étude topologique des singularités de Landau*. Gauthier-Villars, Paris (1967).
7. C. RISK, J. Math. Phys. 9, 2168 (1968).
8. G. SALMON, *Higher Plane Curves*, Dublin (1852) (Reprinted by Chealsea, New York (1980).
9. D. ŞTEFĂNESCU, St. Cerc. Mat., *30*, 465 (1978).

ANALELE UNIVERSITĂȚII BUCUREȘTI, FIZICĂ, XXXIV, 1985, PAG. 15—18

NEW TOOLS FOR AN EFFICIENT USE OF THE FELIX C32 COMPUTER

T. POPESCU, M. N. ȚUGULEA

Faculty of Physics, University of Bucharest *

Abstract. We describe a set of programs which are very useful for physicists in hardware troubleshooting as well as in software debugging.

In the last years considerable efforts have been made in educational and research institutes for the efficient use of the home computer Felix C 32. The original results obtained are of a large practical applicability, especially now, when designers and industry are concentrated on other models.

In this paper we present in a short form (a detailed version will be published elsewhere) a collection of programs which we consider to be very useful for physicists, not only in everyday use of the Felix C 32 computer but also in designing corresponding equivalents for other computers involved in physics.

The programs are of two categories : System programs (I) in machine code used in hardware troubleshooting (1. HARDPACK, 2. DESASSEMBLER, 3. HARDMONTESTS) and Cataloged programs in assembling language-LAF-(II.) ready to use as dedugging tools in Fortran with an LIB-order (1. DUM 3, 2. BIT 1, 3. SCND).

All these programs have been carefully tested in the Computer Lab. of the Faculty of Physics and are available on request.

I.1. HARDPACK

The program provide the facility of hardware operating using EBCDIC punched cards from the card reader and is used instead of the clumsy panel key manipulations or the difficult to produce binary punched cards [1,2], thus avoiding the machine worn out and improving the efficency.

The program (in few binary punched cards) is charged in a memory zone (800—950) and every following EBCDIC punched card is packed in hexa at the hexa-indicated addresses.

We used it as a powerful and elegant tool for carrying out the following two programs.

---

* National Center of Physics, Măgurele, P.O. Box 5211, Bucharest, Romania.

I.2. DESASSEMBLER

The program is designed to replace the MEMORY DUMP [1] in identifying and debugging the operating system anomalies, providing the starting and ending addresses (at console) of an arbitrary zone of memory (instead of dumping all the memory).

The program on EBCDIC punched cards (preceded by the HARDPACK program) is loaded at a suitable place (the corresponding address being punched on a card) and is asking at console the starting and ending addresses of the arbitrary memory zone desired for desassembling. Then, on the printer are listed sequentially memory words in the following format :

address	EBCDIC interpretation	hexa interpretation	machine code desassembling	unused place (for users' commentaries)

This very convenient form of listing and the facility of selecting only arbitrary zones of memory make the system debugging much easier.

I.3. HARDMONTESTS (Hardware tests on auxiliary memory) [3]

The usual Felix C-32 hardware diagnosis [2] is provided only on binary punched cards and therefore is dependent on the condition of cards, card reader and corresponding interface. The problem becomes very difficult in the case of interfering defects.

In order to solve the problem, the hardware tests were loaded in auxiliary memory, modifying the necessary channel program ; the monitor was designed with the following tasks : 1. dialogue with console to select the desired test, 2. console message when inexistent test-name were selected and restart dialogue, 3. select on tape (or disk) the desired test and load it in memory, 4. rewind the tape, 5. start the execution of the test.

The tape (or disk) is structured by blocks (of 256 bytes) in the following order :

I. The monitor — 7 blocks (5 to be loaded at X : '0800', '7800', '7900', '7A00', '7B00', 1 reserved block for corrections and extensions, 1 uniformity block).

II. Hardware tests in the order of the monitor table, to be loaded from X '0058' to X '7058'.

II.1. DUM 3

The subprogram is designed for an effective user's program debugging in the following configuration :

- COMPILE FORTRAN

* LIB DUM 3

```
Main program or procedure
      .
      .
CALL DUM 3 (& 10)
      .
      .                      dumped zone
      .
10 instruction
      .
      .
END
      .
      .
```

The routine will produce a dump of the memory zone between the beginning of the procedure and the first machine instruction contained in the statement with the label specified as argument, so many times as the CALL is activated.

Thus, the clumsy search in the memory dump is very much diminuated and the debugging becomes more pertinent.

II.2. BIT 1

The subprogram is intended for the rapid variables-debugging.

The routine must be used as follows :

```
•          COMPILE FORTRAN
* LIB BIT 1
                         64
           DIMENSION ITAB(or) in main program or a procedure
                         32
           .
           CALL BIT 1 (N, ITAB, VARIAB)
           .
           .
           END
           .
           .
```

and provide the binary content of the variable VARIAB bit-by-bit stored in the one-dimensional array ITAB of 32 (if $N = 0$) or 64 (if $N \neq 0$) locations together with the absolute address and the hexa content.

II.3. SCND

The program is designed for the user's evaluation of the time performances of the programmed sequences.

Usage :

```
•          COMPILE FORTRAN
* LIB SCND
```

BUDAPESTI MŰSZ... PODZOK... 1843 ... KÖNYVTÁR

```
.
.
.
CALL SCND(0) ← first time reference
.
.
.
CALL SCND(1,I1) ← Variable I1 will contain the number of se-
                  conds from the first time reference until pre-
                  sent moment.
.
.
.
CALL SCND(0) ← second time reference
.
CALL SCND(1, I2) ← Variable I2 will contain the number of se-
                   conds from the second time reference until
                   present moment.
.
END
```

Furter on, the number of seconds may be packed for easier manipulation using another routine (DATTIM).

REFERENCES

1. * * * Calculator Felix C32. Documentație software, I.T.C., Buc. 1977.
2. * * * Calculator Felix C32. Documentație hardware, F.C.E., Buc. 1977.
3. M. N. ȚUGULEA, T. POPESCU, M. IONIȚĂ — Communicare la al V-lea Simpozion de Informatică și Conducere, Cluj-Napoca, mai, 1979.

ANALELE UNIVERSITĂȚII BUCUREȘTI, FIZICĂ, XXXIV, 1985, PAG. 19—27

ON THE RADIATIVE PROPERTIES OF A WALL-STABILIZED ARC DISCHARGE

I. IOVA, I. CHERA, GH. ILIE,

Faculty of Physics, University of Bucharest *

Abstract. The experimental results obtained by time integrated spectroscopy (in the spectral range 2200 Å — 5300 Å) of the radiation emitted by a wall stabilized arc discharge (WSAD) are analysed in this paper, with a view to elucidate some of the radiative properties of the Xenon plasma produced in a WSAD pulsed regime. Some arguments concerning the subsequent properties are presented : — in the central zone of the discharge column, the plasma is almost fully ionized (on the first ionization degree), in a local thermodinamical equilibrium ; — the dielectric wall is a spatial limiter for the plasma expansion, due to the ambipolar diffusion and the electrostatic repulsion ; — in accordance with the optical depth and the local equilibrium conditions, a spectral continuum, overlapped by discrete lines, is emitted ; — the radiative recombinations and the cascade transitions originated from highly excited levels, have a dominant contribution to the total radiation.

1. **Introduction**

The wall-stabilized arc discharge (WSAD) is generated by discharging a high electric capacitance in a gaseous gap. The plasma expansion is limited due to the cylindrical tube wall (Fig. 1). The current intensity in the discharge has peak values of tens up to thousands amperes.

Some important characteristics of the WSAD plasma are to be noticed : -a high ionization degree ; -the kinetic pressures in plasma get up to tens of atmospheres ; -the emitted radiant power is considerable. in a large spectral range.

The WSAD — type discharge has important applications in the high speed photographic techniques and the optical pumping of the laser active medium [1—5].

The main questions arised from the study of the radiant emission mechanism are : -the phenomena involved in the production of spectra constituted by a continuum overlapped by a numerous population of spectral lines ; -the influence of the spectral line broadening in the specific pressure and electric current density conditions, on the spectral distribution of the emitted radiation ; -the influence of the local equilibrium or nonequilibrium conditions upon the radiant emission : -the spectral distribution dependence on the dynamics of the discharge (concerning the current intensity time derivative, the thermal and pressure gradients) ; -the plasma interaction with the tube wall, which by the spatial restriction of the plasma expansion, stabilizes the discharge.

---

* National Center of Physics, Bucharest-Măgurele, P. O. Box 5211, Romania.

We shall further present the analysis of some experimental results, obtained by the time integrated spectroscopy of the WSAD radiation (in the spectral range 2200—5300 Å), in order to contribute to the description of the radiative mechanism in the pulsed wall-stabilized arc discharge.

2. Experimental results

The investigations were made on a linear tube (Fig. 1), made of quartz. The gas was pure Xenon (600 mm Hg pressure).

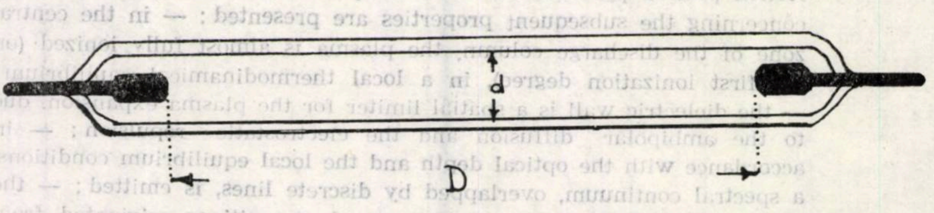

Fig. 1 : The electric discharge tube geometry (D = 100 mm, d = 5 mm).

The electrical circuit driving the discharge (Fig. 2) included a 32,4 μF ICPE capacitor and a 30 μH inductance for the current limitation.

The discharge was initiated by an overvoltage (20—25 kV) applied to the trigger electrode. The initial voltage V_0 on the main capacitor was varied between 300 and 1800 V.

In the normalized differential equation of the discharge circuit [6] :

$$\frac{di}{d\tau} + (\alpha + \beta |i|^{\frac{1}{2}}) \cdot |i|^{\frac{1}{2}} + \int_0^\tau i \cdot d\tau = 1$$

where i — the electric current intensity,

K_0 — the impedance parameter of the discharge,

$$\beta = \frac{r}{Z_0} \quad \alpha = \frac{(V_0 Z_0)^{1/2}}{K_0} \quad I = \frac{iZ_0}{V_0} \quad Z_0 = \sqrt{\frac{L}{C}} \quad \tau = \frac{t}{\sqrt{LC}}$$

the voltage corresponding to the optimal value of the α parameter ($\alpha_{opt} = 0{,}84$) was $V_0 = 1780$ V, the peak current intensity was nearly $9 \cdot 10^2$A and the pulse duration was of hundred of μs.

The spectral investigations were made with a quartz prism spectrograph Zeiss Q-24 and ORWO UV spectral plates as receivers. In the spectral range 3800—5300 Å, the correction of the spectral response was made using a calibrated incandescent filament lamp (of 2800 K colour temperature).

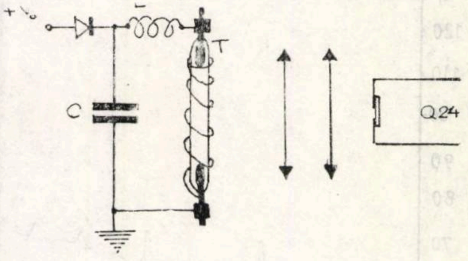

Fig. 2 : The experimental set (T — discharge tube, C — capacitor, L — inductance).

In Table I we present some of the identified spectral lines.

The dominant number of ion lines certifies the fact that almost all the atoms are at least on the first ionization degree, which results in a large number density of free electrons and positive ions in the plasma. Many spectral lines arise from upper levels of high value main quantum numbers. The presence of some cascade transitions is especially to be mentioned.

The most probable excitation processes are : -the dirrect electron collisions ; -the radiative recombinations ; -the cascade transitions from upper excited levels.

The spectral distribution of the emitted radiation in the ultraviolet range (2200—3800 Å) is presented in Fig. 3.

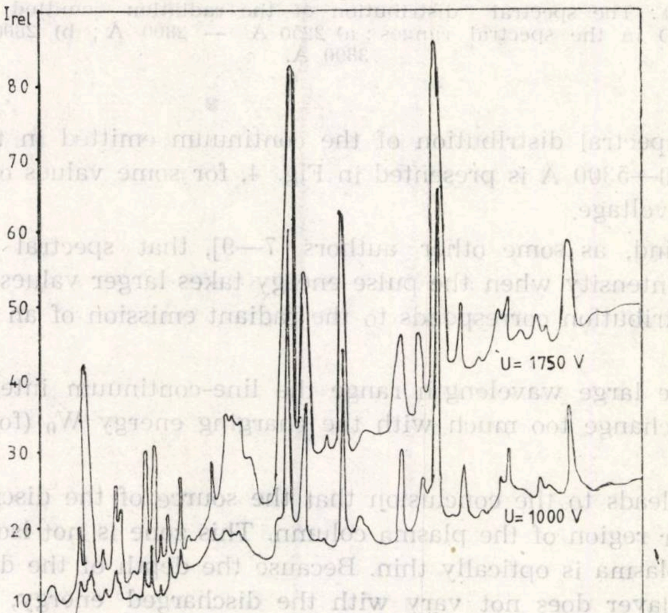

Fig. 3a

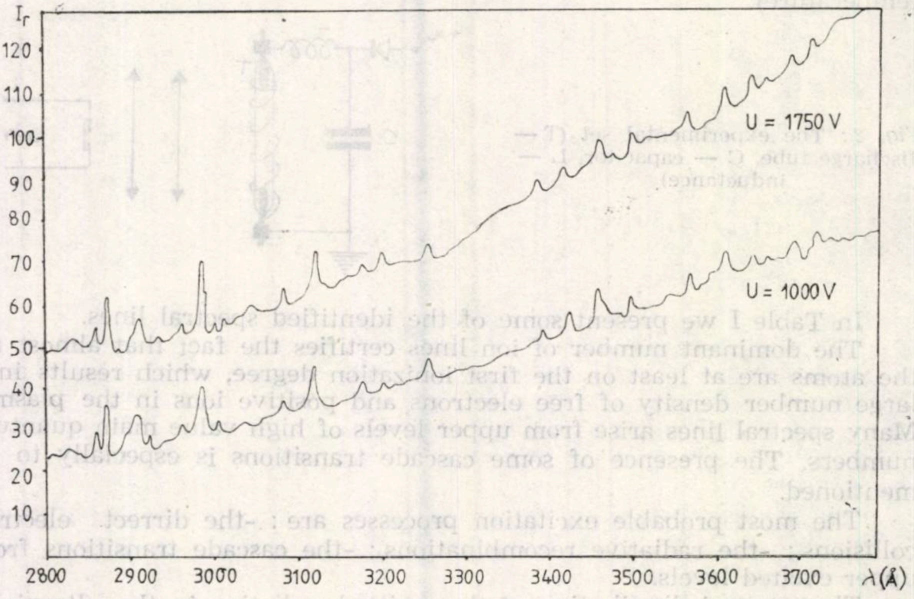

Fig. 3b

Fig. 3 : The spectral distribution of the radiation emitted by the WSAD in the spectral ranges : a) 2250 Å — 2800 Å ; b) 2800 Å — 3800 Å.

The spectral distribution of the continuum emitted in the spectral range 3800—5300 Å is presented in Fig. 4, for some values of the initial capacitor voltage.

We find, as some other authors [7—9], that spectral continuum grows in intensity when the pulse energy takes larger values. The continuum distribution corresponds to the radiant emission of an equilibrium plasma.

In the large wavelength range the line-continuum intensity ratio does not change too much with the charging energy W_0 (for instance, Fig. 5).

This leads to the conclusion that the source of the discrete lines is the border region of the plasma column. This zone is not isothermal [7], and the plasma is optically thin. Because the depth of the discrete lines emitting layer does not vary with the discharged energy, it is to be observed the saturation of the discrete line intensities.

In the ultraviolet spectral range, the line-continuum intensities ratio grows with W_0 in the investigated energy interval, consequently, the emitted radiation at short wavelength is dominated by discrete lines.

Table 1

λ(Å)	Species	E$_{inf}$(ev)	E$_{sup}$(ev)	Transition	J$_i$ — J$_s$
2285,94	Xe II	11,83	17,25	5 d^4 D — 5°	5/2—3/2
2292,40	Xe II	11,83	17,23	5 d^4 D — 3°	5/2—7/2
2294,57	Xe II	11,83	17,23	5 d^4 D — 3°	7/2—7/2
2307,28	Xe II	12,01	17,38	5 d^4 D — 17°	1/2—1/2
2313,70	Xe II	13,20	18,56	5 d^4 P — 37°	5/2—5/2
2316,80	Xe II	11,91	17,26	5 d^4 D — 7°	3/2—3/2
2319,70	Xe II	11,91	17,25	5 d^4 D — 5°	3/2—3/2
2344,47	Xe II	12,01	17,29	5 d^4 D — 9°	1/2—3/2
2368,68	Xe II	11,79	17,02	6 s^4 P — 1°	3/2—3/2
2387,75	Xe II	11,27	16,46	5 p^6 ^{2}S — 6 p′ ^{2}P^0	1/2—1/2
2489,11	Xe II	13,31	18,29	5 d^4 P — 27°	3/2—5/2
2490,76	Xe II	13,31	18,29	5 d^4 P — 25°	3/2—3/2
2526,98	Xe II	13,39	18,30	6 s′ ^{2}D — 29°	5/2—3/2
2576,97	Xe II	11,27	16,08	5 p^6 ^{2}S — 6 p′ ^{2}P°	1/2—3/2
2630,40	Xe II	13,58	18,30	5 d^2 D — 29°	5/2—3/2
2734.14	Xe II	13,25	17,70	5 d^4 P — 23°	1/2—3/2
2740,80	Xe III	15.64	20,16	5 d′ ^{3}F° — 6 p′ ^{3}F	3—3
2864,73	Xe II	13,06	17,38	5 d^2 P — 6 p″ ^{2}P°	3/2—3/2
2907,18	Xe II	13,14	17,40	5 d^2 P — 19°	1/2—3/2
2963,41	Xe II	13,20	17,38	5 d^4 P — 6 p″ ^{2}P°	5/2—3/2
2979,32	Xe II	13,20	17,36	5 d^4 P — 15°	5/2—5/2
3046,27	Xe II	14,23	18,30	5 d′ ^{2}F — 29°	5/2—3/2
3128,40	Xe II	13,06	17,02	5 d ^{2}P — 1°	3/2—3/2
3250,56	Xe II	11,27	15,08	5 p^6 ^{2}S — 6 p^4 S°	1/2—3/2
3420,73	Xe II	11,79	15,41	6 s^4 P — 6 p^2 D°	3/2—3/2
3564,30	Xe II	11,79	15,26	6 s^4 P — 6 p^2 D°	3/2—5/2
3612,36	Xe II	11,83	15,26	5 d^4 D — 6 p^2 D°	7/2—5/2
3644.43	Xe II	12,01	15,41	5 d^4 D — 6 p^2 D°	1/2—3/2
3811,05	Xe II	11,83	15,08	5 d^4 D — 6 p^4 S°	5/2—3/2
3938,92	Xe II	15,41	18,56	5 d″ ^{2}D — 37°	3/2—5/2
4037,59	Xe II	15.02	18,09	6 p^2 S° — 6 d^2 D	1/2—3/2
4158,04	Xe II	15,02	18,00	6 p^2 S° — 6 d^2 P	1/2—1/2
4180,10	Xe II	13,86	16,82	6 p^4 P° — 6 d^4 D	3/2—3/2
4197,81	Xe II	15,26	18,22	6 p^2 D° — 14	5/2—5/2
4208,48	Xe II	13,86	16,80	6 p^4 P° — 6 d^4 D	3/2—7/2
4245,38	Xe II	13,89	16,80	6 p^4 P° — 6 d^4 D	5/2—7/2
4330,52	Xe II	14,07	16,33	6 p^4 D° — 6 d^4 F	5/2—7/2
4369,20	Xe II	14,09	16,93	6 p^4 P° — 18	1/2—1/2
4385,76	Xe I	8,44	11,26	6 s $1^1/_2$° — 4 f $1^1/_2$	1—1
4383.90	Xe I	8,44	11,26	6 s $1^1/_2$° — 4 f $1^1/_2$	1—2
4406,88	Xe II	15,28	18,09	6 p^2 P° — 6 d^2 D	3/2—3/2
4480,86	Xe II	14,48	17,24	6 p^4 D° — 6 d^4 F	3/2—5/2
4524,21	Xe II	12,54	15,28	6 s^4 P — 6 p^2 P°	1/2—3/2
4545,23	Xe II	14,07	16,80	6 p^4 D° — 6 p^4 D	5/2—7/2
4585,48	Xe II	14.10	16,80	6 p^4 D° — 6 d^4 D	7/2—7/2
4603,03	Xe II	11,79	14,48	6 s^4 P — 6 p^4 D°	3/2—3/2
4624,07	Xe I	8,31	10,99	6 s $1^1/_2$° — 7 p $1^1/_2$	2—2
4651,94	Xe II	12,74	15,41	6 s^2 P — 6 p^2 D°	3/2—3/2
4671,23	Xe I	8,31	10,97	6 s $1^1/_2$° — 7 p $1^1/_2$	2—3
4769,05	Xe II	13,38	15,98	5 d^2 D — 6 p′ ^{2}F°	3/2—5/2
4773,19	Xe II	14,76	17,36	5 d″^{2}D — 15°	5/2—5/2
4823,41	Xe II	13,86	16,43	6 p^4 P° — 7 s^4 P	3/2—5/2
4844,33	Xe II	11,54	14,10	6s ^{4} P — 6 p^4 D°	5/7—7/2
4862,54	Xe II	13,89	16,43	6 p^4 P° — 7 s^4 P	5/2—5/2
4883,53	Xe II	12,54	15,08	6 s^4 P — 6 p^4 S°	1/2—3/2
4887,30	Xe II	12,74	15,28	6 s^2 P — 6 p^2 P°	3/2—3/2
4890,03	Xe II	11,54	14,07	6 s^4 P — 6 p^4 D°	5/2—5/2
4921.48	Xe II	12,74	15,26	6 s^2 P — 6 p^2 D°	3/2—5/2
4972,71	Xe II	13,58	16,08	5 d^2 D — 6 p′^{2} P°	5/2—3/2
5226,62	Xe II	15,28	17,65	6 p^2 P° — 7 s^2 P	3/2—3/2
5260,44	Xe II	12,92	15,28	6 s^2 P — 6 p^2 P°	1/2—3/2
5313,87	Xe II	14,10	16,43	6 p^4 P° — 7 s^4 P	7/2—5/2
5339,38	Xe II	14,48	16.80	6 p^4 D° — 6 d^4 D	3/2—7/2

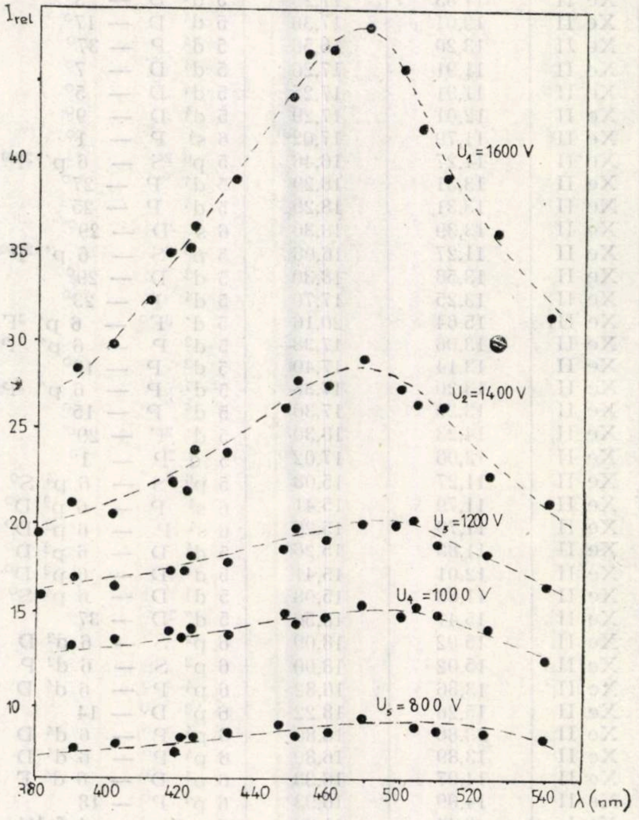

Fig. 4: The spectral distribution of the continuum emitted in the spectral range 3800 Å — 5300 Å.

This fact may be correlated with the plasma column being optically thin for these radiations, due to the low values of the plasma column being opticaly thin for these radiations, due to the low values of the absorbtion-emission coefficient in the WSAD plasma [10].

In fig. 6 we present the intensities of some spectral lines emitted by cascade transitions :

The graphs suggest that the intermediate energy level is populated by dirrect electron colisions and by cascade transitions from upper levels A in some other forms of electric discharges [11], the cascade transitions have an important role concerning the radiative mechanism in WSAD.

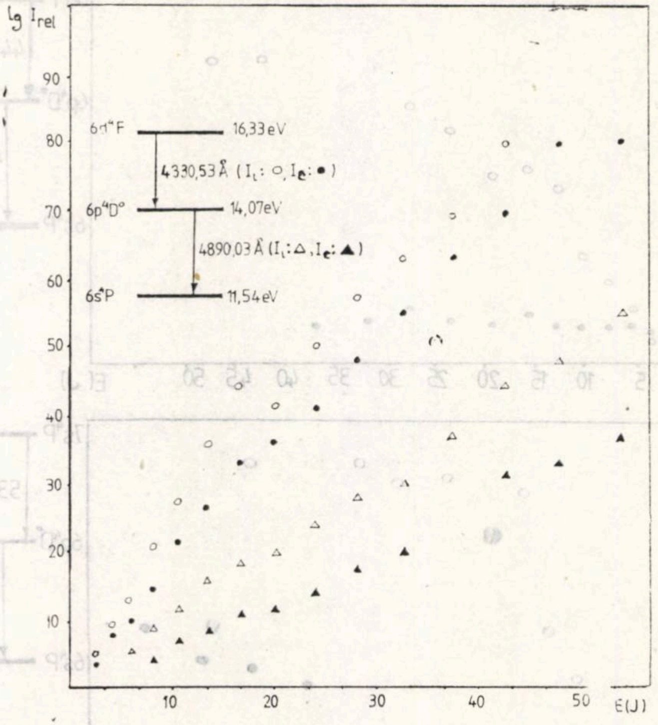

Fig. 5: The line and continuum intensities behaviour as a function of initial capacitor energy for the wave lengths Xe II λ 4330,53 Å and Xe II λ 4890,03 ÅI_c ; line intensity, I_l : continuum intensity).

3. Conclusions

With the probable exception of a short initial time interval, the plasma is fully ionized (on the first ionization degree) and is populated by a large electron and positive ion number density.

Because of the dominant character of the electron collisions, the plasma may be considered in a locally thermodinamical equilibrium. Excepting the border region, the plasma is nearly isothermal.

We suppose that near the quartz wall, the ambipolar diffusion [12] determines the reduction of the effective diameter of the plasma column, because of the electrostatic charging of the dielectric wall.

The growth of the continuum intensity in the visible-infrared spectral range may be correlated with the large values of the emission-absorbtion coefficient [10]. In this spectral interval, the plasma is optically thick, even on the transversal drection of the plasma column.

The visible-infrared spectral distribution is charaterised by the presence of a high intensity of the continuum, corresponding to the equilibrium radiation laws.

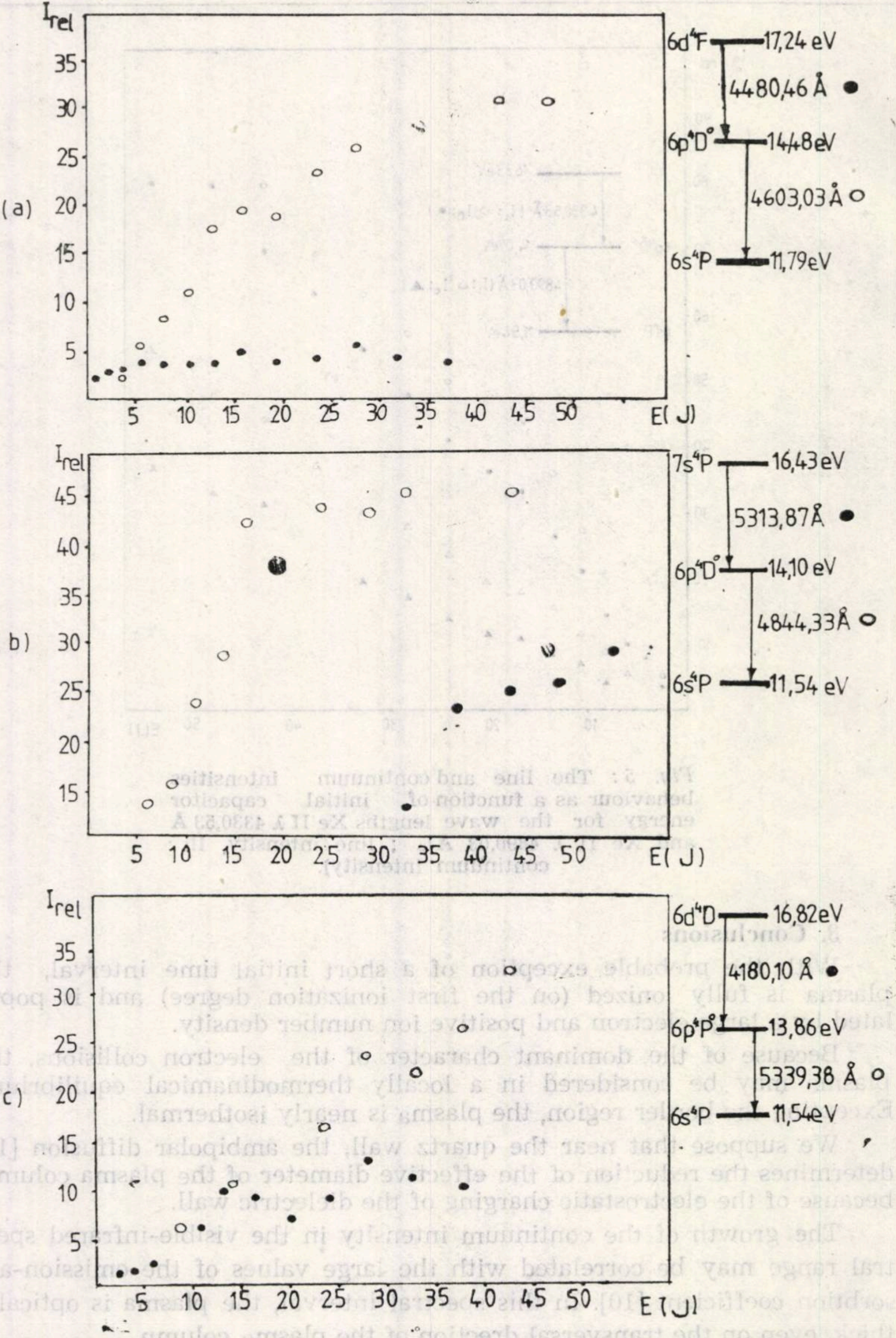

Fig. 6 : The intensity of some special lines, suposed to be emiteed by cascade transitions, as a function of initial capacitor energy :

a) Xe II λ 4480,46 Å (●) and Xe II λ 4603,03 Å (O)
b) Xe II λ 5313,87 Å (●) and Xe II λ 4844,33 Å (O)
c) Xe II λ 4180,10 Å (●) and Xe II λ 5339,38 Å (O)

The predominant character of the spectral continuum may be supplementary due to the large ion number density, which has as effect the action of the pressure and Stark-type electrostatic broadening phenomena, especially at large wavelengths.

The fact that the line-continuum intensity ratio does not change with the discharged energy per pulse may be explained considering the border region as the main source of discrete lines. The central region of the plasma is a permanent supplier of the spectral continuum.

In the ultraviolet spectral range from 2200 Å to 2800 Å, the plasma being optically thin, the radiation is constituted mainly of discrete spectral lines [13].

The radiative recombinations and the cascade transitions, generated from highly excited levels, have a major contribution to the total radiation.

REFERENCES

1. I. IOVA, I. CHERA, GH. ILIE, Sesiunea ICEFIZ "Progrese în Fizică", Craiova, 1983.
2. C. P. LUNGU, A. BALTOG, A. POPESCU, I. MUSTAŢĂ, A. OANCEA, G. MUSA, A V-a Conf. Naţ, "Fizica și Tehnica Plasmei", Iași, 1984.
3. G. NEMEȘ, A. G. SOREANU, Inst. Conf. "Lasers and Applications", Bucharest, 1982.
4. I. LANCRANJAN, S. MICLOȘ, St. Cerc. Fiz. (on press), 1984.
5. D. C. BROWN, *High Power Nd-Glass Laser Systems*, Springer Verlag, Berlin, 1981.
6. J. P. MARKIEWICZ, J. L. EMMETT, IEEE J. Quant. Electronics *JQE*-2, 707, 1966.
7. C. H. CHURCH, R. G. SCHLECHT, I. LIBERMANN, J. Quant. Spectrosc. Radiat. Transfer, *8*, 403, 1968.
8. J. H. GONCZ, P. B. NEWELL, J. Opt. Soc. Am., *56*, 87, 1966.
9. J. H. KELLY, D. C. BROWN, K. TEEGARDEN, Appl. Opt., *19*, 3817, 1980.
10. J. H. TRENHOLME, J. L. EMMETT, Proc. 9th Int. Congress on High Speed Photography, 1970.
11. I. IOVA, Int. Conf. "Lasers and Applications", Bucharest, part I, p. 974, 1982.
12. I. I. POPESCU, I. IOVA, E. TOADER, *Fizica Plasmei*, Ed. Şt. Enc., București, 1982.
13. YU. G. BASOV, J. of Applied Spceroscopy .U.R.S.S.), *XL*, 6, 885, 1984.

ANALELE UNIVERSITĂŢII BUCUREŞTI, FIZICĂ, XXXIV, 1985, PAG. 29—35

A STATISTICAL THEORY OF SURFACE TENSION IN NEMATIC LIQUID CRYSTALS

L. GEORGESCU, V. POPA-NIŢĂ, M. CHIPARĂ

Faculty of Physics, University of Bucharest *

Abstract. The surface tension of a nematic liquid crystal is calculated on the bases of the correlation functions, choosing a new pair interaction potential (9) which describes the coupler of the position variables with the orientational ones. The general form thus obtained is particularized within the framework of the FKB model, in which the position component of the surface tension γ_R depends either on η^2 or on η, while the orientational component γ_θ depends linearly on η, where η is the order parameter.

1. Introduction

In recent years the liquid crystal phase is a matter of rapidly increasing interest, since it plays an important role in technical science. The surface and/or interface properties of liquid crystals is very important and interesting both in theory and application.

The formalism of the statistical mechanics for the surface tension γ of a simple (monoatomic) fluid is wellknown [1—3]. The surface tension is expressed as an integral over the (unknown) pair distribution function for the fluid-fluid transition layer. A simplified and tractable expression for γ [4] in the case of a liquid-gas system has been derived in terms of the pair distribution function for the bulk liquid phase, by assuming an abrupt transition layer from liquid to vapour. Far from critical point (where the transition layer is only one or two molecules thick), the agreement between theory and experiment has been found to be satisfactory for simple fluids.

This formalism was extended in the case of molecular fluids [5, 6], taking into account the angular variables specifying the orientation of each molecule, in addition to the coordinate of the center of mass specifying the position of each molecule. Suppose a one-component fluid consisting of linear molecules, in which each molecule is specified by the coordinate of the center of mass $\vec{R}_i$ and the Euler angles : $\vec{e}_i = (\theta_i, \varphi_i, \chi_i)$. The dividing interface of the two phases of this fluid is assumed to be normal to the z axis. The general expression for the surface tension of a poliatomic fluid is [5] :

$$\gamma = \gamma_R + \gamma_\theta \tag{1}$$

where

$$\gamma_R = -\frac{1}{2}\int_{-\infty}^{\infty} dz_1 \int d\vec{R}\, d\vec{e}_1 d\vec{e}_2 P^{(2)}(z_1,\vec{R},\vec{e}_1,\vec{e}_2) P_2(\cos\theta) R \frac{\partial u(\vec{R},\vec{e}_1,\vec{e}_2)}{\partial R} \tag{2}$$

$$\gamma_\theta = \frac{3}{4}\int_{-\infty}^{\infty} dz_1 \int d\vec{R}\, d\vec{e}_1 d\vec{e}_2 P^{(2)} (z_1,\vec{R},\vec{e}_1,\vec{e}_2) \sin\theta \cos\theta \frac{\partial u(\vec{R},\vec{e}_1,\vec{e}_2)}{\partial \theta} \tag{3}$$

where $\vec{R} = \vec{R}_2 - \vec{R}_1$ is the center of mass vector : $\vec{R} = (R,\theta,\varphi)$; $\vec{e}_1$, $\vec{e}_2$ denote the Euler angles : $\vec{e}_i = (\theta_i, \varphi_i, \chi_i)$; P_2 is the Legendre's polynomial of second order : $P_2(x) = \frac{1}{2}(3x^2-1)$. $P^{(2)} (z_1,\vec{R},\vec{e}_1,\vec{e}_2)$ is the pair, or doublet distribution function defined by the relation [7] :

$$P^{(2)}(z_1\vec{R},\vec{e}_1,\vec{e}_2) = \frac{N(N-1)}{Q}\int \dots \int \exp\left[-\frac{U(\{\vec{R}^N,\vec{e}^N\})}{kT}\right]\left\{d\vec{R}_3^N\right\}\left\{d\vec{e}_3^N\right\} \tag{4}$$

where $\vec{R}^N = \vec{R}_1 \dots \vec{R}_N$; $\vec{e}^N = \vec{e}_1 \dots \vec{e}_N$; $\{d\vec{R}_3^N\} = d\vec{R}_3 d\vec{R}_4 \dots d\vec{R}_N$, N being the number of molecules in thermal equilibrium at temperature T ; Q the configurational partition function and $U(\vec{R}^N, \vec{e}^N\}$ the total potential energy of the system as a function of the configuration $\{\vec{R}^N\}$ of the centers of mass and the orientatons $\{\vec{e}^N\}$ of the molecules. We assume pairwise additivity for the potential :

$$U = \sum_{i<j} u(\vec{R},\vec{e}_i,\vec{e}_j) \tag{5}$$

For a fluid of molecules with isotropic forces $\partial u/\partial\theta = 0$, so that $\gamma_\theta = 0$ and the equation (1) then reduces to the familiar Kirkwood-Buff expression. For a fluid of non-spherical molecules generally γ_θ does not vanish.

Equation (1) is the generalization of the Kirkwood-Buff equation to the case of molecular fluids. In addition to introducing the angular pair distribution function in place of the usual centre of mass function, the extra term γ_θ appears. The expression (1) is intractable as it stands because the function $P^{(2)} (z_1,\vec{R},\vec{e}_1,\vec{e}_2)$ is unknown in the transition layer. In a mean field approximation the local correlations in orientation are ignored, and we replace the pair distribution function $P^{(2)} (z_1,\vec{R},\vec{e}_1,\vec{e}_2)$ by a pair correlation function $g(z_1,z_2,R)$:

$$P^{(2)} (z_1,\vec{R},\vec{e}_1,\vec{e}_2) = P^{(1)} (z_1,\vec{e}_1)\ P^{(1)} (z_2,\vec{e}_2)\ g\ (z_1,z_2,R) =$$

$$= \rho^{(1)} (z_1)\ \rho^{(1)} (z_2)\ f\ (z_1,\vec{e}_1)\ f\ (z_2,\vec{e}_2)\ g\ (z_1,z_2,R) \tag{6}$$

The single particle distribution function $P^{(1)}\ (z_1,\vec{e}_1)$ gives the probability of finding a molecule with orientation $\vec{e}_1$ at position z_1 and is given by [7] :

$$P^{(1)}\ (z_1,\vec{e}_1) = \frac{N}{Q} \int \dots \int \exp\left[-\frac{U(\{\vec{R}^N, \vec{e}^N\})}{kT}\right]\left\{d\vec{R}_2^N\right\}\left\{d\vec{e}_2^N\right\}$$

For an isotropic fluid or for a nematic, but not for a smectic, we can write :

$$P^{(1)}\ (z_1,\vec{e}_1) = p^{(1)}\ (z_1)\ f(z_1,\vec{e}_1) \tag{7}$$

where $f\ (z_1,\vec{e}_1)$ is a purely orientational singlet distribution [8].

2. Potential Model

To proceed further, one first need to specify the potential of interaction between the particles of the system. In the case of the liquid crystals, the intermolecular potential is not known. Even if it is known, the information would not be very helpful in the microscopic calculation (such as expression (1) since it woul certainly be of an inordinately complex nature. As a compromise, when treating such a system, one chooses a model of potential which is tractable within the framework of the theory, but still incorporates certain realistic features.

We use in this paper two potential model :

$$u(\vec{R}, \vec{e}_1, \vec{e}_2) = V(R) + W(R)P_2(\vec{e}_1 \cdot \vec{e}_2) \tag{8}$$

and

$$u(\vec{R}, \vec{e}_1, \vec{e}_2) = V(R) + W(R)P_2(\vec{e}_1 \cdot \vec{e}_2) + v_2(R)\left[P_2(\vec{e}_1 \cdot \frac{\vec{R}}{R}) + P_2(\vec{e}_2 \cdot \frac{\vec{R}}{R})\right] \tag{9}$$

The first model represents the well-known Mc Millan form of the potential [9] which is widely used in the molecular theory of liquid crystals [10]. The last term of the second model, which couples spatial and orientational variables, stands for the leading anisotropic steric correction. This point was discussed more detailed in ref, [11].

With the two potential models we calculate the integral of eq. (1) by appropriate approximations.

3. Nematic-Vapor Interface

We assume that

$$f(z_1, \vec{e}_1) = f(\vec{e}_1) \tag{10}$$

This approximation involves that the z_1 dependence of the distribution function $f(\vec{e}_1)$ is ignored. That is, we assume that the order parameter η has the bulk value up to the free surface.

We may write the expressions (2) and (3) in the following forms :

$$\gamma_R = -\frac{1}{2}\int_{-\infty}^{\infty} dz_1 \int dR P_2(\cos\theta)\, R \left< P^{(2)}(z_1, \vec{R}, \vec{e}_1, \vec{e}_2)\frac{\partial u(\vec{R}, \vec{e}_1, \vec{e}_2)}{\partial R}\right>_{\vec{e}_1, \vec{e}_2} \tag{11}$$

$$\gamma_\theta = \frac{3}{4}\int_{-\infty}^{\infty} dz_1 \int dR \sin\theta \cos\theta \left< P^{(2)}(z_1, \vec{R}, \vec{e}_1, \vec{e}_2)\frac{\partial u(R, e_1, e_2)}{\partial\theta}\right>_{\vec{e}_1, \vec{e}_2} \tag{12}$$

where $< >_{\vec{e}_1, \vec{e}_2}$ denotes an unweighted averaging over the orientations.

We now average the interaction (8) and (9) over a distribution of molecules. Introduce a spherical coordinate system with polar axis $\vec{n}$ (the director) and express $\vec{e}_1$ and $\vec{e}_2$ in this coordinate system. Since the molecules are uniaxial, all azimuthal angles φ_1, φ_2 are equally probable, the average over these angles then works out to be :

$$< u(\vec{R}, \vec{e}_1, \vec{e}_2) >_{\varphi_1, \varphi_2} = V(R) - \frac{1}{2}W(R) + \frac{3}{2}W(R)\cos^2\theta_1\cos^2\theta_2 + \frac{3}{4}W(R)\sin^2\theta_1\sin^2\theta_2 \tag{13}$$

and

$$< u(\vec{R}, \vec{e}_1, \vec{e}_2) >_{\varphi_1, \varphi_2} = V(R) + W(R)\left[\left(\frac{3}{2}\cos^2\theta_1 - \frac{1}{2}\right)\left(\frac{3}{2}\cos^2\theta_2 - \frac{1}{2}\right)\right] + v_2(R)\left(\frac{3}{2}\cos^2\theta - \frac{1}{2}\right)\left(\frac{3}{2}\cos^2\theta_1 - \frac{1}{2} + \frac{3}{2}\cos^2\theta - \frac{1}{2}\right) \tag{14}$$

Next, we average (13) and (14) over the polar angles θ_1, θ_2.. From the symmetry of the nematic state, the distribution function $f(\vec{e}_1)$ is related to the order parameter η by :

$$\eta = \int_0^{\pi/2}\frac{1}{2}(3\cos^2\theta - 1)\sin\theta\, f(\vec{e})\, d\theta \tag{15}$$

In doing the average in (13) and (14) we used the approximation (6). With this approximation, the interactions averaged over all orientations of the two molecules becomes :

— for potentioal model (8) :

$$< u(\vec{R}, \vec{e}_1, \vec{e}_2) >_{\vec{e}_1, \vec{e}_2} = V(R) + W(R)\eta^2 \tag{16}$$

— for potential model (9) :

$$< u(\vec{R}, \vec{e}_1, \vec{e}_2) >_{\vec{e}_1, \vec{e}_2} = V(R) + W(R)\eta^2 + v_2(R)(3\cos^2\theta - 1)\eta \quad (17$$

With the first potential model (8) we obtain the expression (16) which is the well result that the mean field is proportional to η^2. Using the potential model (9) we obtain a term proportional to η (17). If all angles θ are equally probable, $<\cos^2\theta> = \frac{1}{3}$, so that the linear term in η drops out, and (17) reduces to (16). With the expressions (16) and (17) the surface tension γ becomes:

— for potential model (8):

$$\gamma_R = -\frac{1}{2}\int_{\infty}^{-\infty} dz_1\,\rho(z_1)\int d\vec{R}\rho(z_2)\,RP_2(\cos\theta)\,g(z_1, z_2, \vec{R})\,\frac{\partial<u(\vec{R},\vec{e}_1,\vec{e}_2)>_{\vec{e}_1,\vec{e}_2}}{\partial R} \tag{18}$$

$$\gamma_\theta = 0$$

where

$$\frac{\partial<u(R, e_1, e_2)>_{\vec{e}_1,\vec{e}_2}}{\partial R} = \frac{\partial V}{\partial R} + \eta^2\,\frac{\partial W}{\partial R}$$

— for potential model (9)

$$\gamma_R = -\frac{1}{2}\int_{-\infty}^{\infty} dz_1\rho(z_1)\int d\vec{R}\rho(z_2)\,RP_2(\cos\theta)\,g(z_1,z_2,\vec{R})\,\frac{\partial<u>_{\vec{e}_1,\vec{e}_2}}{\partial R} \tag{19}$$

$$\gamma_\theta = \frac{3}{4}\int_{8}^{-\infty} dz_1\rho(z_1)\int d\vec{R}\rho(z_2)\sin\theta\,\cos\theta\,g(z_1,z_2,\vec{R})\,\frac{\partial<u>_{\vec{e}_1,\vec{e}_2}}{\partial\theta} \tag{20}$$

where

$$\frac{\partial<u>_{\vec{e}_1,\vec{e}_2}}{\partial R} = \frac{\partial V}{\partial R} + \eta_2\frac{\partial W}{\partial R}\,(3\cos^2\theta - 1)\,\eta\,\frac{\partial v_2}{\partial R} \tag{21}$$

$$\frac{\partial<u>_{\vec{e}_1,\vec{e}_2}}{\partial\theta} = -6\cos\theta\,\sin\theta\,\eta v_2(R) \tag{22}$$

One easily observe that, in the first case (18), the contribuition γ_θ is lacking since we have assumed the potential function u as it is given by eq. (8). For the model (9), γ_θ does not vanish and the part of the potential energy that causes γ_θ is important if we consider anisotropic physical properties (the case for the nematic liquid crystals).

4. The FKB approximation for surface tension

The general expressions (18), (19), (20) for the surface tension is very difficult to use without further approximation since the density profile and pair correlation function are unknown in the surface region.

At low pressure, the Fowler-Kirkwood-Buff (FKB) approximation [1], [4] leads to a fairly accurate estimation of γ for simple fluids. We use the same approximation in treating the nematic-vapor free surface.

The FKB assumptions ore that: a) the vapor density is negligible, and b) the density of the liquid phase has the bulk value up to the

Gibbs dividing surface, which we take at $z = 0$. These two assumptions imply:

$$\begin{aligned} \rho(z) &= \rho_1 & z &< 0 \\ \rho(z) &= 0 & z &> 0 \end{aligned} \tag{23}$$

In addition we assume the approximation (10) and $g(z_1, z_2, R) = g_1(R)$. With these approximation, the expressions (18), (19), (20) reduce to:

— for potential model (8)

$$\gamma = \gamma_R = \frac{\pi\rho_1^2}{8}\int_0^\infty R^4 g_1(R)\left(\frac{dV}{dR} + \eta^2\frac{dW}{dR}\right) dR \tag{24}$$

— for potential model (9)

$$\gamma_R = \frac{\pi\rho_1^2}{8}\int_0^\infty R^4 g_1(R)\left(\frac{dV}{dR} + \eta^2\frac{dW}{dR} + 2\eta\frac{dv^2}{dR}\right) dR \tag{25}$$

$$\gamma_\theta = \frac{3\pi\rho_1^2}{4}\int_0^\infty R^3 g_1(R)\ \eta v_2(R)\ dR \tag{26}$$

Because sufficiently detailed experimental data for g are absent at present, it is possible to determine g(R) from the equation YBG.

5. Conclusions

Although there were realised investigations of the surface phenomena of the nematic liquid crystals, the statistical treatments on the bases of the correlation functions are very few [15], [16], [17].

In the present paper it is calculated the surface tension coefficient of the nematic liquid crystals by aid of the pair correlation function, using a binary interaction potential, which contains a supplementary term, which describes the coupler of the position variables with the orientational ones (relation 9). Using this potential it was calculated either the general form of the component of the surface tension coefficient γ_R, which contains the position variables, as the component γ_θ which contains the orientational variables (relations (19), 20)). These two relations are applied to a simple structure of the separation surface for the calculation of the two components in the FKB approximations.

There were thus obtained the expressions (25) and (26) for the two components of the surface tension. The component γ_R depends on the square of the order parameter η, as in the older theories (see relation 24) containing also a supplementary term linear in η. The orientational component γ_θ also depends linearly in the order parameter η. Both completions are due to the way in which the new binary interaction potential was defined.

REFERENCES

1. J. G. KIRKWOOD and F. P. BUFF, J. Chem. Phys., 17, 338, 1949.
2. I. Z. FISHER, *Statistical Theory of Liquids*, Chicago, Press, 1966.
3. S. ONO and S. KONDO, *Handbuch der Physik*, ed. S. Flugge, 1960, Vol. 10.

4. R. H. FOWLER, Proc. R. Soc. A, 159, 229, 1937.
5. C. G. GRAY and K. E. GUBBINS, Mol. Phys. 30, 179, 1975.
6. H. T. DAVIS, J. Chem, Phys., 62, 3412, 1975.
7. G. R. LUCKHURST and G. W. GRAY (Ed.). *The Molecular Physics of Liquid Crystals,* Academic Press NY, 1979.
8. V. POPA-NIŢĂ and L. GEORGESCU, Anal. Univ. Buc., Fizică, XXXIII, 27, 1984.
9. W. L. McMILLAN, Phys, Rev. A4, 1238, 1971 ; 6, 936, 1972.
10. L. FEIJOO, V. T. RAJAN and C.-W. WOO, Phys. Rev. A19, 1263, 1979.
11. V. POPA-NIŢĂ and L. GEORGESCU, Stud. şi cerc. de fiz., to be published.
12. J. D. PARSONS, Mol. Cryst., Liq. Cryst. 31, 79, 1975.
13. P. G. de GENNES, Mol. Cryst., Liq. Cryst. 12, 193, 1971.
14. M. G. J. GANNON and T. E. FABER, Phyl. Mag. 37, 117, 1978.
15. J. D. PARSONE, J. Phys. 37, 1187, 1976.
16. J. MURAKAMI, J. of Phys. Soc. of Jap. 42, 210, 1977.
17. L. GEORGESCU, POPA-NIŢĂ VLAD, and R. MOLDOVAN, Rev. Roum. de Phys. 29, 553, 1984.

ANALELE UNIVERSITĂȚII BUCUREȘTI, FIZICĂ, XXXIV, 1985, PAG. 37–93

ELECTRON TRANSFER BANDS OF Fe^{3+} IN TETRAHEDRAL COMPLEXES

ATH. TRUȚIA, FLORIANA IOVA and MIRELLA MANDA

Faculty of Physics, University of Bucharest *

Abstract. The high energy optical absorption bands of Fe^{3+} tetrahedral coordinated in aqueous HCl and CH_2Cl_2 are assigned to electron transfer transitions: $\pi t_1 \to 3de$, $(\pi+\sigma)t_2 \to 3de$, $\pi t_1 \to 3dt_2$ and $(\pi+\sigma)t_2 \to 3dt_2$. The subshell energy difference between dt_2 and *de* orbitals $(-\Delta)$ and the energy difference between the ligand orbitals t_2 and t_1 are calculated from the measured spectra.

1. Introduction

The higher energy optical absorption bands of tetrahedral complexes have been interpreted by molecular orbital theory [1, 2].

The absorption band of lowest energy has been identified with a transition from the highest non-bonding molecular π orbital to the lowest set of two degenerate molecular orbitals of *e* symmetry due to the partly filled shell of the central atom.

The identification of the higher energy bands seems more uncertain. D. S. McClure [3] suggested the following order for the energy levels of the ligand orbitals : πt_1, $(\pi+\sigma)\,t_2$, πe, $(\sigma+\pi)\,t_2$, $\sigma\,a_1$.

Hence the transitions $\pi t_1 \to 3de$, $(\pi+\sigma)t_2 \to 3de$, $\pi t_1 \to 3dt_2$ and $(\pi+\sigma)t_2 \to 3dt_2$ are expected to occur. The energy of the σ — orbitals is so low that the $\sigma t_2 \to dt_2$ or $\sigma t_2 \to$ de transitions have not been observed. The transition $\pi e \to$ de has no electric dipole moment and would be difficult to detect [4]

2. Measurement and results

In the present paper, the spectra of $[FeCl_4]^-$ in aqueous HCl and $[FeBr_4]^-$ in CH_2Cl_2 have been measured,

The optical absorption spectra have been recorded on a UV-VIS-Specord „Zeiss" spectrophotometer. These spectra are shown in the figures 1 and 2 for $[FeCl_4]^-$ and $[FeBr_4]^-$ respectively. The electron — transfer bands are indicated by vertical arrows.

The corrected wave-number, $\tilde{\nu}_{corr}$, of the first band ($\pi t_1 \to 3de$ transition) is related to the difference between the optical electronegativities $x_{opt}(X)$ and $x_{opt}(M)$ of the ligand and the metal ions [5] :

$$\tilde{\nu}_{corr}\ (kK) = 30\ [x_{opt}(X) - x_{opt}(M)] + \tilde{\nu}_{sp} \qquad (1)$$

$\tilde{\nu}_{sp}$ is the spin-pairing energy correction.

---

* National Center of Physics, Bucharest-Măgurele, P. O. Box 5211, Romania.

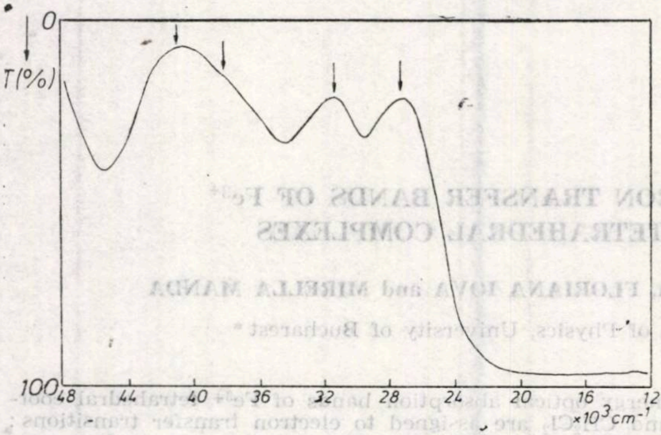

Fig. 1. Absorption spectrum of Fe^{3+} in aqueous HCl.

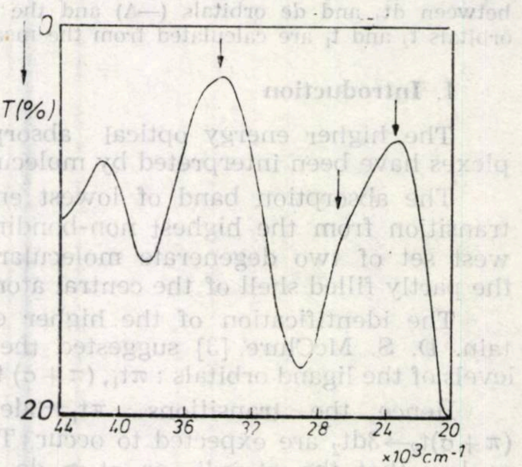

Fig. 2. Absorption spectrum of Fe^{3+} in CH_2Cl_2.

Table I gives the values of ν_{obs} (observed from spectra) and $\tilde{\nu}_{corr}$ (calculated with the formula 1). The values of x_{opt} are those given in literature [5].

Table I

Complex	$x_{opt}(M)$	$x_{opt}(X)$	$\tilde{\nu}_{sp}$(kK)	$\tilde{\nu}_{obs}$(kK)	$\tilde{\nu}_{corr}$(kK)	Transition
$[FeCl_4]^-$	2,4	3	10,6	27,5	28,6	$\pi t_1 \rightarrow de$
$[FeBr_4]^-$	2,4	2,8	10,6	23,2	22,6	$\pi t_1 \rightarrow de$

The bands have the assignement given in fig. 3 and 4, showing a subshell energy difference $-\Delta \simeq -10$ kK between dt_2 and *de* orbitals in $[FeCl_4]^-$ and $-\Delta = -8$kK in $[FeBr_4]^-$. The difference Δ' between the ligand π orbitals energies t_2 and t_1 is close to 3,5 kK in $[FeCl_4]^-$ and 3kK in $[FeBr_4]$.

The band at 41 kK in Fig. 2 could be interpreted as $\pi t_1 \rightarrow$ de transition in $[FeBr_4]^{2-}$ complex or as the same transition in $[FeH_2O]^{2+}$.

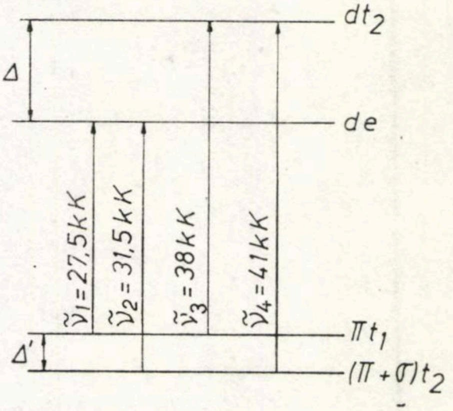

Fig. 3. Energy levels diagram for $[FeCl_4]^-$ complex. The observed transitions are indicated by vertical arrows.

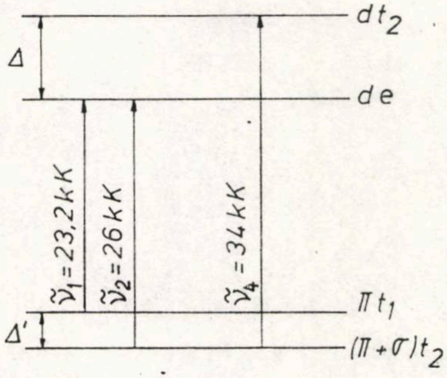

Fig. 4. Energy levels diagram for $[FeBr_4]^-$ complex. The observed transitions are indicated by vertical arrows.

3. **Conclusions**

1. The bonding linear combination of ligand π — orbitals of symetry t_2 has 3,5 kK lower energy than the non-bonding set t_1 in $[FeCl_4]^-$ and 3kK in $[FeBr_4]^-$.

2. The subshell energy difference between dt_2 and de, —Δ is close to — 10kK in $[FeCl_4]^-$ and — 8kK in $[FeBr_4]^-$.

3. The electronegativity of the ligands and central atom can be correlated with the wave-numbers of the electron transfer bands.

REFERENCES

1. M. WOLFSBERG, L. HELMHOLTZ, J. Chem. Phys., 20, 837, 1952.
2. A. CARRINGTON, D. SCHOULAND, M. C. R. SYMONS, J. Chem. Soc., 889, 1960.
3. D. S. McCLURE, Solid State phys., 9, 399, 1959.
4. A. CARRINGTON, C. K. JORGENSEN, Mol. Phys., 4, 395, 1961.
5. C. K. JORGENSEN, Progress in Inorganic Chemistry, 12, 101, ed. S. Lippard, New York, 1970.
6. C. K. JORGENSEN, *Modern Aspects of Ligand Field Theory,* North-Holland Publishing Company, Amsterdam, 1971.
7. ATH. TRUTIA, FLORIANA IOVA, ANA DANCU, Analele Univ. FIZICA, XXXIII, 43, 1983.

ANALELE UNIVERSITĂȚII BUCUREȘTI, FIZICĂ, XXXIV, 1985, PAG. 41–45

ON THE ELECTRON MOBILITY IN n-TYPE InAs

I. LICEA, B. LOGOFĂTU, MICHAELA LOGOFĂTU, I. MUNTEANU, I. DIMA
Faculty of Physics, University of Bucharest *
M. F. LĂZĂRESCU
Institute of Physics and Technology of Materials **

Abstract. In this work some experimental data concerning the dependence of mobility versus the electron concentration at room temperature in n-type InAs are reported. These results agree with the quantitative calculus which take into account, separately, the mobilities determined by the ionized impurity scattering and optical phonon scatering, in the case of predominant electron-electron collisions.

1. Introduction

InAs, like otther III—V compounds. is of great importance because of its use in electronic devices. For an efficient opperation of these materials it is necessary to know the charge carrier mobility, associated with the understanding of the role of the various scattering mechanisms and with the accurate description of the impurified crystal properties.

InAs is a direct gap polar semiconductor with spherically symmetric and nonparabolic conduction band. Although this band structure is closely related to InSb, the experimental and theoretical studies devoted to InAs are less numerous /1/. Some theoretical calculation of the electron mobility, developed for different approximations /2, 3/, were compared with the experimental data on InSb, a III—V compound at which the nonparabolicity is more pronounced.

The purpose of this paper is to present some experimental data on the electron mobility as a function of the electron concentration in uncompensated n-type InAs, at room temperature, and to compare these data with calculations taking into account the predominant mechanisms and the non-parabolic band shape.

2. Experimental

The n-InAs crystals were prepared by a Bridgman horrizontal method, the material being homogeneous, with large single crystal regions. The neutron analysis was used to verify the stoichiometry of the compound. Impurities like Te, Se, Sb associated with point defects in crystal lattice are responsible for n-type conduction of the samples. The samples were prepared under the form of rectangular parallelipipeds ; ohmic contacts have been achieved by alloying with metallic indium, under vacuum conditions (5×10^{-5} torr), at 350°C.

---

* National Center of Physics, P.O. Box 5211, Măgurele — Bucharest.
** National Center of Physics, P.O. Box 5207, Măgurele — Bucharest.

The transport properties were measured /4/ at room temperature so as to determine the carrier type (by thermoelectric method), the electron concentration (from Hall effect), the resistivity (by two points probe method) and the Hall mobility. Magnetic fields in the range 10—15 kilogauss were used so that, for calculations, the value of the Hall coefficient factor (r) has been approximated to unity.

The electron concentrations of the samples ranged from 10^{16}cm^{-3} to 10^{18}cm^{-3} ; these values being by 1—2 order of magnitude higher than the intrinsec concentration ; the mobilities were between 10 000 cm^2/VS and 20 000 cm^2/Vs, corresponding to different doping.

In fig. 1 the experimental data on the mobility as a function of electron concentration, at room temperature, are plotted as open circles. It may be seen that there is a high decrease of the mobility with the increase of electron concentration for $n > 10^{17}$cm^{-3}. A similar behaviour was reported for InAs in /5, 6/. This decrease also appearing for other III—V compounds, is associated with the nonparabolicity of the conduction band and with the increase of the carrier effective mass /1—3, 6, 7/ at high electron concentrations.

Also, we have performed measurements at liquid nitrogen temperature. In this case, the experimental curve presents the same fashion, but mobility values are by one order of magnitude higher than those from fig. 1. Moreover, the same type of measurements were made on samples irradiated with electrons accelerated up to 7Mev or with thermalized neutrons. The results exhibit the same behaviour of the dependence $\mu = \mu(n)$ but mobility values are lower than those from fig. 1.

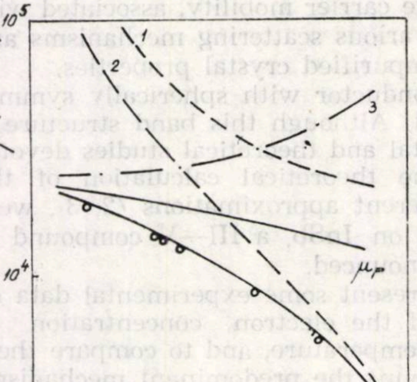

Fig. 1. Electron mobility versus concentration of n-InAs samples, at room temperature.

The following part of this paper deals only with a quantitative evaluation of mobility in non-irradiated samples.

3. Quantitative evaluations. Discussions

A theoretical analysis of the electron mobility must take into account the possible scattering mechanisms. In n-type InAs samples, at room temperature, the following mechanisms are operative /4/: ionized impurity scattering (IIS) and optical phonon scattering (OPS).

The considerations presented in (3) show that the mobility due to simultaneous influence of two scattering mechanisms, in the case of strong electron-electron scattering, may be calculated according to a simple relationship :

$$\frac{1}{\mu} = \frac{1}{\mu_{ii}^{ee}} + \frac{1}{\mu_{op}^{ee}} \tag{1}$$

where μ_{ii}^{ee} and μ_{po}^{ee} are the mobilities evaluated separately, in the limit of strong electron-electron collisions. In this limit case the combination of the mobilities by addition of reciprocal mobilities becomes feasible ; this procedure is not justified in the general case of no electron-electron scattering, when the mobility must be calculated by using the average of an effective relaxation time, defined as $\tau_{ef}^{1} = \tau_{ii}^{1} + \tau_{op}^{1}$.

If the mobility is limited only by ionized center scattering, the process being elastic, the relaxation time approximation may be used to solve the Boltzmann equation. In the case of IIS and a parabolic band shape, the mobility has been described by Brooks-Herring formula. The modification of this formula for a non-parabolic band, in the limit of strong electron-electron collisions, is given in (3) :

$$\mu_{ii} = \frac{\sqrt{2}\, K_o^2 (k_B T)^{1/2}}{\pi e^3 m^{*1/2}} \times \frac{1}{N_1} \times \frac{F_3(\eta)}{F^{3/2}(\eta)} \frac{\varphi(\overline{x})}{s(\overline{x})} \times \left[\frac{1}{2} + (1+e^{-\eta}) \frac{F_{3/2}^2(\eta)}{2F_3(\eta)}\right] \tag{2}$$

where K_0 is the static dielectric constant ; e is the electron charge ; m^* is the effective mass ; k_B is the Botzmann constant ; T is the absolute temperature ; $\hbar = h/2\pi$ and h is the Planck constant ; N_I is the concentration of ionized impurities assumed to be fully ionized and equal to the free electron concentration ; F_α (η) are the Fermi integrals

$$F_\alpha(\eta) = \int_0^\infty \left(-\frac{\partial f_0}{\partial x}\right) x^\alpha dx \tag{3}$$

where $x = E/k_B T$; $\eta = E_F/k_B T$; $f_0 = [1 + \exp(x - \eta)]^{-1}$

$$\eta = \overline{x} - \ln \frac{\overline{x}+3}{\overline{x}-3} \tag{4}$$

$$\varphi(\overline{x}) = \frac{(1+\beta\overline{x})^3}{(1+2\beta)\overline{x}^2} \left[1 + \frac{3}{2}\beta \frac{F_{5/2}(\eta)}{F_{3/2}(\eta)} + \frac{3}{8}\beta^2 \frac{F_{7/2}(\eta)}{F_{3/2}(\eta)} + \dots\right] \tag{5}$$

where $\beta \simeq k_\beta T/E_g$ is the non parabolicity parameter and E_g is the energy gap ; and S(x) is the Takimoto modification of the Brooks-Herring frmula /3/ :

$$S(x) = \ln(x + \alpha x) - (1 + \alpha^{-1})^{-1} \tag{6}$$

with α defined as :

$$\alpha = \frac{(4k_BT)^2Km^*}{3\pi e^2\hbar^2 n}(1+\beta\overline{x})\frac{F_{3/2}(\eta)+\frac{3}{2}\beta F_{5/2}(\eta)+\frac{3}{8}\beta^2F_{7/2}(\eta)+...}{F_{1/2}(\eta)+\frac{5}{2}\beta F_{3/2}(\eta)+\frac{7}{8}\beta^2F_{5/2}(\eta)+...} \tag{7}$$

where we have retained only the second order corrections for non-parabolicity.

The influence of the electron-electron collisions on the impurity mobility is contained between brackets in equation (2).

The electron mobility for a parabolic band shape may be obtained from the above equations for $\beta = 0$.

We performed calculations based on the relations (2) — (7) for : i) the parabolic case $\beta = 0$ (the curve 1 from fig. 1), ii) the non-parabolic case $\beta = 0{,}07$ (the curve 2 from fig. 1). It may be seen that for low electron concentrations the non-parabolicity gives only small corrections to the mobility. But, for electron concentrations $n > 10^{17}\text{cm}^{-3}$, the curve (2) moves away from the curve (1), being close to the experimental data. Therefore, at least for large electron concentrations IIS is the dominant mechanism and the effect of the non-parabolic band must be considered in the calculus. It is noted that the calculated mobility (curve 2) is higher than the observed values, this deviation being particulary pronounced at low concentrations. This fact is due to the influence of OPS, which represents the dominant scattering mechanism in pure polar semicconductors at room temperature /2/.

If the mobility is limited only by OPS, the scatterig process being inelastic for much of the temperature range of interest, the relaxation time concept must be abandoned. The resulting problem has previously been solved by variational calculation /2, 6/. In order to simplify the mathematical calculations, we restricted ourselves making use of the mobility expression, in the parabolic band approximation and in the limit of strong electron-electron collisions. given in /3/ :

$$\mu_{0p} = \frac{2\sqrt{2}\,\hbar^2}{3e(m^*)^{3/2}(k_BT_D)^{1/2}(K_\infty^{-1}-K_0^{-1})}\ x\ \frac{\exp(\Upsilon_0)\text{-}1}{(\Upsilon_0)^{1/2}}\ x\ \frac{F_{3/2}(\eta)}{D_{00}(\eta,\Upsilon_0)} \tag{8}$$

where K_∞ is the high frequency dielectric constant and $T_D = h\nu_{op}/k_B$, where υ_{op} is the longitudinal optical phonon frequency and T_D the corresponding Debye temperature.

The quantity

$$D_{00}(\eta,\Upsilon_0) = 2\int_0^\infty \frac{(x^2+\Upsilon_0x)^{1/2}dx}{(e^{\eta-x}+1)(e^{x-\eta}+e^{-\Upsilon_0})} \tag{9}$$

is an integral which may be evaluated only numerically.

We performed calculations based on the formula (8) and the results are presented in fig. 1 (curve 3). The experimental data agree with theoretical curve (3), at low electron concentrations where OPS plays a significant role

The values of the material parameters used in equations (2) – (9) for numerical-calculations are known from the literature : $K_0 = 14{,}3$; $K_{\infty} = 11{,}5$; $E_g = 0{,}36$ eV ; $m^* = 0{,}025$; $T_D = 334$ K.

The results of combining, by means of equation (1), the polar mobility with the mobility for ionized impurity scattering are presented in fig. 1: i) the curve labelled μ_P corresponds to $\mu_P^{-1} = \mu_{op}^{-1} + \mu_{ii}^{-1}$ ($\beta = 0$); ii) the curve labelled μ_{NP} corresponds to $\mu_{NP}^{-1} = \mu_{op}^{-1} + \mu_{ii}^{-1}$ ($\beta = 0{,}07$). The agreement between the theoretical curve μ_{NP} and the experimental data is satisfactory, even if the calculated values are somewhat higher than the observed values. The deviation may be the result of over estimation of the polar mobility because, it is well known, that the effect of non-parabolicity is to reduce the value of mobility.

At high electron concentrations IIS is the dominant mechanism and the equation (2) takes into account the non-parabolic band shape. The influence of OPS is important at low electron concentrations. The fact that the expression (8) is derived for parabolic band produces only minor errors because at these concentrations the influence of non-parabolicity is small.

The generally good agreement between theory and experiment attests to the accurancy of the present model as well as to the material parameters used in calculations.

REFERENCES

1. P. C. MATHUR, R. SHYAM, SUSHIL JAIN. Phys. Stat. Sol., *50,* 11, 1978.
2. H. EHRENREICH, J. App. Phys. Suppl., *32,* 2155, 1961.
3. R. T. BATE, R. D. BAXTER, F. J. REID, A. C. BEER, J. Phys. Chem. Solids, *26,* 1205, 1965.
4. MICHAELA LOGOFĂTU, Thesis, University of Bucharest, 1984.
5. E. SCHILLMAN, Z. Naturforsch, *11,* 463, 1956.
6. D. L. RODE, Phys. Rev. B, *2,* 1012, 1970.
7. M. CARDONA, Phys. Rev., *121,* 752, 1961.

ANALELE UNIVERSITAŢII BUCUREŞTI, FIZICĂ, XXXIV, 1985, PAG. 47—51

INCREASING THE ANALOG-DIGITAL CONVERTERS PERFORMANCES BY NUMERICALLY CORRECTING THE COMPONENTS' ERRORS

S. I. SPĂNULESCU and I. SPĂNULESCU
Faculty of Physics, University of Bucharest *

Abstract. In this paper a new method for amplification and analog-digital conversion of bipolar signals is presented.

According to the general principle for numerically correcting of errors in the analog part, an experimented model is proposed and analysed.

1. Generalities

As it is known, numerical techniques in electronics come to replace as much as possible the analogic, thus providing further increasing of the performances in a certain application. The main problem that occurs at this point is the analogic nature of the majority of signal sources practically involved, needing a previous analog-numeric conversion before processing. As the final reverse convertion to the original form is not everytime necessary, the general block diagram of the scientific research electronic systhem is like in figure 1,

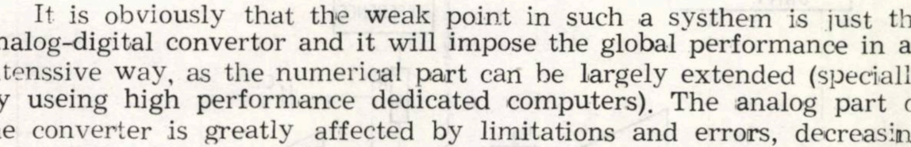

Fig. 1

It is obviously that the weak point in such a systhem is just the analog-digital convertor and it will impose the global performance in an intenssive way, as the numerical part can be largely extended (specially by useing high performance dedicated computers). The analog part of the converter is greatly affected by limitations and errors, decreasing the global performance. To minimize their effects implies sofisticated adjustments, some of them continously and automatically done, a severe selection of the components and sometimes the use of the top performances for them (high speed, high imput impedance amplifiers, very low temperature coefficient for all the components, high stability and many others).

---

* University of Bucharest, Măgurele — Bucharest, P.O. Box MG-11, Romania.

A more attractive way for solving such problems is involving as much as possible the numerical methods even in the analogical part of the convertor and minimising the number of "analogic" components. This permits sometimes the use of low performance analogic components by extending the numerical part and by useing a more sofisticated convertion algorythm.

2. **The four-slope integrating analog/digital convertor**

A simple method for aplying the above principle in a converter is the use of two phase convertion : the first one "measures" the sum of errors in the analogic part and the second the sum of errors and the imput signal. By substracting the two results, the error are severely decreased, no matter their absolute values.

We experimented this principle for a dual slope integrating A/D convertor in a properly modified form and the result was a trimmering, no adjustment systhem. The block diagram of the converter is shown in figure 2.

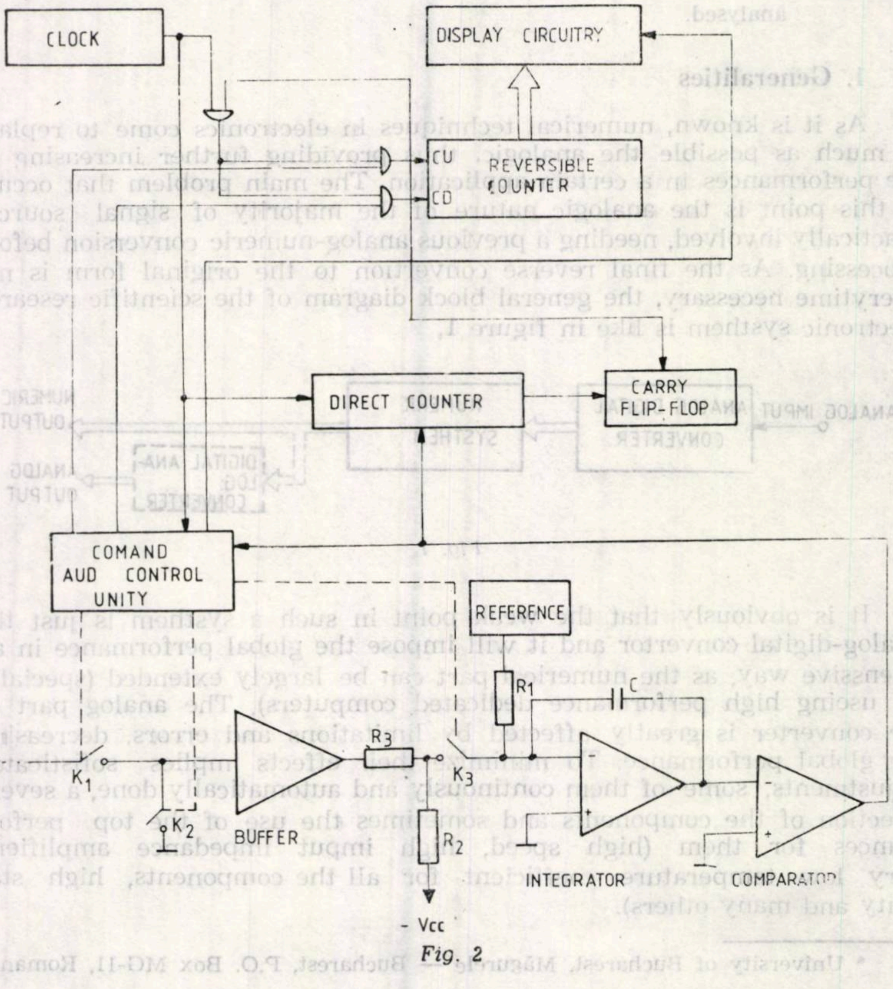
CLOCK
DISPLAY CIRCUITRY
CU
CD
REVERSIBLE COUNTER
DIRECT COUNTER
CARRY FLIP-FLOP
COMAND AUD CONTROL UNITY
REFERENCE
R1
C
R3
K3
K1
K2
BUFFER
R2
INTEGRATOR
COMPARATOR
+
- Vcc

Fig. 2

The numerical part contains : a reversible counter (RC), a direct counter with cary output (DC), a display circuitry (D), and a command and control unity (UC). The analogic part consists in a buffer (1), an opperational amplifier intergrator (2), a comparator (3), a reference source (4) and three analog switches (K_1, K_2, K_3).

As it can be noticed there are some simplification in comparison with other four slope convertors actually known: a single reference source, and only two counters (instead of three or more). In such condition the convertion algorithm is also simplified.

In the waiting period AB (Fig. 3) the switch K_2 is on and K_1, K_3 off. The integrator receives only the refference curent (positive) and it's output is turned to the maximum negative level. Both counters are cleared.

When a start pulse ocurs, K_2 is turned on and a negative curent, greater than the positive reference, is introduced in the integrator imput and so the voltage at the integrator output begins a linear increasing.

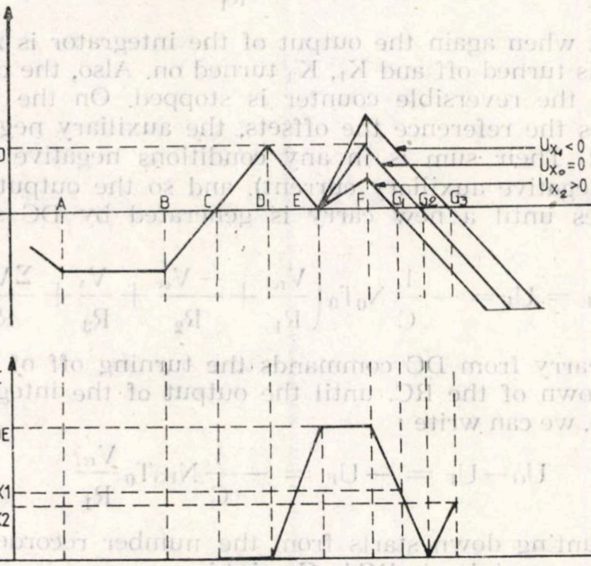

Fig. 3

In point C, when zero crossing, the comparator starts the direct counter ; when it generates a carry the switch K_3 is turned off and the refference current is integrated only, this moment beeing the start of counting up of the reversible counter. So, the output voltage of the integrator varies as following :

$$U_D - U_C = U_D = -\frac{1}{C} N_0 T_0 \left(\frac{V_{ref}}{R_1} + \frac{-V_{cc}}{R_2} + \frac{\Sigma V_{off}}{R_e} \right); \qquad (1)$$

$$U_E - U_D = -U_D = -\frac{1}{C} N_{DE} T_0 \left(\frac{V_{ref}}{R_1} \right). \qquad (2)$$

where :

N_0 — is the capacity of the direct counter ;

N_{DE} — is the count-up number recorded by the reversible counter on the DE slope ;

T_0 — clock period ;

V_{ref} — reference voltage ;

V_{cc} — negative voltage supply ;

ΣV_{off} — the sum of offsets in the conditioner circuitry ;

R_e — equivalent integrating resistance for offsets.

The count up number recorded in RC on DE slope is then :

$$N_{DE} = N_0 \frac{\dfrac{V_{cc}}{R_2} - \dfrac{V_{ref}}{R_1} - \dfrac{\Sigma V_{off}}{R_e}}{\dfrac{V_{ref}}{R_1}} \tag{3}$$

In E point when again the output of the integrator is zero crossing, the switch K_2 is turned off and K_1, K_3 turned on. Also, the direct counter is cleared and the reversible counter is stopped. On the EF slope the integrator takes the reference the offsets, the auxiliary negative current and the signal. Their sum is in any conditions negative (by properly choosing the negative auxiliary current), and so the output of the integrator increases until a new carry is generated by DC started again in E :

$$U_F - U_E = U_F = -\frac{1}{C} N_0 T_0 \left(\frac{V_{ref}}{R_1} + \frac{-V_{ce}}{R_2} + \frac{V_x}{R_3} + \frac{\Sigma V_{off}}{R_e} \right). \tag{4}$$

In F the carry from DC commands the turning off of K_3 and start the counting-down of the RC, until the output of the integrator is zero crossing (G). So, we can write :

$$U_G - U_F = -U_F = -\frac{1}{C} N_{FG} T_0 \frac{V_{ref}}{R_1} \tag{5}$$

As the counting down starts from the number recorded in E, N_{DE}, the final number remaining in RC in G point is :

$$N_x = N_{FG} - N_{DE} = N_0 \frac{\dfrac{V_x}{R_3}}{\dfrac{V_{ref}}{R_1}} \tag{6}$$

The ecuation that describes the convertor is then :

$$N_x = N_0 \frac{R_1}{R_2} \frac{V_x}{V_{ref}} \tag{7}$$

and there are no offsets involved in it althought they were considered from the beginning. This means that autozero function is provided in a numerical way.

3. **Results and conclusions**

Our experiments revealed the opportunity of the method when high resolution and good stability must be achieved with common use components. Thus, even useing low performance operational amplifiers as βA741, precision up to 0.025% was obtained. There is practically no zero temperature coefficient and the whole systhem time and thermal stability depends only by the refferance source. There are no offset adjustments for the operational amplifiers and their speed temperature coefficient and imput currents are not important, these beeing rejected by summing and substracting in the two phases. We consider that using this principle, the performances obtained for a certain set of analog components will increase more than ten times in comparison with the standard dual-slope converters.

REFERENCES

1. * * * CMOS 13-Bit Monolithic A/D convertor AD 7550. Data Sheet in *Analog Devices Data Acquisition Products Catalog*, 1978.
2. E. HNATECK, *A User's Handbook of D/A and A/D Converters*, John Wiley & Sons, 1975.
3. E. RENSCHLER, *Analog to Digital Conversion Techniques*, A/D Conversion Series — Part. 1, MOTOROLA Semic. Applic. Note AN-471.
4. R. C. KIME, Electronics, *46*, No. 11, 1973.
5. J. SHERWIN, *Data Acquisition System Interface to Computers*, NATIONAL SEMICONDUCTORS INC. Application Note, AN-159, 1976.

ANALELE UNIVERSITĂŢII BUCUREŞTI, FIZICĂ, XXXIV, 1985, PAG. 53—56

ON THE EVALUATION OF THE SHORT CIRCUIT CURRENT IN THE THIN FILM Cu_2S-CdS ELECTRON — VOLTAIC CELLS

A. DAFINEI, I. LICEA
Faculty of Physics, University of Bucharest *

Abstract. In this work the short-circuit current appearing in the electron voltaic thin film Cu_2S—CdS cell irradiated with electron beam of a transmission electron microscope (TEM) is analyzed. The relation between some material characteristics of the Cu_2S thin film and its contribution to the short-circuit curent of the cell is establiched.

1. Introduction.

The studies of the β-voltaic effect point out the utility to consider the interaction between the electron beams from the electron microscope and the heterojunction.

As is well known, when the electron beam impinges on an p-n Cu_2S—CdS junction the generation of electron-hole pairs by impact ionization causes a short circuit current I_{sc} to flow. To this short circuit current contribute separately the upper p-Cu_2S layer of the cell, the depletion layer extended mainly in the CdS layer and the n-CdS layer.

In order to determine these contributions, a three dimensional analysis of the electron-hole pairs generation is imposed, For the Si homojunction such a calculus has been performed in [1].

The purpose of this work is to evaluate the contributions of the three layers of the Cu_2S—CdS cell extending the calculus for the Si p-n homojunction in the case of the geometry and specific electrical properties of the Cu_2S—CdS heterojunction.

The used model takes as a basis the assumption that the generation of the charge carriers takes place mainly between the irradiated surface and the electron excitation depth, in a volume far away from upper ohmic contact.

As a result, one may obtain the expressions of the contributions due to everyone of the three heterojunction layers to the short-circuit current. Is pointed out that the contribution of the p-Cu_2S layer to the short-circuit current depends strongly on the electron diffusion lenght L_n and the surface recombination velocity s. The numerical evaluation of the short — circuit current calculated on the basis of the considered model satisfactorily agrees with the experimental data.

2. Theoretical considerations

In order to model the interaction betwen the electron beam and thin film Cu_2S—CdS heterojunction the concret structure of the cell must be considered. The studied structures are typical thin film Cu_2S—CdS cells used both in the study of β—voltaic and foto-voltaic effects. Their construction has been previously presented in the main in [2].

---

* National Centre of Physics, Măgurele — Bucharest, P. O. Box 5211.

The studies of the β—voltaic effect [3, 4] has been performed on some cells for which the upper contact is a grid with a distance of 2 mm between the strips. The electron beam width when this impinge on the cell has been a few tens microns. Therefore, a resonable approximation to model the phenomenon is the consideration that the upper ohmic contact being extended into the half plane $x<0$ to minus infinity and the free surface of p-Cu_2S film into $x>0$ half plane to plus infinity with impunity. As a result, two half spaces joined together at $x=0$ [1].

In order to describe the cell in the z direction let us consider the p-Cu_2S layer being bounded by $z=0$ and $z=d$ planes, the depletion layer bounded by $z=d$ and $z=d+w$ planes and the n-CdS layer bounded by $z=d+w$ and $z=T$ planes.

The interaction between the electron beam and the β — cell may be described by means of two parameters : R and z_1 representing respectively the penetration depth in the material for the electrons of the TEM beam and the excitation depth which is the distance inside the material where pair production is predominant.

In the calculus the existence of the ohmic contact is neglected, i.e. we consider that the electron beam from TEM penetrates the cell in a point situated at some tens diffusion lenghts from the upper ohmic contact. Also we consider that the generation of the secondaries electrons being important only between the upper surface and the excitation depth, such an assumption allowing to consider a source function as [1]:

$$S(x, y, z) = \frac{I'_\circ}{e}\frac{E_o}{E_i}\frac{3\pi^{3/2}}{16\pi}\alpha^3 \exp[-\alpha^2(x^2+y^2+(z-z_1)^2)]\theta(z) \tag{1}$$

wheree I'_0 is the electron beam intensity from the TEM corrected for back-scattered electrons, e is the electron charge, E_0 is the energy of the electrons from beam, E_i is the average ionization energy, $\alpha=R^{-1}$, and θ (z) is the unit step, function.

The determination of the p-Cu_2S layer contribution to the short-circuit current is relatively simple if the upper ohmic contact is completely neglected. For this purpose, we resolve the diffusion equation :

$$(\nabla^2 - L_n^{-2})N(x,y,z) = -D_n^{-1}S(x,y,z) \tag{2}$$

with the boundary conditions :

$$\begin{aligned} &N(x,y,d) = 0, \quad \forall x, \forall y \\ &D_n\frac{\partial N}{\partial y} - sN = 0 \quad \text{for } z=0 \quad \forall x, \forall y \end{aligned} \tag{3}$$

where N(x. y. z) is the density of electrons in excess.

Considering for the short circuit current generated in the p-Cu_2S material the expresion :

$$I_{sc}(n) = eD\int_{-\infty}^{\infty}dx\int_{-\infty}^{\infty}dy\left.\frac{\partial N}{\partial z}\right|_{z=d} \tag{4}$$

and performing the same steps of calculus as in [1] we obtain :

$$I_{sc}(n) = I'_\circ\frac{E_o}{E_i}\frac{3\pi^2}{16}\frac{B+(D_n/L_n-s)e^{-\frac{d}{L_n}}+B-(D_n/L_n+s)e^{\frac{d}{L_n}}}{D_n/L_n\,\mathrm{ch}(d/L_n)+s\,\mathrm{sh}(d/L_n)} \tag{5}$$

where :

$$B_{\pm} = \exp\left[\pm\frac{d-z_1}{L_n} + (2\alpha L_n)^{-2}\right]\left\{\operatorname{erf}[\alpha(d-z_1) \pm (2\alpha L_n)^{-1}] + \right.$$
$$\left. + \operatorname{erf}[\alpha z_1 \mp (2\alpha L_n)]^{-1}\right\} \tag{6}$$

D_n being the diffusion coefficient for electrons in p-Cu_2S layer.

In order to determine the depletion layer contribution to the short-circuit current I_{se} (DL), we consider that each pair generated in this layer is immediately separated by the electrical junction field so that the recombination current must be neglected. Therefore, we have

$$I_{sc}(DL) = 2e\int_{-\infty}^{\infty} dx \int_{-\infty}^{\infty} dy \int_{d}^{d+w} dz\, S(x,y,z) \tag{7}$$

so that taking into account the source expresion (1) we obtain :

$$I_{sc}(DL) = I'_{\circ}\frac{E_o}{E_i}\frac{\pi^2}{16}\left\{\operatorname{erf}[(d+w-z_1)\alpha] - \operatorname{erf}[(d-z_1)\alpha]\right\} \tag{8}$$

The contribution to the short-circuit current of the n-CdS layer, Isc(p), may be directly obtained from the relation (5) replacing the thickness d by T-d-w the excitation depth z_l by z_1-d-w, the diffusion lenght L_n by L_p and the diffusion coefficient D_n and D_p. Moreover, we consider a good bottom ohmic contact with the n CdS layer, i.e. $s=\infty$. In these conditions

$$I_{sc}(p) = I'_{\circ}\frac{E_o}{E_i}\frac{3\pi^2}{64}\frac{C_- e^{(T-w-d)/Lp} - C_+ e^{-(T-w-d)/Lp}}{sh[(T-w-d)/L_p]} \tag{9}$$

where

$$C_{\pm} = \exp\left[\pm\frac{T-z_1}{L_p} + (2\alpha L_p)^{-2}\right]\left\{\operatorname{erf}[\alpha(T-z_1) \pm (2\alpha L_p)^{-1}] + \right.$$
$$\left. + \operatorname{erf}[\alpha(z_1-d-w) \mp (2\alpha L_p)^{-1}]\right\} \tag{10}$$

The whole short-circuit current is obtained by

$$I_{se\ total} = I_{c}(n) + I_{sc}(DL) + I_{sc}(p) \tag{11}$$

The contribution of the p-Cu_2S layer (5) decends strongly on the parameters Ln and s, which are hard to controle.

3. Comparison with Experimental Data and Discussion

In order to compare the expression (11) of the short circuit current with the experimental data, the knowledge of a great number of parameters is required.

From these, E_0 and $I'_{\circ}$ depend only on the used radiation source (TEM), and can be measured by means of the technics previously described [6]. The obtained values for the studied cell has been E_0=50 keV and $I'_{\circ}$ = 0,2 μA, respectively.

Other quantities as d, w, and T are determined from the concrete geometry of the cell. The whole thickness of the two CdS and Cu_2S layers, $T = 15$ μm has been determined by a direct measurement with an indicating micrometer. The thickness of the Cu_2S layer $d = 0{,}15$ μm has been measured using the technics of the electrochemical analysis of the composition and thickness previously exposed [4]. At last, the thickness of the depletion layer $w = 0{,}5$ μm has been estimated from measurements of the electron concentration and electrical resistivity. This value agrees with the other data from the literature obtained for similar cells.

The knowledge of cell parameters describing the interaction between the radiation and the heterojunction as z_1, R and E require special measuring methods, The values has been given from the literature [7].

Finally, some parameters as the diffusion lenght, the diffusion coefficients and the surface recombination velocity, must be evaluated. The diffusion coefficients $D_n = 0{,}02$ cm²/s and $D_p = 0{,}018$ cm²/s has been estimated from mobility measurements effectuated by Corbino disk method using the technics described in [8]. The diffusion lenght for holes in CdS layer has been evaluated to be $L_p = 0{,}2$ μm.

The parameters L_n and s for the Cu_2S layer are more difficult to evaluate. The allowable values in the literature are in a large range. In the present calculus we consider that $L_n = 0{,}3$ μm and $s = 10^4$ cm/s.

At finally, the experimental value of the short-circuit current, $I_{sc}^{exp} = 78{,}75$ μA has been measured by the technics previously described in [6] which is used succesfully in the study of the β-voltaic effect. This value is comparable to the calculated value $I_{sd} = 101{,}75$ μA by means of the relation (11) and using the mentioned above values for the different parameters. A more good agreement between the experimental and calculated value of the short-circuit current may be obtained for others more suitable values of the parameters L_n and s. Such a fit may be accomplished by plottig a family of curves $I_{se} = I_{sc}(I_o; L_n, s)$ for different values of Ln and s and comparing these curves with experimental one. In this way a more adequated values for L_n and s may be obtained too. This problem will be treated in an apart study.

REFERENCES

[1] O. von RÖSS, olid State Electronics, *21,* 1067 (1978) ; *21,* 1069 (1978).

[2] I. DIMA, I. SECĂREANU, I. LICEA, Analele Univ. București, Fizica, XXVI, 89 (1977).

[3] A. DAFIEI, I. DIMA, Conferința Națională de Fizică, București, 1982, pag. 316.

[4] A. DAFINEI, I. LICEA, Analele Univ. București, Fizica, XXXIII, 43 (1984).

[5] I. LICEA, A. DAFINEI, Al III-lea Colocviu Național de Fizica și Tehnologia Materialelor Cristaline și Amorfe, Iași, 1984, pag. 97.

[6] I. LICEA, A. DAFINEI, I. DAFINEI, Lucrările Conferinței anuale de Semiconductoare, Timișu de Sus, 1984, pag. 167.

[7] E. PFISTERER, H. W. SCHOCK, G. H. HEWIG, Proc. 2nd Photovoltaic Solar Energy Conference, Berlin, 1979, pag. 352.

[8] A. DAFINEI, I. LICEA, Al II-lea Colocviu Național de Fizica Materialelor cristaline și Amorfe, Iași 1984, pag. 99 ; idem, pag. 101.

ANALELE UNIVERSITĂŢII BUCUREŞTI, FIZICĂ, XXXIV, 1985 PAG. 57—67

RELAXATION TIMES ASSOCIATED WITH 2-PHONONS PROCESES IN METALIS CRYSTALS

C. CIUCU
Faculty of Physics, University of Bucharest *

R. P. LUNGU
Polytechnic Institute of Bucharest

Abstract. The probabilities associated whith 2-phonons processes in metallic isothropic crystals are presented. With the results obtained for these probabilities in the Debye approximation and high temperature limit the corresponding relaxation times were calculated.

1. Introduction

The Hamiltonian of a metallic crystal with 1 monovalent ion in the elementary cell and in the adyabatic approximation is [1, 2, 3, 4] :

$$\hat{H} = \hat{H}_e + \hat{H}_I + \hat{H}_{eI} \qquad (1—1)$$

Introducing the creation and annihilation operators ($\hat{C}^{+}_{\vec{k},\sigma}$ and $\hat{C}_{\vec{k},\sigma}$ on the 1-electronic states $U_{\vec{k},\sigma}$, the electronic Hamiltonian is :

$$\hat{H}_e = \sum_{k}\sum_{\sigma} \varepsilon_{\vec{k}} \hat{C}^{+}_{\vec{k},\sigma} \hat{C}_{\vec{k}\,\sigma} \qquad (1—2)$$

and the electronic state vector is :

$$| \psi^{e}_{R^{0},n} > = | \ldots, n_{\vec{k},\sigma}, \ldots > \qquad (1—3)$$

where $n_{\vec{k},\sigma} = 0, 1$ are the occupation numbers on the 1-electronic states $u_{\vec{k},\sigma}$.

Introducing the normal coordinate operators $\hat{Q}_{\vec{q},\lambda}$ and the phonon creation and annihilation operators on the $(\vec{q}, \lambda))$—mode $(\hat{a}^{+}_{\vec{q}}$ and $\hat{a}_{\vec{q},\lambda})$ we express in the second quantisation the ionic Hamiltonian ($\hat{H}_I$), the ionic state-vector ($|\psi^{I}_{n,\nu}>$) and the elongation on the n node ($\vec{U}_{\vec{n}}$ [1,6]:

$$\hat{H}_I = \sum_{\vec{q}}\sum_{\lambda} h\omega_{\vec{q}\lambda} (\hat{a}^{+}_{\vec{q}\lambda} \hat{a}_{\vec{q}\lambda} + \frac{1}{2}\hat{1}) \qquad (1—4)$$

$$| \psi^{I}_{n,\nu} > = | \ldots, n_{\vec{q},\lambda}, \ldots >$$

$$\vec{U}_{\vec{n}} = \frac{1}{\sqrt{MN}} \sum_{\vec{q}} \sum_{\lambda} \sqrt{\frac{h}{2\omega_{\vec{q}\lambda}}} \hat{a}_{\vec{q}\lambda} + \hat{a}^{+}_{-\vec{q}\lambda}) \vec{\in} (\vec{q},\lambda)\, e^{i\vec{q}\cdot\vec{R}^{\circ}_{\vec{n}}} \qquad (1—5)$$

---

* National Center of Physics, P.O. Box 5211, Bucharest, Romania.

where $\vec{\epsilon}\,(q, \lambda)$ and $\omega_{\vec{q},\lambda}$ are the polarisation vector and respectively the proper pulsation on the $(\vec{q}, \lambda)$—mode.
The electron-lattice interaction problem :

The non-adyabatical term $\hat{H}_{el} = \hat{V}_{el} - \hat{V}^{o}_{el} - E^{e}_{n}\,(R^{\circ})\hat{1}$ is considered as a perturbation which induce correlated transitions in the electronic and ionic systems. The third term $E^{e}_{n}\,(R^{\circ})\hat{1}$ is an C-number, thus it bring no contribution to the electron-lattice interaction, and we develope in power series of ionic elongations $\hat{\vec{R}}_{\alpha} = \hat{\vec{R}}^{o}_{\alpha} + \hat{\vec{U}}_{\alpha}$ to obtain the interaction Hamiltonian in the second order [1, 6, 8] :

$$\hat{H}^{el}_{int} = \hat{V}_{el} - \hat{V}^{o}_{el} = \sum_{j=1}^{N}\sum_{\alpha=1}^{N}\left\{\hat{v}(\hat{\vec{r}}_j - \hat{\vec{R}}_{\alpha}) - \hat{v}(\vec{r}_j - \hat{\vec{R}}^{o}_{\alpha})\right\} = \hat{H}^{(1)}_{el} + \hat{H}^{(2)}_{el} \qquad (1—6)$$

where :

$$\hat{H}^{(1)}_{el} = \sum_{j=1}^{N}\sum_{\alpha=1}^{N}\left(\frac{\partial\hat{v}\,(\vec{r}_j - \vec{R}_{\alpha})}{\partial\vec{R}_{\alpha}}\right)_{\vec{R}_{\alpha} = \vec{R}^{o}_{\alpha}}\cdot\hat{\vec{U}}_{\alpha} \qquad (1—7)$$

$$\hat{H}^{(2)}_{el} = \frac{1}{2}\sum_{j=1}^{N}\sum_{\alpha=1}^{N}\hat{\vec{U}}_{\alpha}\cdot\left(\frac{\partial^{2}\hat{v}\,(\vec{r} - \vec{R}_{\alpha})}{\partial\vec{R}_{\alpha}\,\partial\vec{R}_{\alpha}}\right)_{\vec{R}_{\alpha} = \vec{R}^{o}_{\alpha}}\cdot\hat{\vec{U}}_{\alpha} \qquad (1—8)$$

are the corresponding terms of the eleectron-lattice interaction associated with the 1-phonon processes and respectively 2-phonon processes.
Using the Nordheim approximation

$$\left(\frac{\partial^{n}\vec{v}(\vec{r}_j - \vec{R}_{\alpha})}{\partial\vec{R}^{n}_{\alpha}}\right)_{\vec{R}_{\alpha} = \vec{R}^{o}_{\alpha}} = \frac{\partial^{n}\hat{v}\,(\vec{r}_j - \vec{R}_{\alpha})}{\partial\vec{R}^{on}_{\alpha}}$$

and considering the periodicity property of the electron-lattice potential: $\hat{v}\,(\vec{r}_j - \vec{R}^{o}_{\alpha}) = \hat{v}\,(\vec{r}_j - \vec{R}^{o}_{\alpha} + \vec{R}^{o}_{\beta})$ we develope in Fourier serie the potential $\hat{v}(\vec{r}_j - \vec{R}^{o}_{\alpha})$:

$$\hat{v}\,(\vec{r}_j - \vec{R}^{o}_{\alpha}) = \frac{1}{\Omega}\sum_{\vec{k}}\tilde{v}\,(\vec{k})\,e^{i\vec{\kappa}\cdot(\hat{\vec{r}}_j - \hat{\vec{R}}^{o}_{\alpha}} \qquad (1—9)$$

We exprese in the second quantisation the operator $\sum_{j} e^{i\vec{\kappa}\vec{r}_j}$ and we use (1—5) for $\hat{\vec{U}}_{\vec{n}}$ to obtain the interaction hamiltonians in the second quantisation version :

$$\hat{H}^{(1)}_{el} = \sum_{\vec{q},\lambda}\ \sum_{\vec{k},\sigma} A_{\vec{q},\lambda}(\hat{a}_{\vec{q}} + \hat{a}^{+}_{-\vec{q},\lambda})\hat{c}^{+}_{\vec{k},\sigma}\hat{c}_{\vec{k}-\vec{q},\sigma} \qquad (1—10)$$

$$\hat{H}^{(2)}_{el} = \sum_{\vec{q},\vec{q}'}\ \sum_{\lambda,\lambda'}\ \sum_{\vec{k},\sigma} B_{\vec{q}\lambda;\vec{q}'\lambda'}(\hat{a}_{\vec{q}\lambda} + \hat{a}^{+}_{-\vec{q},\lambda})(\hat{a}_{\vec{q}'\lambda'} + \hat{a}^{+}_{-\vec{q}'\lambda'})\hat{c}^{+}_{\vec{k}'\sigma}\hat{c}_{\vec{k}-\vec{q}'-\vec{q},\sigma'}$$

(1—11)

where :

$$A_{\vec{q}\lambda} = \frac{-i}{\Omega}\sqrt{\frac{hN}{2M\omega_{\vec{q}\lambda}}}\, v(\vec{q})(\vec{q}\cdot\vec{\epsilon}_{\vec{q},\lambda}) \qquad (1—12)$$

$$B_{\vec{q}\lambda;\,\vec{q}',\lambda'} = -\frac{h}{4M\Omega}\,\frac{1}{\sqrt{\omega_{q\lambda}\,\omega_{\vec{q}'\lambda'}}}\,\tilde{v}(\vec{q}+\vec{q}')\,[(\vec{q}+\vec{q}')\cdot\vec{\epsilon}_{\vec{q}\lambda}]\,[(\vec{q}+\vec{q}')\cdot\vec{\epsilon}_{\vec{q}'\lambda'}] \qquad (1—13)$$

To consider the collective effects of the quasi-free electron system, we evaluate the Fourier transformation of the interaction potential $\tilde{v}(\vec{k})$ in the approximation Thomas-Fermi [4, 7] (approx. ord. I) :

$$\tilde{v}(\vec{q}) = \frac{-4\pi Ze^2}{q^2 + k^2_{TF}} \qquad (1—14)$$

where k_{TF} is the Thomas-Fermi wave vector :

$$k^2_{TF} = \frac{12\pi me^2}{h^2}\,\frac{n_0}{k^2_F} \qquad (1—15)$$

In the case of simple lattice $\vec{q}\cdot\vec{\epsilon}_{\vec{q},\lambda} = q\sigma_{\lambda L}$, thus to the 1-phonon interaction there are contribution only from the longitudinal phonons, and the interaction Hamiltonian is decomposed in 2 terms for $H^{(1)}_{el}$ and in 4 terms for $H^{(2)}_{el}$:

$$\hat{H}^{(1)}_{el} = \hat{H}^{(1)}_{el+} + \hat{H}^{(1)}_{el-} \qquad (1—16)$$

$$\hat{H}^{(2)}_{el} = \hat{H}^{(2)}_{el--} + \hat{H}^{(2)}_{el-+} + \hat{H}^{(2)}_{el+-} + \hat{H}^{(2)}_{el++} \qquad (1—17)$$

where :

$\hat{H}^{(1)}_{el+} = \sum_{\vec{q}}\sum_{\vec{k},\sigma} A_{\vec{q}}\,\hat{a}_{\vec{q},L}\,\hat{c}^{+}_{\vec{k},\sigma}\,\hat{c}_{\vec{k}-\vec{q},\sigma}$ (1-phonon emission hamiltonian)

$\hat{H}^{(1)}_{el-} = \sum_{\vec{q}}\sum_{\vec{k},\sigma} A^{*}_{\vec{q}}\,\hat{a}^{+}_{\vec{q}L}\,\hat{c}^{+}_{\vec{k},\sigma}\,\hat{c}_{\vec{k}+\vec{q},\sigma}$ (1-phonon absorbtion hamiltonian)

$\hat{H}^{(2)}_{el--} = \sum_{\vec{q}\lambda}\sum_{\vec{q}'\lambda'}\sum_{\vec{k}'\sigma} B_{\vec{q}\lambda,\vec{q}'\lambda'}\,\hat{a}_{\vec{q}\lambda}\,\hat{a}_{\vec{q}'\lambda'}\,\hat{c}^{+}_{\vec{k}\sigma}\,\hat{c}_{\vec{k}-\vec{q}-\vec{q}',\sigma}$ (2-phonon absorbtion hamiltonian)

$\hat{H}^{(2)}_{el-+} = \sum_{\vec{q}\lambda}\sum_{\vec{q}'\lambda'}\sum_{\vec{k}\sigma} B_{\vec{q}\lambda,\vec{q}'\lambda'}\,\hat{a}_{\vec{q}\lambda}\,\hat{a}^{+}_{\vec{q}'\lambda'}\,\hat{c}^{+}_{\vec{k}\sigma}\,\hat{c}_{\vec{k}-\vec{q}-\vec{q}',\sigma}$ (1-phonon absorbtion and 1-phonon emission hamiltonian'

$\hat{H}^{(2)}_{el+-} = \sum_{\vec{q}\lambda}\sum_{\vec{q}'\lambda'}\sum_{\vec{k}\sigma} B_{\vec{q}\lambda,\vec{q}'\lambda'}\,\hat{a}^{+}_{\vec{q}\lambda}\,\hat{a}_{\vec{q}'\lambda'}\,\hat{c}^{+}_{\vec{k}\sigma}\,\hat{c}_{\vec{k}-\vec{q}-\vec{q}',\sigma}$ (1-phonon emission and 1-phonon absorbtion hamiltonian)

$$\hat{H}^{(3)}_{el++} = \sum_{\vec{q}\lambda} \sum_{\vec{q}'\lambda'} \sum_{\vec{k}\sigma} B_{\vec{q}\lambda,\vec{q}'\lambda'}\, \hat{a}_{\vec{q}\lambda}\, \hat{a}_{\vec{q}'\lambda'}\, \hat{c}^{+}_{\vec{k}\sigma}\, \hat{c}^{+}_{\vec{k}-\vec{q}-\vec{q}',\sigma} \qquad \text{(2-phonon emission hamiltonian)}$$

and

$$A_{\vec{q}} = \frac{i}{\Omega}\, 4\pi Ze^2 \sqrt{\frac{hN}{2M\omega_{\vec{q}\lambda}}}\, \frac{q}{q^2 + k_{TF}^2}$$

2. Electron-lattice transition probabilities

a) The lattice in pure states

We consider the system consisting of one electron $(\vec{k}, \sigma)$ and the lattice $(\{n_{\vec{Q}\Lambda}\})$. The interaction $\hat{H}_{el}$ produces transitions between the states $|i\rangle = |\ldots, n_{\vec{Q}\Lambda}, \ldots\rangle|0, \ldots, 0, 1_{\vec{k},\sigma}, 0\ldots\rangle$ and $|f\rangle = |\ldots, n'_{\vec{Q},\Lambda}, \ldots\rangle|0, \ldots, 0_{\vec{k}'\sigma}, \ldots, 1_{\vec{k}\sigma}, \ldots\rangle$ which have the energies

$$E_i = \sum_{\vec{Q}\lambda} h\omega_{\vec{Q}\lambda}\, n_{\vec{Q}\lambda} + \varepsilon_{\vec{k}} \quad \text{and} \quad E_f = \sum_{Q\lambda} h\omega_{\vec{Q}\lambda}\, n'_{Q\lambda} + \varepsilon_{\vec{k}'}$$

The transition probability $|i\rangle \rightarrow |f\rangle$ in the first order of the perturbation theory [1] is :

$$P(i,f) = \frac{2\pi}{h} \,|\langle f \,|\, \hat{H}_{int} \,|\, i\rangle|^2 \delta(E_f - E_i) \tag{2—1}$$

Because $\langle f|\hat{H}^{(1)}_{el}|i\rangle \langle f|H^{(2)}_{el}|i\rangle = 0$, the transition probability is decupled in 2 terms :

$$P\,(i,\, f) = P^{(1)}\,(i,\, f) + P^{(2)}\,(i,\, f) \tag{2—2}$$

where :

$$P^{(1)}\,(i,\, f) = \frac{2\pi}{h} \,|\langle f \,|\, \hat{H}^{(1)}_{el} \,|\, i\rangle|^2 \,\delta(E_f - E_i) \tag{2—3}$$

is the transition-probability associated with 1-phonon processes.

$$P^{(2)}\,(i,\, f) = \frac{2\pi}{h} \,|\langle f \,|\, \hat{H}^{(2)}_{el} \,|\, i\rangle|^2 \,\delta(E_f - E_i) \tag{2—4}$$

is the transition probability associated with 2—phonon processes.

The 1—phonon transition probability is decomposed in the 1 phonon absorbtion term and the 1—phonon emission term :

$$P^{(1)}\,(i,\, f) = P^{(1)}_{-}(i,f) + P^{(1)}_{+}(i,f) \tag{2—5}$$

The 2—phonons transition probability is decomposed in 5 terms :

$$P^{(2)}(i,f) = P^{(2)}_{2+}(i,f) + P^{(2)}_{2-}(i,f) + P^{(2)}_{++}(i,f) + P^{(2)}_{--}(i,f) + P^{(2)}_{+-}(i,f) \tag{2—6}$$

2° The lattice at thermal equilibrium

In the preceding sub-section we have considered the transition probabilities of the electron-lattice system with the lattice in pure states the phonon occupation numbers on each vibration mode are well defined). If the lattice is at thermal equilibrium there are only the probability that on the $(Q\Lambda)$ — mode exist $n_{\vec{Q}\Lambda}$ phonons : $P(n_{\vec{Q}\Lambda}\,;T)$, and the mean number of photons on each mode is described by the Bose-Einstein distribution function :

$$N_{\vec{Q}\Lambda} = \sum_{n_{Q\Lambda}=0}^{\infty} n_{\vec{Q}\Lambda}\, P(n_{\vec{Q}\Lambda}\,;T) = [\exp(Bh\omega_{\vec{Q}\Lambda}) - 1]^{-1} \tag{2—7}$$

Because the interesting quantity is the electronic transition probability when the lattice is at thermal equilibrium, without considering the electronic spin orientation and the final state of the lattice, we make the following operations : 1° summation on the initial and final electron spin states ; 2° take the statistical average on all initial phononic states ; 3° summation on all possible final phononic states [9].

In the Debye approximation ($q \leqslant q_D$, $\omega_{qL} = sq$, where s is the longitudinal sound velocity) we obtain the transition probabilities :

$$P_{-}^{(1)}(\vec{k},\vec{k}') = \frac{16\pi^3(Ze^2)^2N}{\Omega^2 Ms} \sum_{\vec{q}} \frac{q}{(q^2+k_{TF}^2)^2} N(q) \times \delta\left[\frac{h^2}{2m^*}\left(q^2 + 2\vec{k}\vec{q}\right) - hsq\right] \delta_{\vec{k}',\vec{k}+\vec{q}} \tag{2—8}$$

$$P_{+}^{(1)}(\vec{k},\vec{k}') = \frac{16\pi^3(Ze^2)^2N}{\Omega^2 Ms} \sum_{\vec{q}} \frac{q}{(q^2+k_{TF}^2)^2} \times [N(q)+1]\delta$$

$$\left[\frac{h^2}{2m^*}\left(q^2 - 2\vec{k}\cdot\vec{q}\right) + hsq\right] \delta_{\vec{k}',\vec{k}-\vec{q}} \tag{2—9}$$

$$P_{2+}^{(2)}(\vec{k},\vec{k}') = \frac{64\pi^3 h(Ze^2)^2N}{M^2\Omega^2 s^2} \sum_{\vec{q}} \frac{q^2}{4q^2+k_{TF}^2)^2} [N(q)+1] \times$$

$$\times [N(q)+2]\, \delta\left[\frac{h^2}{2m^*} 4\left(q^2 - \vec{k}\cdot\vec{q}\right) + 2hsq\right] \delta_{\vec{k}',\vec{k}-2\vec{q}} \tag{2—10}$$

$$P_{2-}^{(2)}(\vec{k},\vec{k}' = \frac{64\pi^3 h(Ze^2)^2N}{M^2\Omega^2 s^2} \sum_{\vec{q}} \frac{q^2}{(4q^2+k_{TF}^2)^2} N(q)\,[N(q)-1] \times$$

$$\times\, \delta\left[\frac{h^2}{2m^*} 4\left(q^2 + \vec{k}\vec{q}\right) - 2hsq\right] \delta_{\vec{k}',\vec{k}+2\vec{q}} \tag{2—11}$$

$$P_{++}^{(2)}(\vec{k},\vec{k}') = \frac{4\pi^3 h(Ze^2)^2}{M^2\Omega^2 s^2} \sum_{\vec{q},\vec{q}'}{}' \frac{|\vec{q}+\vec{q}'|^4}{[(\vec{q}+\vec{q}')^2 + k_{TF}^2]^2} \times \frac{[N(q)+1]\,[N(q')+1]}{qq'}\,\delta$$

$$\left[\frac{h^2}{2m^*}\{(\vec{q}+\vec{q}')^2 - 2\vec{k}\cdot(\vec{q}+\vec{q}')\} + hs(q+q')\right] \cdot \delta_{\vec{k}',\vec{k}-(\vec{q}+\vec{q}')} \tag{2—12}$$

$$P_{--}^{(2)}(\vec{k},\vec{k}) = \frac{4\pi^3 h(Ze^2)^2}{M^2\Omega^2 s^2} \sum_{\vec{q},\vec{p}'} \frac{|\vec{q}+\vec{q}'|^4}{[(\vec{q}+\vec{q}')^2 + k_{TF}^2]^2} \frac{N(q)-N(q')}{q\cdot q'} \times$$

$$\times\, \delta\left[\frac{h^2}{2m^*}\{(\vec{q}+\vec{q}')^2 + 2\vec{k}\cdot(\vec{q}+\vec{q}')\} - hs(q+q')\right] \delta_{\vec{k}',\vec{k}+(\vec{q}+\vec{q}')} \tag{2—13}$$

$$P^{(2)}_{+-}(\vec{k}\vec{k}') = \frac{8\pi^3 h(Ze^2)^2}{M^2\Omega^2 s^2} \sum_{\vec{q},\,\vec{q}'} \frac{|\vec{q}+\vec{q}'|^4}{[(\vec{q}+\vec{q}')^2 + k^2_{TF}]^2} \frac{[N(q)+1]N(q')}{q\cdot q'} \times$$

$$\times\ \delta\left[\frac{h^2}{2m^*}\{(\vec{q}-\vec{q}')^2 - 2\vec{k}\cdot(\vec{q}-\vec{q}')^2\} + hs(q-q')\right]\delta_{\vec{k}',\vec{k}-(\vec{q}-\vec{q}')} \qquad (2-14)$$

where $N(q) \equiv N_{q,L} = [\exp(\beta hsq) - 1]^{-1}$, and the summations $\sum_{\vec{q}}$ are efectuated inside the Debye spehere ($q \leqslant q_D$).

3. The electronic relaxation times associated with the 1-phonon and 2-phonons processes

We consider the high temperature limit ($T \gg \Theta_D$ where Θ_D is the Debye temperature) when $h\omega_D \equiv hsq_D \ll k_B T$ and the following approximations are valid :

1° $\varepsilon_{k'} - \varepsilon_k \ll k_B T$, thus the electron-phonon scatterings are quasi-elastic and the scattered electrons are in states near the Fermi level ($k \simeq k' \simeq k_F$).

2° $N(q) \simeq N(q) \pm 1 \simeq N(q) \pm 2 \simeq \dfrac{k_B T}{hsq}$.

3° $\dfrac{2ms}{hq_D} \simeq 10^{-3} \ll 1$ and $q_D \simeq k_F \cdot [2,4]$

In the case of quasi-elastic scatterings, the Boltzmann equation, which describe the transport processes, may be solved with the well-known relaxation time aproximation [2, 4]. If the electronic iso-energetic surfaces are spherical and the magnetic field is absent the relaxation time is [2, 4, 6] :

$$\frac{1}{\tau(\vec{k})} = \sum_{\vec{k}'} (1 - \cos\theta_{\vec{k},\vec{k}'})\, P(\vec{k},\vec{k}') \qquad (3-1)$$

where $\theta_{\vec{k}',\vec{k}}$, is the angle between electronic wave vectors $\vec{k}$ and $\vec{k}'$.

Using the decomposition of transition probabilities in 1-phononic terms $P(\vec{k},\vec{k}') = P^{(1)}(\vec{k},\vec{k}') + P^{(2)}(\vec{k}\vec{k})$ and the eq. (2—8, 2—14), we obtain :

$$\frac{1}{\tau(\vec{k})} = \frac{1}{\tau^{(1)}(\vec{k})} + \frac{1}{\tau^{(2)}(\vec{k})} \qquad (3-2)$$

where :

$$\frac{1}{\tau^{(1)}(\vec{k})} = \frac{1}{\tau^{(1)}_{+}(\vec{k})} + \frac{1}{\tau^{(1)}_{-}(\vec{k})} \qquad (3-3)$$

$$\frac{1}{\tau^{(2)}(\vec{k})} = \frac{1}{\tau^{(2)}_{2+}(\vec{k})} + \frac{1}{\tau^{(2)}_{2-}(\vec{k})} + \frac{1}{\tau^{(2)}_{++}(\vec{k})} + \frac{1}{\tau^{(2)}_{--}(\vec{k})} + \frac{1}{\tau^{(2)}_{+-}(\vec{k})} \qquad (3-4)$$

a) The relaxation times associated with the 1—phonon processes.

Transforming the sums into the integrals : $\sum_{\vec{k}'} f_{\vec{k}'} \rightarrow \frac{\Omega}{(2\pi)^3} \int_{R^3} d^3\vec{k}' f_{\vec{k}'}$ and using (2—27, 28) when $k' = \vec{k} \mp \vec{q}$ thus $\int_{R^3} d^3\vec{k}' f_{\vec{k}'} = \int_{(q<q_D)} d^3 \vec{q} f_{\vec{k} \pm \vec{q}}$ we obtain :

$$\frac{1}{\tau_{\pm}^{(1)}(\vec{k})} = \frac{\Omega}{2\pi^3} \int_{(q<q_D)} d^3\vec{q} \, (1 - \frac{\vec{k}\cdot(\vec{k} \mp \vec{q})}{k|\vec{k} \mp \vec{q}|} \frac{32\pi^3 m^* N}{\Omega^2 h^3} \frac{k_B T}{Ms^2} (Ze^2)^2 \times$$

$$\times \frac{1}{(q^2 + k_{TF}^2)^2} \delta\left[q^2 \mp 2\vec{k}\cdot\vec{q} \mp \frac{2m^* s}{h} q\right] \qquad (3—5)$$

The integrals are effectuated in spherical coordinates with the polar axis parallel with $\vec{k}$ and after the angular integrations we obtain :

$$\frac{1}{\tau_{\mp}^{(1)}(\vec{k})} = \frac{4\pi m^*(Ze^2)^2}{\Omega_0 h^3 k} \frac{k_B T}{Ms^2} \int_0^{q_D} \frac{1}{(q^2 + k_{TF}^2)^2} \left[1 - \frac{2k^2 \mp \frac{2ms}{h} q - q^2}{2k\, k^2 \mp \frac{2ms}{h} q}\right] \times$$

$$\times \theta(\mp \frac{2ms}{h} - 2k \leqslant q \leqslant \mp \frac{2ms}{h} + 2k \qquad (3—6)$$

where : $\Omega_0 = \frac{\Omega}{N}$ (the volume of elementary cell)

$$\theta(a \leqslant x \leqslant b) = \begin{cases} = 1 \text{ if } x \in [a,b] \\ = 0 \text{ if } x \in [a,b]. \end{cases}$$

Introducing the adimensional variables $\eta = \frac{q}{q_D}$, $\alpha = \frac{k_{TF}}{2q_D}$ and using the approximations $k \simeq k_F \simeq q_D$, $\frac{2ms}{hq_D} \simeq 0$ we obtain :

$$\frac{1}{\tau_{\mp}^{(1)}(k)} = \frac{2\pi m^*(Ze^2)^2}{\Omega_0 h^3 k_F^3} \frac{k_B T}{Ms^2} \int_0^1 d\eta \frac{\eta^3}{(\eta^2 + 4\alpha^2)^2} \qquad (3—7)$$

and the total relaxation time associated with the 1—phonon processes for $k \simeq k_F$ is;

$$\frac{1}{\tau^{(1)}(k_F)} = \frac{4m^*(Ze^2)^2}{3\pi h^3} \frac{k_B T}{Ms^2} N(2\alpha) \qquad (3—8)$$

where :

$$N(\alpha) \equiv \int_0^1 d\eta \frac{\eta^3}{(\eta^2 + \alpha^2)} = \frac{1}{2}\left[\ln\left(1 + \frac{1}{\alpha^2}\right) - \frac{1}{1+\alpha^2}\right] \qquad (3—9)$$

$$k_F = (3\pi^2 n)^{1/3} = \left(\frac{3\pi^2}{\Omega_0}\right)^{1/3} \quad [1,2]$$

b) The relaxation times associated with the 2—phonons processes $\tau_{2\pm}^{(3)}$ (k) is calculated analogous with the 1—phonon relaxation times and the result is

$$\frac{1}{\tau_{2\pm}^{(2)}(k_F)} = \frac{m^* (ze^2)^2}{3\pi h^3} \left(\frac{k_B T}{Ms^2}\right)^2 N(\alpha) \tag{3—10}$$

but an inspection of the expressions of the transition probabilities in the high temperature limit (2.29—30) reveals that $\tau_{\pm}^{(2)}$ (k) are automatically included in $\tau_{++}^{(2)}$ and $\tau_{--}^{(2)}$ if we relaxe the restriction $q \neq q'$ in the expressions for $\tau_{\pm\pm}^{(2)}$. Therefore the relaxation times associated with 2—phonons (identical or different) in the high temperature limit are :

$$\frac{1}{\tau_{\pm}^{(2)}(k)} = \frac{1}{\tau_{2\pm}^{(2)}(k)} + \frac{1}{\tau_{\pm\pm}^{(2)}(k)} = \frac{m^*(Ze^2)^2}{8\pi^3 h^3} \left(\frac{k_B T}{Ms^2}\right)^2 \int_{(q \leq q_D)} d^3\vec{q} \times$$

$$\int_{(q' \leq q_D)} d^3\vec{q} \, \frac{1}{q^2 q'^2} \left[1 - \frac{k^2 \mp \vec{k}\cdot(\vec{q} + \vec{q}')}{k\,|\vec{k} \mp (\vec{q} + \vec{q}')|} \frac{(\vec{q} + \vec{q}')^4}{[(\vec{q} + \vec{q}')^2 + k_{TF}^2]^2} \delta\,[2\vec{k}\cdot(\vec{q} + \vec{q}') \mp \right.$$

$$\left. \mp (\vec{q} + \vec{q}')^2 - \frac{2m^* s}{h}(q + q') \right] \tag{3—11}$$

We introduce $\vec{P} = \vec{q} + \vec{q}'$ and $\tau_{\pm}^{(2)}$ become :

$$\frac{1}{\tau_{\pm}^{(2)}(k)} = \frac{m^*(Ze^2)^2}{8\pi^3 h^3} \left(\frac{k_B T}{Ms^2}\right)^2 \int_{R^3} d^3P \, \frac{P^4}{(P^2 + k_{TF}^2)^2} \times$$

$$\times \left[1 - \frac{k^2 \pm \vec{k}\cdot\vec{P}}{\sqrt{k^2 + P^2 \mp 2\vec{k}\cdot\vec{P}}} \right] I_{\pm}\left(P, k, \frac{2m^* s}{h}\right) \tag{3—12}$$

where :

$$J_{\pm}\left(P; k, \frac{2m^* s}{h}\right) = \int_{(q \leq q_D)} d^3q \, \frac{\theta\left(q_D - \sqrt{P^2 + q^2 - 2\vec{P}\cdot\vec{q}}\right)}{q^2(P^2 + q^2 - 2\vec{P}\cdot\vec{q})} \times$$

$$\times \left[\delta\, 2\vec{k}\cdot\vec{P} \mp P^2 - \frac{2m^* s}{h}\left(q + \sqrt{P^2 + q^2 - 2\vec{P}\cdot\vec{q}}\right) \right] \tag{3—13}$$

We choose the polar axis parallely to $\vec{P}$ and after effectuating the angular integrations $J_{\pm}$ is reduced at the form :

$$J_{\pm}\left(\vec{P}; k, \frac{2m^* s}{h}\right) = \frac{2\pi}{P} \frac{h}{2m^* s} \int_0^{q_D} dq \, \frac{1}{q\left[\frac{h}{2m^* s}(2\vec{k}\cdot\vec{P} \mp P^2) - q\right]} \times$$

$$\times\, \theta\left[q_D - \frac{h}{2m^* s}(2\vec{k}\cdot\vec{P} \mp P^2) \right] \theta\left[|\vec{P} - \vec{q}| \leqslant \frac{h}{2m^* s}(2\vec{k}\cdot\vec{P} \mp \vec{P}^2) \leq P + q \right] \tag{3—14}$$

We introduce $Q_{\pm} \equiv \frac{h}{2ms}(2\vec{k}\vec{P} \mp P^2)$, and observing that the Heaviside's functions have the only effect to limit the integration domain, we obtain:

$$J_{\pm}\left(\overline{P}; k, \frac{2ms}{h}\right) \equiv I_{\pm}(P,Q) = \frac{2\pi}{P}\frac{h}{2m^{*}s}\int_{q_m^{(\pm)}}^{q_n^{(\pm)}} \frac{dq}{q(Q_{\pm}-q)} =$$

$$= \frac{h}{2m^{*}s}\frac{2\pi}{Q\cdot P_{\pm}}\ln\left|\frac{q_M^{(\pm)}}{q_m^{(\pm)}}\frac{q_m^{(\pm)}-Q_{\pm}}{q_M^{(\pm)}-Q_{\pm}}\right|$$

The analysis of the integration domains lead to the result :

$$= \frac{h}{2m^{*}s}\frac{4}{PQ_{\pm}}\ln\left|\frac{Q_{\pm}+P}{Q_{\pm}-P}\right| \quad \text{if } 0 \leqslant P \leqslant Q_{\pm} \leqslant q_D \quad \text{or } 0 \leqslant P \leqslant 2q_D - Q_{\pm}$$

$$J_{\pm}(P,Q_{\pm}) = \frac{h}{2m^{*}s}\frac{4}{PQ_{\pm}}\ln\left|\frac{q_D}{Q_{\pm}-q_D}\right| \quad \text{if } q_D \leqslant P \leqslant Q_{\pm} \leqslant 2q_D \quad \text{or} \qquad (3\text{—}16)$$

$$2q_D - Q_{\pm} \leqslant P \leqslant q_D \text{ and } q_D \leqslant Q_{\pm} \leqslant 2q_D$$

$$= 0 \text{ in rest}$$

We introduce $J_{\pm}$ in eq. (3—12), making the change of variables in the integral after the polar angle $\theta_k = \frac{P_z}{P}$ to the integration after Q, and with the following adimensional quantities :

$$\eta = \frac{P}{2q_D}, \quad \varphi = \frac{Q}{2q_D}, \quad \alpha = \frac{k_{TF}}{2q_D}, \quad \upsilon = \frac{m^{*}s}{hq_D} \quad \text{we obtain :}$$

$$\frac{1}{\tau_{\pm}^{(2)}(k_F)} = \frac{m^{*}(Ze^2)^2}{2\pi h^3 k_F}\left(\frac{k_B T}{Ms^2}\right)^2 2q_D \int_0^{\infty} d\eta \frac{\eta^4}{(\eta^2+\alpha^2)^2} \times$$

$$\times \int_{-\frac{1}{\upsilon}\left(\frac{k_F}{q_D}\eta \mp \eta^2\right)}^{\frac{1}{\upsilon}\left(\frac{k_F}{q_D}\eta \mp \eta^2\right)} \frac{d\varphi}{\varphi}\left[1 - \frac{2\frac{k^2}{4q_D^2} - \eta^2 \mp \upsilon\varphi}{\frac{k}{q_D}\sqrt{\frac{k^2}{4q_D^2} \mp \upsilon\varphi}}\right] F(\eta,\varphi)\,\theta(0 \leqslant \eta \leqslant \varphi \leqslant 1) \qquad (3\text{—}17)$$

where :

$$F(\eta,\varphi) = \begin{cases} = \ln\left|\dfrac{\varphi+\eta}{\varphi-\eta}\right| & \text{if } 0 \leqslant \eta \leqslant \varphi \leqslant 0{\cdot}5 \text{ or } 0 \leqslant \eta \leqslant 1-\varphi \text{ and } 0{\cdot}5 \leqslant \varphi \leqslant 1 \\ = -\ln|2\varphi - 1| & \text{if } 0{\cdot}5\eta \leqslant \varphi \leqslant 1 \text{ or } 1-\varphi \leqslant \eta \leqslant 0{\cdot}5 \text{ and } 0{\cdot}5 \leqslant \varphi \leqslant 1 \end{cases} \qquad (3\text{—}18)$$

Considering in the conditions of the above aproximations $k \simeq k_F \simeq q_D$ and $\nu << 1$, the relaxation times become :

$$\frac{1}{\tau_{\pm}^{(2)}(k_F)} = \frac{4m^*(Ze^2)^2}{\pi h^3}\left(\frac{k_B T}{Ms^2}\right)^2 M_1(\alpha) \qquad (3\text{—}19)$$

where :

$$M_1(\alpha) = \int_0^1 d\eta \frac{\eta^6}{(\eta^2+\alpha^2)^2} L_1(\eta) \qquad (3\text{—}20)$$

$$L_1(\eta) = \begin{cases} = \int_{\eta}^{1-\eta} \frac{d\varphi}{\varphi} \ln\frac{\varphi+\eta}{\varphi-\eta} - \int_{1-\eta}^{1} \frac{d\varphi}{\varphi} \ln(2\varphi-1) \text{ if } 0\leqslant\eta\leqslant 0.5 \\ = -\int_{2}^{1} \frac{d\varphi}{\varphi} \ln(2\varphi-1) \qquad \text{if } 0.5\leqslant\eta\leqslant 1 \end{cases} \qquad (3\text{—}21)$$

The relaxation time $\tau_{+-}^{(2)}(k)$ calculated in a similar manner with $\tau_{\pm}^{(2)}(k)$and we obtain

$$\frac{1}{\tau_{+,-}^{(2)}(k_F)} = \frac{8m^*(Ze^2)^2}{\pi h^3}\left(\frac{k_B T}{Ms^2}\right)^2 M_2(\alpha) \qquad (3\text{—}22)$$

where :

$$M^2(\alpha) = \int_0^1 d\eta \frac{\eta^6}{(\eta^2+\alpha^2)^2} L_2(\eta) \qquad (3\text{—}23)$$

$$L_2(\eta) = \begin{cases} = \int_0^{\eta} \frac{d\varphi}{\varphi} \ln\left[(1-2\varphi)\frac{\eta+\varphi}{\eta-\varphi}\right] \text{ if } 0\leqslant\eta\leqslant 0.5 \\ = \int_0^{1-\eta} \frac{d\varphi}{\varphi} \ln\left[(1-2\varphi)\frac{\eta+\varphi}{\eta-\varphi}\right] \text{ if } 0.5\leqslant\eta\leqslant 1 \end{cases} \qquad (3\text{—}24)$$

Combining the preceding results (eq. 3—19) and 3—22), we obtain the total relaxation time associated with the 2—phonons processes (in the high temperature limit) :

$$\frac{1}{\tau^{(2)}(k_F)} \simeq \frac{8m^*(Ze^2)^2}{\pi h_3}\left(\frac{k_B T}{Ms^2}\right)^2 M(\alpha)$$

where :

$$(\alpha) = \int_0^1 d\eta \frac{\eta^6}{(\eta^6+\alpha^2)^2} L(\eta)$$

$$L(\eta) = \begin{cases} \int_{\eta}^{1-\eta} \frac{d\varphi}{\varphi} \ln\frac{\varphi+\eta}{\varphi-\eta} \int_{1-\eta}^{1} \frac{d\varphi}{\varphi} \ln(2\varphi-1) + \int_0^{\eta} \frac{d\varphi}{\varphi} \ln\left[(1-2\varphi)\frac{\eta+\varphi}{\eta-\varphi}\right] \text{ if } \eta\leqslant 0.5 \\ -\int_{\eta}^{1} \frac{d\varphi}{\varphi} \ln(2\varphi-1) + \int_0^{1-\eta} \frac{d\varphi}{\varphi} \ln\left[(1-2\varphi)\frac{\eta+\varphi}{\eta-\varphi}\right] \text{ if } \eta\leqslant 0.5 \end{cases} \qquad (3\text{—}25)$$

4. **Conclusions**

The present expressions of 2—phonons relaxation time contain integrals which cannot be expressed by a finit number of elementary functions, therefore it can obtain only approximate values using numerical analysis, The evaluation of the contribution of the 2—phonons processes in the transport phaenomena will be reported in future [10]. We remark that our method correct some analogues results [9], evidentiating the transition probabilities (and the relaxation times) associated with the emission and the absorbtion of 2 identical phonons, which can be absorbed in the analogous quantities associated with 2 different phonons, only in the high temperature limit.

1. KITTEL, C., *Quantum Theory of Solids,* John Willey and Sons, Inc. NY-London (1963)
2. ZIMAN M. I., *Principles of Solid State Physics,* Cambridge, 1964.
3. HARRISON W. A., *Solid State Theory,* McGraw Hill, 1970.
4. PINES D., *Elementary Excitations in Solids,* Benjamin, 1963.
5. BORN M., HUANG K., *Dynamical Theory of Crystal Lattices,* Oxford, 1954.
6. CALLAWAY J., *Quantum Theory of the Solid State,* Academic Press, 1974.
7. FEITER A. L., WALLECKE J. D., *Quantum Theory of Many Particle Systems,* McGraw Hill, New York, 1971.
8. MOHAN G. D., *Many Particle Physics,* Plenum Publishing Co., 1981.
9. NATTA M., Journal de Physique, *29,* 1019, 1968.
10. LUNGU R. P., CIUCU C., PLAVITU C., Rev. Roum. Phys., (to be published)

ANALELE UNIVERSITĂȚII BUCUREȘTI, FIZICĂ, XXXIV, 1985, PAG. 69—73

STUDY OF RUMANIAN RUBBER CAROM IN WORKING CONDITIONS OF BEARING PACKINGS TYPE RS

LIVIA MARIA IONESCU
Faculty of Physics, Bucharest University *

MARIANA CIOAREC
Bearings Factory, Alexandria

Abstract. **In order to get bearing packings type RS and 2RS, utilization of some mixtures with Rumanian rubber CAROM as substitute of imported BUTACRYL BT 308, was proposed.**

Complex analysis of mechanical behaviour for samples of vulcanizated rubber and for various components in specific conditions of utilization permite to indicate Rumanian product as better one, in different climate conditions.

Introduction

In order to take more advantage of all raw materials of our country, the BUTACRYL BT 308 rubber was replaced with a Rumanian mixture of CAROM rubber for the manufacture of bearing packings type RS and 2RS.

Rumanian rubber CAROM (made in Borzești) is a butadiene-acrylonitrile copolymer sulphur vulcanizate, or by other means of vulcanization.

Butadiene-acrylonitrile copolymers

First of all we have to point out that butadiene-acrylonitrile copolymers are special rubbers (nitrile rubbers), new materials with modern and intresting practical utilizations /1, 2/. Such rubbers are known for their high resistance at mineral and vegetable oils, at abrasion, at warm air and a reduce permeaebility for gases, between working temperatures of various components (—30°C and +100°C). This resistance is dependent on acrylonitrile content which is between 18 and 45%.

Another specific feature of these copolymers is done by the necessity of adding a great number of ingredients in order to get the wares. Usually such ingredients are: fillers, plasticizers, vulcanization, protecting, swelling, fireproofing and treating agents. Such a system with all these ingredients is a mixture.

Usually a mixture has at least ten supplementary ingredients with a weight comparable to the elastomer weight. A good choise of the mixture and of its constituents, taking in account the conditions of manu-

---

* National Center of Physics, P.O. Box 5211, Bucharest—Măgurele, Romania.

facture of wares and their properties, is necessary in order to improve the techniques of rubber processing /3, 4/.

Structural analysis, relaxation mechanism of the strength /5/, dielectric properties and their influence in swelling conditions /6/ for some mixtures with butadiene-acrylonitrile rubber are known also.

Bearing packings type RS and 2RS

The rubber used in order to get bearing packings type RS and 2RS has in its composition nitrile medium NBR-CAROM with an acrylonitrile content of 31.80%.

Packings are made from mixture rubber-metal fittings ; the brazing of the rubber on the metal is realized by vulcanization at high temperature in matrix.

In order to get a good and uniform adhesion of the rubbr on the metal fittings, we have to prepare adequately both the surfaces of the rubber and of the metal fittings.

Technical conditions imposed for packings include the rubber mixture utilized and the system rubber-metal fittings equally.

Experimental

A complex analysis on mechanical behaviour of samples prepared from CAROM rubber and of wares in specific working conditions was made.

Analysis of samples from CAROM rubber

Basic physico-mechanical features as : Mooney visozity, pre-vulcanization time, specific weight, sulphur dispersion, Shore hardness, breaking tension, tensile strenght /7/ were comparatively studied for Rumanian rubber and for imported BUTACRYL 308, in air and normal temperature conditions (20°C$\pm$2°).

The losses in ageing conditions (oxidation in oven at 100°C, during 70 hours) and after mineral oils immersion (ASTM 1, ASTM 3) of the Shore hardness, tensile strength and breaking tension are determinated also. The conclusion is : the BUTACRYL BT 308 rubber is not resistant at the oxidation in oven (the test-pieces are broken and can not be tested). Tensile strenght and breaking tension are done as relative values (%) using initial values (before ageing and oil immersion) as references. For example, tensile strenght after oxidation in oven T_0 is done by relation :

$$T_0 = R_{T_0} - 100$$

R_{T_0} being the ratio between tensile strength after ageing and before ageing. Also breaking tension after ageins is :

$$E_0 = R_{E_0} - 100$$

R_{E_0} being the ratio between breaking tension after ageing and before ageing.

The data from such experiments and other specific parameters values as remanent compresion at constant deformation (in ageing conditions in oven) and change of volume at mineral oils immersion are listed in table 1, and they are in good agrement with the Strandards /8, 9/.

The Rumanian rubber CAROM is more resistant at ageing and specially at various fluids action, the decrease of its physico-mechanical properties being less important in comparison with imported rubber. This is definitely a great advantage.

Table 1

Parameter/units	Standard limit values	Effective values CAROM	Effective values BUTACRYL BT 308
Mooney viscozity (U.M.)	22—35	28	
Pre-vulcanization time (min)	4— 8	4	
Specific weight (g.cm^{-3})	1.25± 0.02	1.23	1.21
Sulphur dispersion	good	good	good
A. In air at 20°C ± 2°			
Shore hardness (°Sh)	60± 3	60	59
Tensile strength (daN.cm^{-2})	min. 125	195	173
Breaking tension (%)	min. 350	405	400
B. Oxidation in oven (100°C, 70 h)			
Shore hardness (°Sh)	min. ±15	22	
Tensile strength (%)	max. —20	— 19	
Breaking tension (%)	max. —50	— 43	
Compresion (%)	max. +35	33	
C. ASTM 1 oil immersion (100°C, 70 h)			
Shore hardness (°Sh)	max. — 5 — +40	12	— 15
Tensile strength (%)	max. —20	7.9	— 13
Breaking tension	max. —50	— 10	— 43
Volume (%)	max. —10 — + 5	— 9	
D. ASTM 3 oil immersion (100°C, 70 h)			
Shore hardness (°Sh)	max. —10 — + 5	5	— 7
Breaking tension (%)	max. —35	11.2	— 10
Tensile strength (%)	max. —40	4.7	— 21
Volume (%)	max. 0 —25	3	

Teasting of bearing packings type RS and 2RS

In a second stage the testing of wares — bearing packings type RS and 2RS — was made in specific working conditions.

The data obtained for percentage weight variation of packings after immersion in various mineral oils and greases (protecting fluid UP 7, CASTROL grease, ASTM 1 oil, ASTM 3 oil) at 100°C ± 2° during 70 hours and White Spirit at 20C° ± 2° during 22 hours, are listed in table 2. These data are average values for three samples, from two different lots : 6205 and 6206. All values are in good agreement with the Standards /9, 10/.

Table 2

Lot	22 hours 20°C ± 2° WHITE SPIRIT		UP 7		CASTROL		ASTM 1		ASTM 3	
	Our data	Standard values	Our data	Standard values	Our data	Standard values	Our data	Standard values	Our data	Standard values
6205	0.77	—5—+5	—0.02	—10—+5	0.44	0—15	—1.51	—10—+5	1.28	0—0;25
6206	0.92		—7.02		0.93		—3.05		1.03	

In order to find the capacity of packings to maintain protecting grease in various conditions of utilization, the grease loss in time was studied. The packings are tested on the test-stand in simulated working conditions of wares (maximum load, working time).

The weight of grease maintained in packing is ploted as a function of time (during 80 hours) for three samples, from two different lots : 6205 (fig. 1) and 6206 (fig. 2).

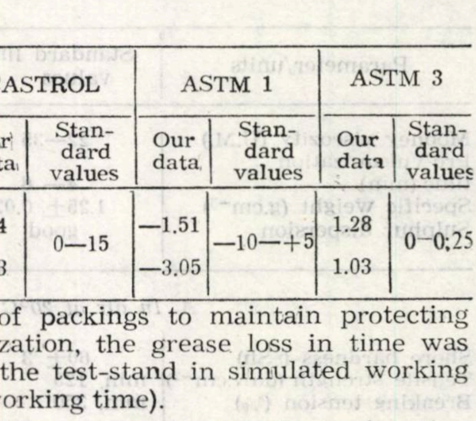

Fig. 1. **Weight of grease maintained by three bearing packings type 2RS from the lot 6205 as a function of time. ● : packing 1 ; 0 : packing 2 ; × : packing 3. Average percentage loss of grease after 80 hours : 15%.**

Average values of percentage grease losses after 80 hours calculated for the packings from the two lots : 6205 and 6206 are 15% and 19% respectively.

All these data indicate a good behaviour of peckings ; they keep the grease in good conditions time enough (80 hours), average working time imposed for such bearing packings being 40—50 hours.

Determinations of detachment strength of rubber from metal and of fatigue resistance in different medium and temperature conditions (in air, protecting fluid UP 7, CASTROL grease at 100°C±2°, during 70 hours) show a good behaviour of packings in working conditions ; the rubber does not easily comme of from the metal fittings.

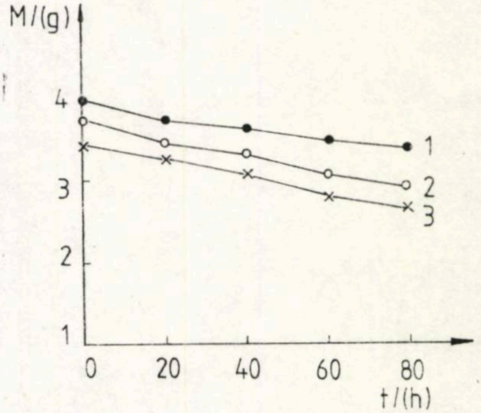

Fig. 2. Weight of grease maintained by three bearing packings type 2RS from the lot 6206 as a function of time. ● : packing 1 ; 0 : packing 2 ; × : packing 3. Average percentage loss of grease after 80 hours : 19%.

Conclusions

Our results are a justification of using Rumanian rubber CAROM for bearing packings without a chemical supplementary protection in temperature climate, warm-humid and warm-dry.

REFERENCES

1. I. PETREA, L. M. IONESCU, *Fizica elastomerilor. Reologie*, E.D.P., București, 1981.
2. J. CURCHOD, *Les élastomères*, in *Propriétés physiques des polymères. Mise en oeuvre*, G.F.P. Ed., Strasbourg, 1981.
3. C. WIPPLER, *Mise en oeuvre des matières plastiques*, in *Propriétés physiques des polymères. Mise en oeuvre*, G.F.P. Ed., Strasbourg, 1981.
4. F. R. EIRICH, *Science and Technology of Rubber*, Academic Press Inc., 1978.
5. M. COJOCARU, I. PETREA, C. A. STĂNESCU, Anal. Univ. București, Fizică, XXVII, 29, 1978.
6. M. COJOCARU, L. M. IONESCU, I. PETREA, C. A. STĂNESCU, Anal. Univ. București, Fizică, XXXI, 71, 1982.
7. L. M. IONESCU, I. PETREA, M. CIOAREC, Communication in 29 th International Symposium on Macromolecules IUPAC-MACRO '83, Bucharest.
8. S. TURNER, *Mechanical Testing of Plastics*, Published for the Plastics Institute. London, ILIFFE Books.
9. A. WEILL, *Normes et eessais, in Propriétés physiques des polymères. Mise en oeuvre*, G.F.P. Ed., Strasbourg, 1981.
10. * * * Anual Book of ASTM Standards, part 27-Plastics-General Methods of testing-Nomenclature-American Society of Testing and Materials, Philadelphia.

ANALELE UNIVERSITĂȚII BUCUREȘTI, FIZICĂ, XXXIV, 1985, PAG. 75—79

SUR LA FLEXIBILITÉ DES CHAINES MACROMOLÉCULAIRES DANS DES COPOLYMERES METHACRYLIQUES AVEC DES GROUPES LATERAUX LONGS

M. COJOCARU, LIVIA MARIA IONESCU

Faculté de Physique, Uinversité de Bucarest *

Résumé. La flexibilité thermodynamique des chaînes macromoléculaires de certains copolymères statistiques appartenant à la série des méthacrylates est étudiée à partir des résultats obtenus par des méthodes optiques et hydrodynamiques. Après des comparaisons avec d'autres composés macromoléculaires de la même série, les auteurs arrivent à la conclusion que la distribution statistique des radicaux n-lauryle et n-cétyle le long des chaînes macromoléculaires du copolymère ne change pas sensiblement la fléxibilité des chaînes.

1. Introduction

Parmi les nombreuses études concernant les copolymères en solutions diluées /1—5/, celles qui s'occupent des copolymères statistiques de la série des méthacrylates avec des groupes latéraux longs sont assez rares, bien que cette catégorie des composés macromoléculaires soit intéressante par ses applications pratiques /6—8/. Ce travail a pour but de mettre en évidence, pour deux copolymères de la série des méthacrylates, l'influence des groupes latéraux longs sur la flexibilité thermodynamique de la chaîne macromoléculaire principale.

2. Technique expérimentale. Echantillons

Nous avons étudié deux copolymères statistiques (F 20 et F 22) obtenus par la copolymérisation du n-méthacrylate de lauryle et n-méthacrylate de cétyle. L'homogénéité en composition des deux copolimères étant la même, la copolymère F 20 est différent du F 22 par la masse moléculaire, ainsi que par d'autres paramètres (tableaux 1 et 2). L'indice de polymolécularité $I = \overline{M}_w / \overline{M}_{SD}$ inférieur à 1,3 et les fonctions de dis-

Tableau 1

Résultats obtenus par diffusion de la lumière, en benzène, à 20°C.

	$[\eta]$ $(dl \cdot g^{-1})$	$A_2 \cdot 10^4$	$\overline{M}_w \cdot 10^{-5}$	$\frac{A_2 M}{[\eta]}$	$(\overline{h^2})^{1/2}$ **(Å)**	a	$(\overline{h^2_\Theta})^{1/2}$ **(Å)**	$\left(\frac{\overline{h^2_\Theta}}{M}\right)^{1/2} \cdot 10^8$	$\left(\frac{\overline{h^2_\Theta}}{\overline{h^2_f}}\right)^{1/2}$
F 20	0.56	0,94	**4,3**	0,72	480	0,72	**400**	**0,61**	**2,4**
F 22	0,60	0,79	**5,1**	0,67	530	0,76	**430**	**0,60**	**2,4**

---

* Centre National de Physique, Măgurele—Bucarest, B.P. 5211, Romania.

Tableau 2

Résultats obtenus par ultracentrifugation de sédimentation en hexane-heptane 1 : 1, à 20°C.

	$[\eta]$ $(dl \cdot g^{-1})$	$S_0 \cdot 10^{13}$	$D_0 \cdot 10^7$	$(\overline{h^2})^{1/2}$ (Å)	$\overline{M}_{SD} \cdot 10^{-5}$	$\alpha = \left(\frac{\overline{h^2}}{\overline{h^2_\Theta}}\right)^{1/2}$	$\frac{\overline{M}_w}{\overline{M}_{SD}}$
F 20	0,26	**10,4**	**2,3**	**350**	**3,6**	1,21	**1,20**
F 22	0,28	**11,1**	1,6	**380**	**4,0**	**1,22**	**1,27**

tribution d'après la constante de sédimentation présentées dans les figures 1 et 2, suggérent une bonne homogénéité d'après la masse moléculaire.

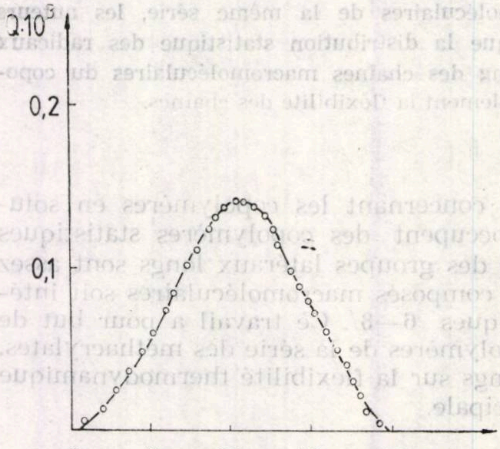

Fig. 1 — La fonction de distribution d'après la constante de sédimentation, pour le copolymère F 20, 3700 s après la réalisation de la vitesse de régime et pour une concentration c = 0,4 g/dl.

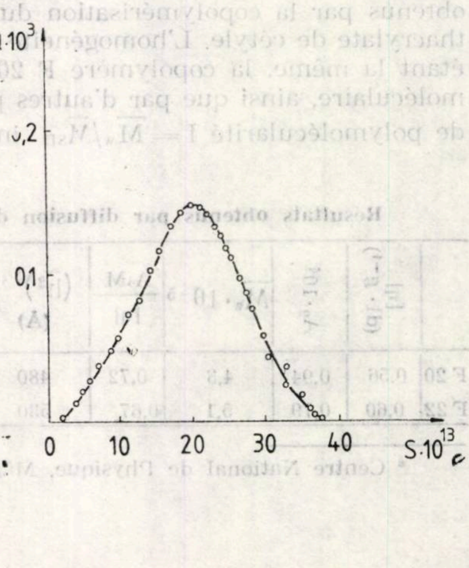

Fig. 2 — La fonction de distribution d'après la constante de sédimentation, pour le copolymère F 22, 3700 s après la réalisation de la vitesse de régime et pour une concentration c = 0,5 g/dl.

3. **Résultats et discussions**

Dans le tableau 1 sont présentés les résultats obtenus à partir de la théorie thermodynamique de Flory pour les solutions macromoléculaires /9/, ainsi que l'exposant a de la loi viscosimétrique de Mark—Kuhn—Houwink ($[\eta] = K\,M^a$) évalué par une méthode proposé par Loucheux, Weill, Benoît /10/. La valeur élevée de l'exposant a ainsi calculée (0,72 dans le cas du F 20 et 0,76 dans le cas du F 22) peut être expliquée soit par la rigidité élevée des copolymères en discution, soit par la perméabilité hydrodynamique partielle de la pelote statistique par rapport au solvant respectif /11/.

La flexibilité thermodynamique de la chaîne macromoléculaire peut être exprimée par le rapport

$$\left(\frac{\overline{h^2_\Theta}}{\overline{h^2_f}}\right)^{1/2} \tag{1}$$

où $(\overline{h^2_\Theta})^{1/2}$ représente les dimensions statistiques de la pelote en solvant Θ et $(\overline{h^2_f})^{1/2}$ — les dimensions statistiques de la pelote dans l'hypothèse de la rotation libre autour des liaisons simples du type C—C, aussi bien que par le rapport équivalent

$$\left(\frac{\overline{h^2_\Theta}}{M}\right)^{1/2} \tag{1'}$$

Les mesures de l'intensité de la lumière diffusée par les solutions en benzène des copolymères F 20 et F 22 nous ont permis d'obtenir directement les dimensions $(\overline{h^2})^{1/2}$ et la masse moléculaire $\overline{M}_w$.

Par l'intermède des relations /9, 12/ :

$$A_2 = \frac{2^{5/2}\pi N_A}{3^3\varphi}\cdot\frac{[\eta]}{M}\cdot\ln\left[1+\frac{\sqrt{\pi}}{2}(\alpha^2-1)\right] \tag{2}$$

et

$$\left(\frac{\overline{h^2}}{\overline{h^2_\Theta}}\right)^{1/2} = \alpha \tag{3}$$

nous avons passé des dimensions $(\overline{h^2})^{1/2}$ aux dimensions $(\overline{h^2_\Theta})^{1/2}$.

Les paramètres A_2, $\overline{h^2}$, $\overline{M}_w$ et $[\eta]$ ont été obtenus par des mesures directes effectuées sur des solutions diluées des copolymères F 20 et F 22 en benzène.

Les valeurs du coefficient de gonflement α et les dimension $(\overline{h^2_\Theta})^{1/2}$ sont présentées aussi dans les tableaux 1 et 2.

La valeur du rapport $(\overline{h^2_\Theta}/M)^{1/2}$ calculée à l'aide de $(\overline{h^2})^{1/2}$ et de $\overline{M}_w$ est égale à $0{,}6 \cdot 10^{-8}$. Eskin et Nesterov /13/ ont trouvé pour polypropylènesulfide, polymère aux chaînes flexibles, $(\overline{h^2_\Theta}/M)^{1/2} = 0{,}60 \cdot 10^{-8}$, la même valeur que celle calculée pour le polyméthacrylate de cétyle en utilisant les données de la littérature /14/.

La flexibilité de la chaîne peut être exprimée encore par la relation :

$$(\overline{h_f^2})^{1/2} = 0,256\sqrt{M} \quad (\text{Å}) \tag{4}$$

vérifiée pour les polymères de la série des polyméthacrylates /9, 15/.

Avec $(\overline{h_\Theta^2})^{1/2}$ donné par la relation (3) et $(\overline{h_f^2})^{1/2}$ donné par la relation (4), nous avons calculé pour les deux copolymères étudiés :

$$\left(\frac{\overline{h_\Theta^2}}{\overline{h_f^2}}\right)^{1/2} = 2,4 \tag{5}$$

Nous avons déjà montré que la valeur élevée de l'exposant a de l'équation de Mark—Kuhn—Houwink (voir le tableau 1), pourrait être expliquée par la perméabilité hydrodynamique partielle des pelotes statistiques des copolymères étudiés.

D'après les théories connues /12, 16/, la propriété de perméabilité ou d'imperméabilité hydrodynamique des pelotes macromoléculaires est valable seulement lorsqu'il s'agit des solvants bons du point de vue thermodynamique et peut être caractérisée par le rapport

$$\frac{A_2 M}{[\eta]} \tag{6}$$

Dans le cas des suspensions sphériques, qui peuvent être comparées aux pelotes statistiques complètement imperméables, le rapport (6) a la valeur 1,6, tandis que pour de nombreux polymères statistiques de masse moléculaire élevée ($M > 10^4$) dissous en bons solvents, les expériences montrent que le même rapport (6) a des valeurs comprises entre 1,1 et 1,4.

Le benzène, le solvent dans lequel ont été étudiés les copolymères F 20 et F 22 par diffusion de la lumière, est un solvant bon par rapport à ces composés macromoléculaires. Dans ces conditions. si on prend en compte que le rapport (6) doit diminuer jusqu'à zero lorsqu'on s'approche du point Θ indépendamment de la perméabilité hydrodynamique de la pelote /11/, il est indiqué de penser à une flexibilité un peu diminuée de la chaîne, plutôt qu'à la perméabilité hydrodynamique partielle des pelotes macromoléculaires étudiées.

Les copolymères que nous avons étudiés sont statistiques à cause de la distribution au hasard des radicaux n-lauryle et n-cétyle sur une chaîne de la série des méthacrystales. Dans ces conditions, une comparaison entre la flexibilité de la chaîne des copolymères étudiés et la flexibilité de la chaîne des autres polymères avec des groupes latéraux n-alkyle de longueurs différentes et appartenant à la série des méthacrylates est tout à fait permise. En effet, si on examine les données du tableau 3, on peut observer que la rigidité de la chaîne augmente lorsque la longueur du radical latéral n-alkyle augmente.

Dans ce contexte des faits, une liaison entre la valeur élevée de l'exposant a de la loi viscosimétrique et la flexibilité de chaîne diminuée dans le cas des copolymères F 20 et F 22, parait tout à fait justifiée.

La flexibilité des chaînes macromoléculaires en fonction de la longueur du radical latéral n-alkyle /11, 17, 18/.

Tableau 3

Polymère	$\left(\frac{\overline{h^2_\Theta}}{\overline{h^2_f}}\right)^{1/2}$	$A \cdot 10^8$ (cm) (segment statistique de Kuhn)
Polyméthacrylate de méthyle	1,8	15
Polyméthacrylate de butyle	2,1	17
Polyméthacrylate d'octyle	2,3	20
Polyméthacrylate de lauryle	2,85	31

REFERENCES

1. D. FROELICH, H. BENOIT, Makromol. Chem., *92*, 240 (1966).
2. H. BENOIT, P. REMPP, A. DONDOS, J. Polym. Sci. B, *4*, 293 (1966).
3. L. M. IONESCU, Rev. Roum. Phys., T. 24, *1*, 81 (1979).
4. L. M. IONESCU, C. PICOT, R. DUPLESSIX, M. DUVAL, H. BENOIT, J. P. LINGELSER, Y. GALLOT, J. Polym. Sci : Polym. Phys Ed., *19*, 1033, (1981).
5. L. M. IONESCU, I. C. PETREA, I. IONESCU-BUJOR, I. DEMETRESCU, Makromol. Chem. *184*, 1005 (1983).
6. I. I. BORISOVA, L. L. BURSTEIN, Visokomol. Soed., *10*, 2106 (1972).
7. E. A. BEKTUROV, R. E. LEGKUNETZ, Visokomol. Soed., *12*, 626 (1970).
8. E. T. SRINIVASAN, M. SANTOPA, Makromol. Chem., *27*, 61 (1958).
9. P. J. FLORY, *Principles of Polymer Chemistry*, Cornell Univ. Press, Ithaca, New York (1953).
10. C. LOUCHEUX, G. WEILL, H. BENOIT, J. Chim. Phys., 55, 540 (1958).
11. V. N. TZVETKOV, V. E. ESKIN, S. I. FRENKEL, *Strunktura makromolekul v rastvorah*, Izdvo. Nauka, Moskva (1964).
12. T. OROFINO, P. J. FLORY, J. Chem. Phys., *26*, 1067 (1957).
13. V. E. ESKIN, A. E. NESTEROV, Visokomol. Soed., *1*, 141 (1966).
14. V. N. TZVETKOV. D. HARDY, I. N. STENIKOVA, E. V. KORNEEVA, G. F. PIROGOVA, K. NITRAY, Visokomol. Soed., *2*, 349 (1969).
15. M. V. VOLKENSTEIN, *Configurational Statistics of Polymers*, John Wiley (1972).
16. A. S. ALBRECHT, J. Chem. Phys., *27*, 1002 (1957).
17. S. CHINAI, R. RESNIK, H. LEE, J. Polym. Sci., *33*, 471 (1958).
18. H. LEE, D. LEVI, J. Polym. Sci., *47*, 449 (1960).

ANALELE UNIVERSITĂŢII BUCUREŞTI, FIZICĂ, XXXIV, 1985, PAG. 81—86

INFLUENCE DE LA MASE MOLECULAIRE SUR LA CINETIQUE DE CRISTALLISATION ISOTHERME DU POLYETHYLENE

E. BARNA, LIVIA MARIA IONESCU

Faculté de Physique, Université de Bucarest *

Résumé. Le cinétique de la cristallisation isotherme du polyéthylène a été étudiée par microscopie optique, dépolarisation de la lumière et diffusion de la lumière aux petits angles, dans l'intervalle de températures 100—110°C. En dessous de 100°C les mesures cinétiques deviennent pratiquement impossibles à cause des vitesses de germination et de croissance élevées. Les mesures ont été effectuées sur des fractions de polyéthylène indigène de masse moléculaire M_v située dans le domaine 10^4—10^5, en obtenant un maximum de la vitesse de croissance en fonction de la masse moléculaire. La valeur non entière de „l'exeposant d'Avrami" n ainsi obtenue est expliquée par la superposition de deux mécanismes de germination et de croissance.

1. **Introduction**

Un grand nombre de propriétés des technopolymères sont dépendentes non seulement du pourcentage de la phase cristalline, mais encore de la morphologie des formations cristallines se formant pendant le processus de cristallisation à partir de l'état surfondu. Le polyéthylène indigène est un tel polymère ; les études de la cinétique de cristallisation ont eu pour but de déterminer la vitesse de cristallisation isotherme, les mécanismes de germination et de croissance, ainsi que l'effet de certains paramètres sur le processus de cristallisation.

Les résultats obtenus ont été interprétés à l'aide de l'équation d'Avrami :

$$1 - \Theta = \exp\,(-kt^n) \tag{1}$$

dans laquelle Θ est le degré de cristallinité au temps t, k une constante qui dépend de la géométrie de croissance et du type de germination, n un nombre entier dont la valeur dépend du mécanisme de germination et de la forme de croissance du cristal (fibrille, disque, sphérolite) /1/.

La masse moléculaire joue un rôle important dans le processus de cristallisation. Dans cet article, continuant l'étude du polyéthylène indigène /2—6/, les auteurs vérifient l'aplicabilité de l'équation d'Avrami pour des fractions de polyéthylène de masse moléculaire M_v comprise entre 10^4 et 10^5, mettant en évidence la dépendence des paramètres k et n de la masse moléculaire.

La température de cristallisation et le temps de fusion ont été choisis de telle manière, que l'effet de l'histoire thermique du processus de cristallisation soit éliminé, ce qui a fait possibles des mesures dans des conditions de surrefroidissement programmé.

---

* Centre National de Physique, Măgurele, Bucarest, B.P. 5211, Roumanie.

2. Technique expérimentale. Echantillons

Les expériences ont été effectuées sur cinq fractions de polyéthylène indigène de masse moléculaire M_v comprise dans l'intervalle 10^4—10^5 : P_1 — 80 000, P_2 — 120 000, P_3 180 000, P_4— 230 000, P_5 — 280 000, la polydispersité d'après la masse moléculaire de ces fractions n'étant pas connue.

Le processus de cristallisation dans des films de polyéthylène ayant une épaisseur comprise entre 10^{-2} et 1 mm, a été suivi par microscopie optique, diffusion de la lumière aux petits angles et dépolarisation de la lumière.

Le temps de fusion a été de 5 minutes, et la température dépassait de quelques degrés la temperature de fusion T (en fonction de la masse moléculaire), en prenant soin d'éivter la dégradation tehrmique de l'échantillon.

Etant donné qu'aucune modification de la vitesse de croissance n'a pas été observée lorsque la température ou le temps de traitement augmentaient, nous avons considéré que dans tous les cas, la cristallisation se produit à partir de l'état surfondu, en conditions d'équilibre.

Afin d'éliminer les tensions thermiques, le température de cristallisation T_c a été atteinte par l'intermède d'une température suffisamment élevée pour qu'elle ne permet pas l'amorçage du processus de cristallisation.

3. Résultats et discussions

Tout d'abord nous avons étudié la variation du temps après lequel le système est amené à la température de cristallisation en fonction de l'intervalle de refroidissement ΔT (fig. 1). Cette dépendence élimine la majorité des erreurs sur le temps d'induction t_0.

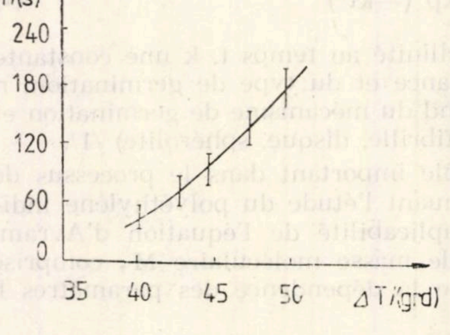

Fig. 1. Le temps t après lequel le système est amené à la température de cristallisation en fonction de l'intervalle de refroidissement ΔT.

Les résultats de dépolarisation de la lumière ont été analysés d'après la méthode de Magill /7/, en suivant la variation de la lumière transmise normalisée en fonction du temps :

$$\frac{I_c - I_t}{I_c - I_0} = f\ (\ln t) \qquad (2)$$

où I_0 et I_c représentent respectivement les intensités initiale et finale, et I_t l'intensité transmise au moment t. Si le rapport normalisé est Θ, alors n peut être obtenu directement à l'aide de la courbe :

$$\ln(-\ln \Theta) = f\ (t) \qquad (3)$$

La méthode peut être appliquée, avec de bons résultats, seulement pour des systèmes capables de croissance sphérolitique et dans lesquels on admet une dépendence linéaire entre la biréfringence et le volume de la phase cristalline /8/.

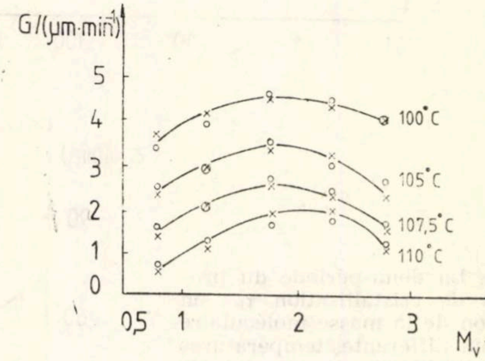

Fig. 2. La vitesse de croissance isotherme libre des sphérolites G en fonction de la masse moléculaire M_v pour les fractions P_1, P_2, P_3, P_4, P_5 : × microscopie optique ; ○ diffusion de la lumière aux petits angles.

Dans la figure 2 est représentée la variation de la vitesse de croissance des formations sphérolitiques G en fonction de la masse moléculaire M_v. On observe un maximum de la vitesse de croissance (vitesse déterminée pour un processus isotherme), d'autant plus accentué que la température de cristallisation est plus élevée. Ces résultats sont confirmés et par des mesures de diffusion de la lumière aux petits angles /6/.

Par contre, la vitesse de croissance des sphérolites, mesurée en croissance isotherme, pour beaucoup d'autres polymères tels que : poly (tétraméthyl-p-silphénylène)-xyloxane, poly(succinate d'éthylène), poly (téréphtalate d'éthylène), diminue lorsque la masse moléculaire augmente, sur tout le domaine en question /9/. Tous ces polymères ont des vitesses de cristallisation beaucoup plus basses que le polyéthylène (pour un ΔT équivalent, leur vitesse de croissance est environ 100 fois plus petite).

Dans la figure 3 sont présentés les résultats de dépolarisation de la lumière, en mentionnant en même temps les valeurs obtenues pour n. Dans ce cas, t inclue et la correction pour le temps d'induction.

On peut remarquer le changement de pente de n=4 à n=3, lorsque le diamètre des sphérolites s'approche de l'épaisseur des échantillons, pour des valeurs élevée de la tempèrature de cristallisation, ce qui indique une modification des mécanismes de germination et de croissance.

Dans la figure 4 est présentée la dépendence du $\tau_{1/2}$ (la demipériode du processus de cristallisation) de la masse moléculaire et de la tempé-

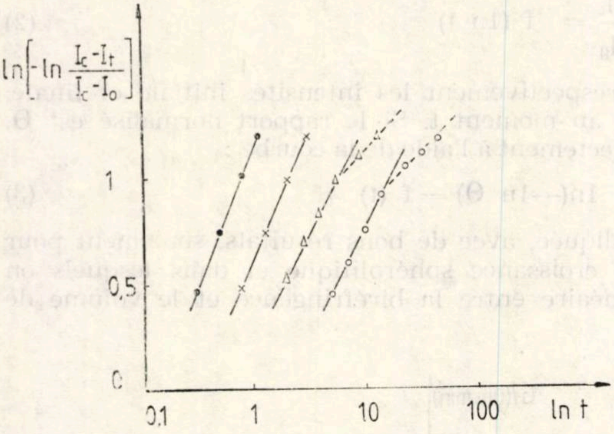

Fig. 3. Diagrammes de cristallisation obtenus par dépolarisation de la lumière pour le polyéthylène (échantillon P_3) : ● $T_c = 100°C$, $n = 3{,}9 \pm 0{,}1$; × $T_c = 105°C$, $n = 3{,}9 \pm 0{,}1$; Δ $T_c = 107{,}5°C$, $n = 3{,}8 \pm 0{,}1$, ... $n = 3{,}2 \pm 0{,}1$; ∘ $T_c = = 110°C$, $n = 4{,}0 \pm 0{,}1$, ... $n = 3{,}1 \pm 01$.

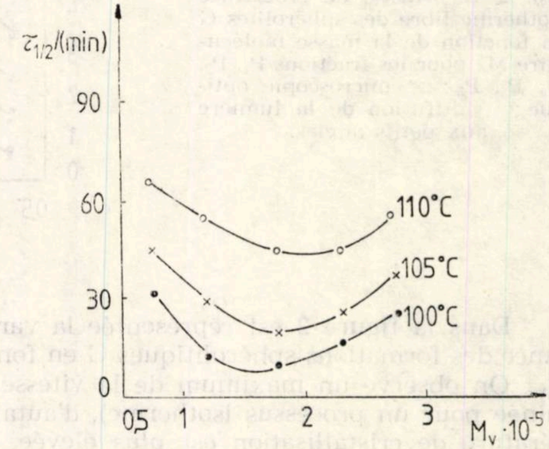

Fig. 4. La demi-période du processus de cristallisation $\tau_{1/2}$ en fonction de la masse moléculaire M_v pour différentes températures de cristallisation : ● 100°C ; × 105°C ; ∘ 110°C.

rature de cristallisation. On voit le déplacement du minimum vers des valeurs basses de la masse moléculaire, lorsque la température de cristallisation diminue, ainsi qu'un minimum plus accentué aux températures de cristallisation T_c élevées.

Les variations de la constante k de l'équation d'Avrami en fonction de la température de cristallisation et de la masse moléculaire sont données dans la figure 5.

La variation de l'exposant n avec l'épaisseur de l'échantillon montre l'existence d'un seuil entre la croissance tridimensionnelle et celle bidimensionnelle, ainsi qu'un changement des mécanismes de germination, seuil qui est pratiquement indépendent de la masse moléculaire, mais dépendent du temps de cristallisation. Le phénomène a été mis en évidence sur des épaisseurs en dessous de 50 μm cristallisés aux températures supérieures à 105°C. Le changement des mécanismes de germination et de croissance doit être atribué plutôt à la capacité de l'échantillon de changer la chaleur dans cette géomètrie et à la possibilité de rejéction des impurités par les fronts de croissance dans les zones intercristallines, qu'aux dimensions de cet échantillon. Il est probable que ce processus détermine l'augmentation de l'intervalle ΔT par l'augmentation simultanée de la température de fusion T_f, ce qui permet d'obtenir une configuration dense des formations cristallines et une plus grande résistance par rapport aux conditions de fusion.

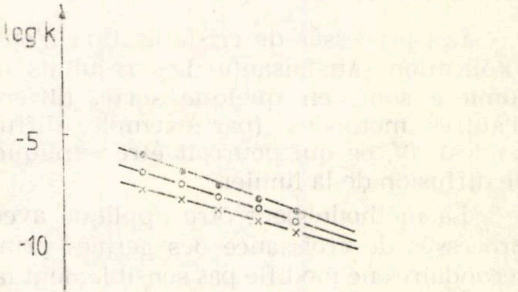

Fig. 5. L'influence de la température de cristallisation T_c sur la constante k (équation d'Avrami): × P_1 ; o P_3 ; ● P_5.

Les données représentées dans la figure 6 confirment ce changement des mécanismes de germination et de croissance.

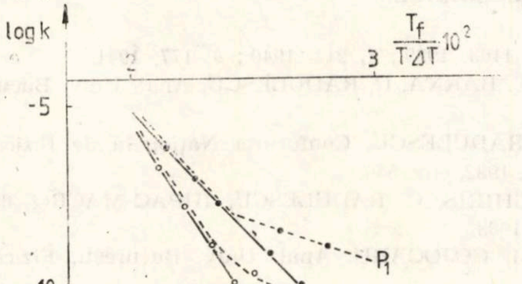

Fig. 6. Le changement du mécanisme de germination pour deux échantillons :
● P_1 (épaisseur de l'échantillon 40 μm) ; o P_4 (épaisseur de l'échantillon 50μm).
— $T_f / T_c \cdot \Delta T$; …… $T_f^2 / T(\Delta T)^2$.

D'après la théorie /10/, la relation entre la vitesse de cristallisation et la température doit être linéaire. Pour des croissances pendant la cristallisation secondaire-bidimensionnelle, la dépendence :

$$\log k = f\left(\frac{T_f}{T_c \cdot \Delta T}\right) \tag{4}$$

doit être linéaire ; la croissance tridimensionnelle des germes secondaires doit donner aussi une dépendence linéaire :

$$\log k = f\left(\frac{T_f^2}{T(\Delta T)^2}\right) \tag{5}$$

Cela permet, en même temps, d'expliquer les valeurs expérimentales non entières de l'exposant d'Avrami n, soit par les processus simultanés, ou succesifs de cristallisation, ayant des mécanismes différents (germination homogène, ou hétérogène), soit par la superposition des effets de cristallisation primaire et secondaire.

4. Conclusions

Les processus de cristallisation n'ont pas trouvé jusqu'à présent une explication satisfaisante. Les résultats obtenus par dépolarisation de la lumière sont, en quelque sorte, différents des résultats obtenus par d'autres méthodes (par exemple, diffusion de la lumière aux petits angles) /6/, ce qui pourrait être expliqué par l'apparition du phénomène de diffusion de la lumière.

La méthode peut être appliqué avec de bons résultats à l'étude du processus de croissance des germes primaires ; la croissance des germes secondaires ne modifie pas sensiblement la biréfringence.

La cristallisation isotherme peut être décrite par une équation du type Avrami à l'exposant non entier pour la croissance sphérolitiques, si on admet l'apparition des systèmes contenant des régions avec des possibilités différentes de cristallisation.

REFERENCES

1. M. AVRAMI, J. Chem. Phys., 7, 1103, 1939 ; *8*, 212 ,1940 ; *9*, 177, 1941.
2. I. C. PETREA, L. M. IONESCU, E. BARNA, C. RĂDULESCU, Anal. Univ. București, Fizică, XXX, 35, 1981.
3. I. C. PETREA, E. BARNA, C. RĂDULESCU, Conferința Națională de Fizică, București, 21—23 octombrie, 1982, pag. 556.
4. I. C. PETREA, E. BARNA, S. CHIRIS, C. RĂDULESCU, IUPAC-MACRO '83, Bucharest, september 5—9, 1983.
5. E. BARNA, L. M. IONESCU, M. COJOCARU, Anal. Univ. București, Fizică, XXXIII, 71, 1984.
6. L. M. IONESCU, E. BARNA, Colocviul Național de Optică, Ed. a III-a, București, 14—15 iunie, 1984.
7. J. H. MAGILL, Polymer, *2*, 221, 1961.
8. F. L. BINSNBERGEN, J. Macromol. Sci. (B), *4*, 837, 1970.
9. B. WUNDERLICH, *Macromolecular Physics*, vol. 2, Academic Press, Ney York, 1976.
10. L. MANDELKERN, *Crystallisation of Polymers*, McGrow-Hill, New York, 1964.

ANALELE UNIVERSITĂŢII BUCUREŞTI, FIZICĂ, XXXIV, 1985, PAG. 87—94

CORRELATION BETWEEN THE INDOOR ADN THE OUTDOOR PARTICLE CONCENTRATION

ELENA DECU, ŞT. LASCU, SAEED BAFAYAD [**]

Faculty of Physics, Bucharest University [*]

Abstract. The outdoor and indoor data collected in Bucharest on the Măgurele Platform over the interval 1976—1977 and 1983 reveal that the indoor particle concentration at various levels is greater than the outdoor one. Our studies point out that reduction of the indoor particle concentration does not necessarily accompany height reduction, unlike the outdoor particle concentration which decrease, as highlighted by measurements from as high as 42 m altitude. The ratio between the indoor and the outdoor concentration is variable and dependent, among other factors, on the season in which the measurements are performed.

In Bucharest the polluting particle concentration almost doubled over the 1971—1978 period while on the Măgurele Platform it was approximately 1.5 times bigger in 1983 as compared with 1976.

1. Introduction

Atmospheric pollution has been variously defined, still the definition suggested by the Comission of the European Council for the Prevention and Control of Pollution, in February 1967, seems to us the most comprehensive of all /1/. The definition reveals that the highest levels of pollution are to be encountered about the plants and the great industrial complexes, in this case the pollution being either simple or complex; however, high levels are also registered in towns where, given the innumerable and various polluting sources, pollution always has a complex character. Besides, other elements may turn polluting. such as a normal atmospheric component which at a certain moment exceeds a given concentration limit or any other component which appears in the atmosphere beyond its normal limits within an area.

The study of atmospheric pollution has been constantly tackled in many papers, a large number being due to collectives of Romanian researches /11, 12, 13, 14/; most of the papers point to the noxious effects of the various types of polluting agents, contributing further information for the study of many other such effects, insufficiently examined before. We consider the conclusions of some of our previous papers as relevant in this respect, all the more so as the conclusions were based on the study of the solid aerosol concentrations in the outdoor atmosphere as evidenced by the measurements performed over the interval

---

[*] National Center of Physics, Măgurele — Bucharest, P.O. Box MG—11, R—76900, Romania.

[**] On leave from the Physics Department, University of Aden, D.P.R. Yemen.

1970—1980 in Bucharest, Braşov and on the Măgurele Platform, the results being interpreted by means of analytical and graphical methods /2, 5, 8, 9, 10/ as well as by statistical methods /2, 3, 4, 5, 7/.

2. Working method and material employed

Most of the pollution studies bearing on particle concentration were carried out in the outdoor atmosphere. Still, on the average, man spends some 80% of his time indoor and the effects of pollution are even more consequential to the persons spending more than 80% of their life-time indoor.

That is why we have examined particle concentration and generation in the indoor atmosphere as well as particle penetration from the outside into the buildings. In the present paper we attempted the establishment of certain correlations between the concentrations of the outdoor particles polluting the indoor atmosphere. The identifications will be treated in a future paper.

The level of indoor pollution is expressed in percentages in relation to the outdoor level (indoor concentration / outdoor concentration X 100). This ratio has been widely used for it affords a better definition of indoor pollution as a function of outdoor pollution. The identification of the correlations between indoor and outdoor pollution could facilitate the estimation of the indoor levels on the basis of the data relevant for outdoor pollution which are by far more numerous.

The concentration measurements were carried out in 1976, 1977 and 1983 in a building on the Măgurele Platform situated at 50 m from the nearest road ; the building consisted of a semi-basement, ground floor, first floor, second floor and open terrace (terrace I had $h = 12$ m). The determination of the concentrations (particles/cm^3) of the particles having a wide dimensional spectrum was achieved by the simultaneous employment of two apparatus /2, 10/ : the Scholz meter for Aitken nuclei, C_A, (0.01—0.1μ) for the great and huge ones, C_G, (0.1—5μ) an impactor represented by the Zeiss Conimeter. In view of the fact that in the distribution log r — number the maximum value C_A for Aitken particles was obtained for a radius of 0.03μ in our determinations with the Scholz meter we took into account this maximum concentration with a radius of 0.05μ.

While performing the measurements of the particle concentrations we also measured the meteorological parameters both inside and outside; as concerns the indoor activity we made various observations bearing on the operation of the installations, the people working in the lab cleaming conditions a.c.

The radio soundings performed at the Mogoşoaia — Bucharest Aerological Observatory were employed in the outdoor studies.

In 1976 measurements were made both in a semi-basement lab and outside the building (near the respective lab) at the height of 2 m. The measurements of 1976 were performed one day per week and, in addition, one representative week per season, hour by hour. Thus daily, monthly, seasonly, and yearly mean values were obtained. Starting with June 1977 in a ground floor room a space was separtted by means of plastic walls ; in this restricted area particle filters were mounted both in the window and the ceiling ; the space thus separated became a „clean room". The filters placed in the „clean room" influenced also the quality of the air in the rest of the lab (denominated „lab" in the references contained in this paper) ; filters were also mounted in a recess in the lab wall, Under these indoor circumstances the determinations were made at the respective hours almost simultaneously in the lab, the clean room and the recess.

În 1977 the measurements were made a representative week per season as follows :

— outdoor : at ground level, at the height of 2 m terrace I, at the height of 12 m.

— indoor : semi-basement groung floor — lab, clean room, recess first floor, second floor.

In order to offer an accurate image of the evolution of pollution in time the measurements were resumed in 1983, the results concerning the correlation between indoor and outdoor pollution depending mostly on the measurements performed in 1976, 1977 and on the methodology worked out in /10/. The measurements made in 1983 were meant to highlight the evolution rate of pollution : the concentration of polluting particles on the Măgurele Platform is approximately 1.5 times larger than the one registered in 1976.

3. **Correlations between the indoor and the outdoor particle concentration**

When determining these correlations we took into account only the measurements performed in 1976 on the Măgurele Platform. that is almost 212 individual measurements for each category of particles: Aitken nuclei, large and huge nuclei having the concentrations C_A and $C_G = C_1 + C_3 + C_5$ /10/, respectively.

The results of the studies are presented synthetically in Table 1, by means of the monthly, seasonly, and yearly mean values.

Conclusions

The analysis of the Aitken nuclei points out the following : — with no exception all the monthly and seasonly mean values reveal higher concentrations indoor than outdoor. If the monthly mean values are considered, the ratio indoor / outdoor appears to vary between 109% and 306% ; 8 cases are below 200% and 4 cases above 200%. In cold seasons the indoor / outdoor ratio is high (in winter 189% and in autumn 261%) while in warm seasons is much smaller (in summer 121% and in spring 143%).

— the great variation of the indoor / outdoor ratio, reaching values even over 200%, leads to the conclusion that the outdoor concentrations and man's presence and indoor activities which are permanent and persistent sources for such particles have an equally important role.

The analysis of the large and huge nuclei highlights the following :

— indoor concentrations are greater than outdoor concentrations, although the variations are quite reduced. As concerns the indoor / outdoor ratio for the monthly mean values of the three categories of particles the following data are relevant :

Table 1

Locality and room type	Month, season or year	CONCENTRATION (particles/cm³)														
		INDOOR					OUTDOOR					INDOOR/OUTDOOR %				
		C_A	C_G	C_1	C_3	C_5	C_A	C_G	C_1	C_3	C_5	C_A	C_G	C_1	C_3	C_5
the Măgurele Platform lab	I	34,896	292	253	36	3	26,309	253	218	32	3	132	115	116	112	100
	II	98,669	288	223	52	13	36,803	269	213	43	13	268	107	104	120	100
	III	47,136	203	129	53	21	28,581	289	215	62	12	168	70	60	85	175
	IV	42,020	258	180	66	12	30,567	187	149	29	9	137	137	121	227	133
	V	44,652	313	253	46	14	34,182	257	203	44	10	131	122	125	105	140
	VI	42,143	209	188	15	6	38,792	253	228	18	7	109	83	82	83	86
	VII	27,733	265	234	25	6	17,173	266	234	26	6	161	99	100	96	100
	VIII	34,000	506	432	66	8	29,950	508	434	65	9	136	99	99	101	88
	IX	61,200	474	417	50	7	20,000	466	412	48	6	306	102	101	104	117
	X	47,897	377	316	47		23,097	388	330	48	10	201	97	96	98	140
	XI	38,632	306	271	26	9	13,300	288	248	28	12	290	106	109		75
	XII	33,422	412	350	47	15	24,935	417	354	45	18	134	99	99	104	83
	winter	55,672	330	275	45	10	29,349	312	261	40	11	189	106	105	113	100
	spring	44,603	282	212	55	15	31,110	244	189	45	10	143	116	112	122	91
		34,625	326	284	35	7	28,638	341	298	36	7	121	95	95	91	150
	autumn	49,243	385	334	41	10	18,799	380	330	41	9		101	101	100	111
	1976	46,050	331	276	47	11	29,630	303	254	39	10	155	109	109	113	110

(0.1—1μ), with values ranging between 60% (minimum value) and 125% (maximum value) ; 6 cases $\leqslant$ 100% and 6 cases $>$ 100% ;

(1—3μ), with values : 83% minimum and 127% maximum ; 5 cases $<$ 100% and 7 cases $>$ 100% ;

(3—5μ), with values : 75% minimum and 175% maximum ; 7 cases $\leqslant$ 100% ;

— with all the large and huge particles C_1, C_3, C_5 there is no difference between the indoor and the outdoor concentrations in the cold seasons (winter and autumn), the ratio being constantly around 100%. In summer the ratio is $<$100%, to reach even higher values in spring : 112%, 122% and 150% ;

— as regards large and huge particles, their indoor levels are totally dependent on outdoor changes ; the generation of such particles in the daily activities can have certain effects but they are generally short lived and, consequently they are not directly reflected in the daily variations of the indoor concentrations.

Natural ventilation which has an immediate influence on the outdoor concentrations also affects the concentration of the indoor particles. Table 1 reveals a seasonly decrease from summer time to winter of the indoor / outdoor ratio ; as natural ventilation is intenser in summer the / outdoor concentration is small and the ratio is high while in winter the situation is quite reverse (owing to thermal inversions the natural ventilation is reduced, the outdoor concentration is high and the ratio is small).

4. Indoor particle concentration at various levels, in relation with outdoor concentration

In order to afford a more detailed examination of the problem under discussion, in 1977 we employed five units for simultaneous measurements installated on the Măgurele Platform in one and the same building, as follows : outdoor at the ground level (h=2m) and on the first terrace (h=12 m) and indoor on the ground floor, the first floor, the second floor, and in winter and spring, in the semi-basement. The results are synthetically presented in table 2 by means of the seasonly mean values of the concentrations of the different-sized particles $\overline{C}_A, \overline{C}_G = \overline{C}_1 + \overline{C}_3 + \overline{C}_5$ for various indoor and outdoor levels. In June installations for air foltering were mounted in the ground floor lab.

Conclusions

The analysis of the seasonly mean values of the particle concentrations (table 2) for various indoor levels of the building (the ground floor with no filters) in winter and spring revealed wide variations from one level to the other. Theoretically, the pollution degree (mostly the particle concentration) decreases with height. However, this law is not observed to the letter inside buildings because of the internal sources of pollution which can be numerous and intenser at a higher level, depending on the human activity : production activity, smoking, outsweeping in the morning before performing the measurements, variable number of persons walking the corridors, introduction of external polluting agents by window-and door-opening, etc.

Table 2

Locality and year	Indoor or Outdoor	Position	Room type	Season	Concentration (particles/cm^3)				
					$\bar{C}_A$	$\bar{C}_G$	$\bar{C}_1$	$\bar{C}_3$	$\bar{C}_5$
1	2	3	4	5	6	7	8	9	10
the Măgurele Platform, 1977	Outdoor	ground level h = 2 m		winter	41,111	251	185	41	25
				spring	18,501	257	175	57	25
				summer	23,738	302	250	35	17
				autumn	47,411	257	169	45	43
	Indoor	semi-basement	Corridor	winter	38,080	275	231	25	19
				spring	42,823	328	185	90	53
	Indoor	ground floor	Corridor	winter	38,905	294	202	58	34
				spring	28,635	251	161	55	35
			Lab	summer	6,152	265	228	31	6
			Clean room	summer	2,492	164	148	14	2
			Recess	summer	4 059	236	201	31	4
			Lab	autumn	9,850	131	114	10	7
			Clean room	autumn	4,450	63	57	4	2
			Recess	autumn	5,700	81	75	3	3
		ground floor / ground level	Lab / ground level %	summer	26	88	91	89	35
			Clean room / ground level %	summer	10	54	59	40	11
			Recess / ground level %	summer	17	78	80	89	23
	Indoor / Outdoor	ground level / ground floor	Lab / ground level %	autumn	21	51	67	22	16
			Clean room / ground level %	autumn	9.4	24	33	8	4
			Recess / ground level %	autumn	12	32	44	6	7
	Indoor	1st floor	Corridor	winter	52,000	272	184	54	34
				spring	42,240	279	181	66	32
				summer	46,080	272	210	43	19
				autumn	65,926	248	165	45	38

Table 2 (continued)

1	2	3	4	5	6	7	8	9	10
the Măgurele Platform, 1977	Indoor	2nd floor	Lab	winter	63,641	283	206	48	29
				summer	34,285	289	182	74	33
				autumn	31,836	239	180	40	19
				spring	40,133	224	160	34	30
	Outdoor	1st terrace h = 12 m		winter	54 506	259	189	44	26
				spring	26,392	260	175	58	27
				summer	40,258	279	220	42	17
				autumn	34,400	224	153	38	33
	Indoor / Outdoor	1st floor / ground level %		winter	126	108	99	131	136
				spring	288		103	115	128
				summer	198	90	84	123	112
				autumn	139	96	97	100	88
	Indoor / Outdoor	2nd floor / ground level %		winter	155	113	111	117	116
				spring	185	112	104	130	132
				summer	134	79	72	114	111
				autumn	85	87	95	76	70
	Indoor / Indoor	2nd floor / 1st floor %		winter	123		112	89	85
				spring	81		100	112	103
				summer	69		86	94	100
				autumn	61		91	76	79
	Outdoor / Outdoor	1st terrace / ground level %		winter	132	103	101	107	290
				spring	142	101	100	101	220
				summer	170	111	90	120	271
				autumn	72	88	110	84	300
	Indoor / Indoor	2nd floor / semi-basement %, 1976		winter	167	103	89	192	152
				spring	80	88	98	82	
	Indoor / Indoor	2nd floor / ground floor %		winter	163	98	102	83	85
				spring	119	115	115	135	94
the Măgurele Platform 197	Indoor / Outdoor	ground floor / ground level %		winter	95	117	109	141	136
				spring	154	97	92	96	140
	Indoor / Outdoor	semi-basement / ground level %		winter	93	109	128	60	76
				spring	231	127	105	157	212

The indoor / indoor ratio, above all the ratio of 2nd floor / 1st floor, 2nd floor / semi-basement in 1977, 2nd floor / semi-basement im 1976 and 2nd floor / ground floor, in all 60 values, 35 cases $\leqslant 100\%$ and 25 cases $> 100\%$ points to a decreasing tendency of the concentration in parallel with the growing height of the indoor level, both with the Aitken particles and with the large and huge particles, this tendency being more marked in summer and autumn (most of the ratio values are smaller than 100%).

On account of the indoor / outdoor ratio, that is 2nd floor / ground level, 1st floor / ground level, ground floor / ground level, and semi-basement / ground level for which we obtained 60 values, 21 cases $\leqslant 100\%$ and 39 cases $> 100\%$, the values of the concentration inside the building at various levels appear to be greatert han the outdoor values.

The outdoor / outdoor ratio, namely 1st terrace / ground level, for which 20 values were available, 10 cases $\leqslant 101\%$ and 10 cases $> 101\%$, demonstrates that the measurements made in 1977 were too scanty to enable us to derive a variation law of the outdoor concentration of particles in relation to height. The measurements dit not suffice in point of number and the 1st terrace height ($h = 12$ m) was also not statisfactory. One could still notice a decrease of the large and huge particle concentration on the 1st terrace as compared to the ground level.

The measurements resumed in 1978, this time also on an outdoor terrace which was 42 m high, revealed that the outdoor particle concentration decreases with height /2/.

REFERENCES

1. CHOVIN P., ROUSSEL A., *Physicochimie et physiopathologie des polluants atmosphériques*, Masson et Cie. Éditeurs, 1973.
2. DECU ELENA, *Contribuţii la studiul componentei solide din aerosolul atmosferic*, Doctoral thesis, Univ. Buc., 1981.
3. DECU ELENA, LASCU ŞT., Anal. Univ. Buc., Fizică, XXVIII, 1979, 117—121.
4. DECU ELENA, LASCU ŞT., Anal. Univ. Buc., Fizică, XXXII, 1983, 91—94.
5. DECU ELENA, LASCU ŞT., DIACONU OTILIA, Anal. Univ. Buc., Fizică, XXXI, 1982, 97—102.
6. DECU ELENA, LASCU ŞT., EŞEANU D., Anal. Univ. Buc., Fizică, XXVII, 1978, 97—101.
7. DECU ELENA, LASCU ŞT., EŞEANU D., Rev. Roumaine de Géologie, Géophys., Géograph., série Géophys., Tome 27, 1983, 33—36.
8. DECU E., PĂSTÎRNAC A., LASCU ŞT., VIŞOIU D., Bul. Univ. Braşov, seria C, XIX, 1977, 105—109.
9. DECU E., PĂSTÎRNAC A., PASCU, ŞT., VIŞOIU D., Bul. Univ. Braşov, seria C, XIX, 1977, 111—116.
10. DECU ELENA, VIŞOIU D., SANDU I., Rev. Roumaine de Géologie, Géophys., Géograph., série Géophys., Tome 21, Nr. 2, 1977, 213—226.
11. DIACONU BH., FRIMESCU M., MOROIANU I., MOROIANU AL., *Culegere de lucrări de meteorologie*, Bucureşti, I.M.H., 1967.
12. ROMANOF N., ELEKES I., TUMANOV S., *Meteorology and Hydrology*, Bucureşti, I.M.H., 2, 1977.
13. TUMANOV S., MIHU D., *Meteorology and Hydrology*, Bucureşti, I.M.H., 2, 1975.
14. TUMANOV S., *Meteorology and Hydrology*, Bucureşti, I.M.H., 2, 1977.

ANALELE UNIVERSITĂȚII BUCUREȘTI, FIZICĂ, XXXIV, 1985, PAG. 95—99

NUMERICAL SIMULATION SCHEME OF THE CLOUD COALESCENCE PROCESS

SABINA ȘTEFAN, D. BORȘAN
University of Bucharest, Faculty of Physics *
IOLANDA OSVATH
Institute of Meteorology and Hydrology, Bucharest **

Abstract. The Gillespie algorithm, based on the Monte-Carlo method for simulating the stochastic coalescence process in a warm cloud is used. The scheme includes explicit coalescence kernel and a Khrgian-Mazin distribution function and allows the study of the evolution of droplet size spectra.

1. Introduction

The study of the development undergone by the dimensional cloud droplet spectrum in time is particularly important in establishing the moment and conditions for precipitations formation.

The mechanism of cloud droplet growth by stochastic coalescence proved significant in the formation of precipitations. Various techniques may be employed in modelling the coalescence process.

The authors made it their object to present in this paper a numecal simulation of the cloud droplet mass spectrum developing in time based on the Monte-Carlo method.

The Gillespie [Gi 75] algorithm was used for the stochastic model of cloud droplet coalescence starting from the following hypotheses :

— the cloud is homogeneous in space ;

— the cloud behaves as a dispersed aerosol so that the interactions of more than two droplets simultaneously are ignored.

The fundamental postulate on which the Gillespie algorithm is based assumes the existence of a function $C_{kl} \equiv C(X_k, X_l)$ called coalescence kernel which expresses the collision-coalescence probability depending on the X masses of the droplets.

The probability for the cloud droplets k and l to coalescence in the infinitesimal time interval $d\tau$ is expressed by means, C_{kl} through relation :

$$Q(X_k, X_l) = C_{kl}\, d\tau \tag{1}$$

Let a space homogeneous cloud of droplets developing in time consequence; to the collision-coalescence process. N will denote the number of droplets at moment t and X , the mass of droplet i (i = 1, 2, . . . N). The density of probability function of the coalescence process $Q(\tau, i, j)$ is defined by :

$$Q(\tau, i, j) = P(\tau, i, j)\, d\tau \tag{2}$$

where $Q(\tau, i, j)$ denotes the probability at time t for the folowing coalescence to take place in the time interval ($t + \tau$, $t + \tau + d\tau$) and to involve droplets i and j ($i < j$).

---

* Bucharest, Măgurele, P. O. Box 5211, Romania.

** I.M.H. București, Șoseaua București-Ploiești, 97.

Function $P(\tau, i, j)$ defined over the space of the constinuous variable τ and the discrete variables i and j stands for basis of Gillespie simultation algorithm and is inferred from the fundamental postulate (1).

The probability density for the coalescence process is considered a function of the following form [Gi 75 pg. 1979].

$$P(\tau, i, j) = C_{ij} \exp\left[-\sum_{k=1}^{N-1} \sum_{l=k+1}^{N} C_{kl}\tau\right]$$

for $\tau \in R$, $0 \leqslant \tau \leqslant \infty$, i, j N, $1 \leqslant i \leqslant j \leqslant N$ and is normalized over its domain of definition.

The schematic simulation algorithm of the time development undergone by the dimensional cloud droplet spectrum lies in the following steps :

Step 0 : The initial values are specified at moment $t=0$, for the mass of the N droplets : $X_1, X_2, ..., X_N$ and a set of $\frac{N(N-1)}{2}\{C_{kl}\}$ numbers are computed.

A series of moment $t_1 < t_2 < ..$, are specified with particular stress on the development stage of the cloud droplet mass spectrum and moment t-stop up to which the cloud model development is interesting.

Step 1 : By employing suitable Monte-Carlo technique, generate a random triplet (τ, i, j) according to the joint probability density function $P(\tau, i, j)$.

Step 2 : Using the values τ, i, j obtained in step 1, the time variable t is attached the new value $t + \tau$; the droplets i and j are withdrawn from the spectrum and a droplet having the mass $(X_j + X_i)$ is introduced the spectrum containing a droplet less at this moment. The droplets are again number and $\{C_{kl}\}$ is reconsidered.

Step 3 : If t became larger than t_i a frequency histogram is drawn as a function of the instantaneous values X_i at moment t_i or the characteristics studied for the mass distributio are assessed and represented. If $t \geqslant t_i$ — stop (or if there is only one drop let left) the computation is closed, otherwise, return to step 1.

A statistically completed-image of the coalescence process is accomplished by the repeated application of the algorithm to the same time material [0, t]. From the mass distribution of the droplets at moment t, the number of droplets may be determined **Nk (X, δx ; t)** as obtained in the k achievement of the coalescence process, with the mass traceable in the mass interval $[X, X + \delta X]$, at moment t, for any value of X and δX. If the algorithm was repeated of K times, the average number of droplets at moment t with the mass somewhat between X and $X + \delta X$ may be expressed as :

$$\bar{N}(X, \delta X ; t) = \frac{1}{K}\sum_{k=1}^{K} N_k(X ; \delta X ; t)$$

and the rms magnitude of the ± fluctuations which may reasonably be expected to occur about this average is :

$$\Delta(X, \delta X; t) \asymp \left\{ \frac{1}{K} \sum_{k=1}^{K} \left[N_k(X, \delta X; t) \right]^2 - \left[\frac{1}{K} \sum_{k=1}^{K} N_k(X, \delta X; t) \right]^2 \right\}^{1/2} \qquad (5)$$

$\overline{N}$ becomes an exact quantity while Δt tends to zero, when $K \to \infty$

Practically for any value of K situated between 3 and 10 [Gi 75] a complete image may be obtained over the droplet mass spectrum at moment t, t obe relied on in estimating any quantity associated to this spectrum.

2. Coalescence simulation programme using the Monte-Carlo method

The programme worked out is an implementation of the Monte-Carlo step using the partial-conditioning method [Gi 75].

This programme may be applied to any form of initial mass spectrum and of coalescence kernel achieving the simulation of any population of cloud droplets for which the stochastic model hypotheses are valid and for which the form of coalescence kernel is known.

Input data of the programme :

1. Initial mass spectrum of the cloud droplets included in a massive whole the dimension of which is given by the initial number of droplets.

If the spectrum may be described in analytical terms only the parameters required in spectrum determination are specified.

The programme computes initial mass spectra for population droplets with diameters are distributed according to Poisson and Khrgian-Mazin, having as initial data :

a) minimum diameter, maximum diameter, average diameter and the number of droplets for the Poisson distribution.

b) minimum diameter, maximum diameter, average, diameter and the amount of liquid water within the cloud. for the Khrgian-Mazin distribution.

2. The moments at which the instantaneous droplets mass spectrum is reprezented. These moments may be computed function of the time required in producing a coalescence and of the total number of drop lets so that significant reprezentations were obtained.

3. The diameter up to which the process is studied, possibly the lowest limit of the precipitating droplet diameters (100 μm). If, consequence to the coalescence processes, droplets of limit diameter occur in the spectrum represented for the moment in question and the computtion interpreted.

4. The time interval for which cloud development is of interest.

Programme running results in :

1. The analytical expression of distribution turned particular for the conditions specified by the input data.

2. The total amount of droplets computed when the initial distribution is of Khrgian-Mazin type).

3. The total droplet mass.

4. The droplet mass wtih a limit diameter.

5. The mass spectrum in rising order : the mass in grams of the droplets existing in the cloud at moment t.

6. The coalescence number, the total number of drop lets at moment t.

7. Table wit droplet distribution over mass ranges of 1ng length centered around full values of the mass at moment t.

8. The efficiency of partial conditioning ; for a greater efficiency C^* [Gi 75] was computed by relation $C^* = C[X(N), X(N-1)]$, the massive (X(V) having rising-ordered elements so that C^* is the upper limit of the set of values in the coalescence kernel for the $\frac{N(N-1)}{2}$ distinct pairs of droplets.

9. The random triplet produced.

10. The masses of droplets i, j involved in coalescence and the mass of the resulting droplet.

11. The mass spectrum at moment t : the hystogram showing the droplet number and the mass (in ng).

12. The dimensional spectrum at moment t : the hystogram showing the number of droplets and the diameter (in μm).

3. **Results obtained**

A. The program was tested by simulating the development of a cloud droplet population initially characterized by a symmetrical dimensional distribution and by a coalescence nucleus proportional to the sum of volumes. The Poisson distribution was employed ; the number of droplets having the diametetr D, $N_0(D) = NP(D)$ where N stands for the total number of droplets and $P(D) = \frac{D^{-D} e^{-\bar{D}}}{D!}$ denotes the Poisson probability density.

One hundred droplets were considered the diameters of which cover a range of values from 10 to 100 μm and an average diameter of 55 μm.

It was noticed that :

a) only 8 % of the number of droplets involved in the coalescence process have diameters below 50 μm which point to the fact that small droplets are hardly subject to coalescence. This characteristic of small droplets is accounted for by the hydrodynamic interaction mechanisms butailing cloud droplets and determining the shape of the coalescence kernel.

b) the spectrum evolves to a bimodal shape which agrees with the results obtained by numerical integration of SCE in similar conditions [A1 79b].

c) the time lapse between two coalescence instants is longer with the spectrum development towards larger sizes ; the development becomes slower in time.

B. Further on the gravitational coalescence process was simulated in a homogeneous space volume of 1 cm^3 belonging to a continental cloud of a stratus type, at the state resulting from the increase due to diffusion and vapour condensation into droplets considering an initial distribution of Khrgian-Mazin type.

The water content is $W_L = 1gm^{-3}$ and the spectrum acquires the form :

$$n(D) = AD^2 \exp(-BD) cm^{-3} cm^{-1}$$

where, n(D)dD is the number of droplets cm^{-3} having the diameter somewhat between D and (D + dD). Parameters A and B, the total number of droplets cm^{-3} as functions of the liquid water content W_L. water density ρ_w and the expressed in μm are given by [KP 78]

$$A \simeq 2{,}32 \cdot 10^{7} \frac{W_L}{\rho_W \overline{D}^{6}} \qquad \rho_W \text{ in } gcm^{-3}$$

$$B = \frac{3}{\overline{D}} \qquad W_L \text{ in } gm^{-3}$$

$$N = 8{,}56 \; 10^{5} \frac{W_L}{\rho_W \overline{D}^{3}} cm_{-}{}^{3} \qquad \overline{D} \text{ in } \mu m$$

The coalescence kernel given by Long's polynomial approximation [KP 78] was used.

The Khrgian-Mazin distribution is characterized by a value of the distribution average diameter $D = 20$ µm, including droplets of 10 to 30 µm.

The programme was run on an IBM 360 computer. The outcomes to the simulation of a single achievement of the coalescence process are the following :

1) The initial spectrum consisting in 143 droplets of Khrgian-Mazin distribution has the expression below :

$$n(D) = 0{,}362 \; D^2 \exp(-0{,}15 \; D) cm^{-3} cm^{-1}$$

and the total mass of the droplets $m = 0{,}618 \; 10^{-6}$ g.

2) The spectrum develops towards a bimodal shape which fully agrees with the observations and results obtained by SCE. This is accounted for, in terms of gravitational coalescence [AI 75 b], by the fact that in the very nature of the coalescence process, the small droplets are hardly involved which confers them a longer life-time.

This effect tends to preserve unaltered the distribution of the droplets within the range of small radius values while the medium and large size droplets, easily coalescing, grow rapidly leading to the formation of the two maxima observed. The coalescence process, therefore makes manifest for particles of over 40 µm diameter, only.

This tendency is much weaker with turbulent coalescence as the turbulent coalescence efficiency being less discriminating to the small droplets, all droplets take active part in the coalescence process.

3) The duration of cloud development up to the occurrence of precipitation drops, obtained by simulation, is one order of magnitude longer than the one observed in nature. This discrepancy is, to the authors, due to ignoring turbulence which favours coalescence processes in any real cloud.

Similarly, the hypothesis of space homogeneousness excluded the fluctuations in liquid water content.

4) The time required for a coalescence instant is longer with spectrum development ; the development becomes slower as the droplets get fewer although the value of the coalescence kernel is greater with greater droplet masses.

REFERENCES

AL 79a de ALMEIDA, F. C., Jour. Atmos. Sci., 1979, vol. 36, pag. 1534.

AL 79b de ALMEIDA, F. C., Jour. Atmos. Sci., 1979, vol. 36 pag. 1957.

GI 75 GILLESPIE D., Jour. Atmos. Sci., 1975, vol. 32, pag. 1977.

KP 78 KLETT J., PRUPPACHER H., *Microphysics of Cloud and Precipitation*. 1978.

L'académicien ȘERBAN ȚIȚEICA

(1908—1985)

Le 28 mai 1985, la science roumaine a souffert une grande perte par la mort du professeur Șerban Țițeica, physicien de haute réputation. Il est difficile de parler de notre professeur au passé cependant nous allons essayer de passer en revue les principales étapes de son activité prodigieuse, ainsi que ses accomplissements les plus importants.

Șerban Țițeica naquit à Bucarest, le 27 mars 1908, comme troisième enfant du professeur Gheorghe Țițeica, mathématicien illustre, et de Florica Țițeica (née Thierrin, d'origine suisse), musicienne distinguée, licenciée ès lettres.

Il fit ses études à Bucarest. Au lycée „Mihai Viteazul" il suivit les cours de physique du professeur Roman, grâce auxquels il acquit une bonne compréhension de la physique. Ensuite, il fut étudiant à la Faculté des Sciences de Bucarest, où il obtint en 1929 la licence ès Sciences physiques et chimiques, ainsi que la licence ès Sciences mathématiques, avec la mention „très bien". En même temps, il a fréquenté les cours de théorie, solfège, harmonie et de contrepoint (avec le compositeur Alfons Castaldi), au Conservatoire de Bucarest.

Un moment décisif dans l'évolution du très jeune Șerban Țițeica fut occasionné par les conférences sur la physique atomique données à Bucarest par Enrico Fermi, en 1929. En apprenant le désir de Țițeica de s'initier à la physique quantique, Fermi lui suggéra de continuer ses études à Leipzig, avec Heisenberg. Il s'ensuivit que, durant l'automne de 1930, après avoir fait son service militaire, Țițeica se fit inscrire pour le doctorat à la Faculté philosophique de Leipzig. Cette ville était à ce temps-là parmi les quelques centres européens où on développait la mécanique quantique récemment créée: c'était le temps des grandes applications. Pendant quatre ans, Țițeica étudia assidument la physique théorique, les mathématiques et la géophysique. Il fréquenta les cours et les séminaires des professeurs et docents Peter Debye, Fritz Hund, Werner Heisenberg, Bartel Leendert van der Waerden et Felix Bloch. En même temps, guidé par Heisenberg, il préparait sa thèse. Par sa dissertation [1], achevée en décembre 1934 et qui obtenu la mention „mit ausgezeichnetem Erfolge bestanden", Țițeica élabora la théorie quantique de la conductibilité des métaux en présence d'un champs magnétique d'intensité arbitraire. La formule de Ţiţeica contient comme cas limite la dépendance quadratique bien connue de la résistivité par rapport à l'intensité du champ, lorsque celui-ci est faible ; elle explique en outre les résultats expérimentaux de Piotr Kapitsa pour les champs magnétiques forts (1928), à savoir l'isotropie de la résistivité et sa dépendance linéaire par rapport à l'intensité du champ. Ce travail de Ţiţeica, qui inspira des travaux ultérieurs, est considéré comme fondamental et actuel, cinquante ans après son apparition. Nous citons [2] : „The exciting history of quantum magnetotransport theory began in 1935 with the ingenious work by Ţiţeica. Following his ideas is still the best approach for understanding quantum magnetotransport phenomena ; it is also an excellent introduction to more elaborate theories".

---

[1] Ș. Țițeica, *Über die Widerstandsänderung von Metaller im Magnetfeld*, Ann. d. Physik, 1. Folge, *22*, 129—161 (1935).

De retour en Roumanie, Şerban Ţiţeica devint pendant les années 1935—1941 maître-assistant à l'Ecole Polytechnique et maître de conférences à la Faculté des Sciences de Bucarest, enseignant surtout l'analyse mathématique. Il étudia le problème de l'absorption des particules chargées lourdes dans la substance [3, 4], complétant les résultats théoriques de N. Bohr, F. Bloch et E. J, Williams. D'abord, il évalua l'énergie moyenne d'excitation d'un atome par la méthode de Thomas-Fermi [3]. Ensuite, il établit les conditions de validité de la formule de Bohr pour la probabilité d'une perte d'énergie cinétique ; de même il obtint l'expression de la valeur moyenne du carré de l'énergie cinétique transmise à un atome, ainsi que son ordre de grandeur [4]. Il faut signaler aussi sa contribution originale à la théorie des positrons [5].

Pendant les années de l'avant-guerre, à l'aide de la grande pianiste Silvia Şerbescu, Şerban Ţiţeica devint lui-même un fin pianiste.

Entre les années 1941 et 1948, il fut professeur à l'Université de Jassy, enseignant le cours de structure de la matière. Il publia ses travaux sur le temps propre en mécanique quantique et sur la polarisation du vide.

Şerban Ţiţeica se maria en 1951 avec Maria-Marta Mişu, docteur en médicine, chargée de cours à l'Institut de Médicine et Pharmacie de Bucarest. Ils eurent deux filles : Ştefana (née en 1952, violoniste) et Maria (née en 1955, physicienne).

De 1948 jusqu'à sa retraite en 1977, Şerban Ţiţeica fut professeur de physique théorique à l'Université de Bucarest. Son activité didactique fut prodigieuse. Il a donné les cours généraux de mécanique classique, électrodynamique, mécanique quantique, thermodynamique et physique statistique, Il enseigna, comme cours spéciaux, la théorie du noyau, des chapitres de mécanique quantique avancée, la théorie des groupes, les algèbres de Lie.

---

[2] J. Hajdu and G. Landwehr. *Quantum Transport Pheonmena in Semiconductors in High Magnetic Fields*, en *Strong and Ultrastrong Magnetic Fields and Their Applications*, F. Herlach ed., p. 38 (Springer. Berlin, 1985).

[3] Ş. Ţiţeica, *Über die Absorption der Korpuskularstrahlen*, Zs. f. Physik. *101*, 378—397 (1936).

[4] Ş. Ţiţeica, *Sur la fluctuations de parcours des rayons corpusculaires*, Bull. Soc. Roum. Phys. *38*, 81—100 (1937).

[5] Ş. Ţiţeica, *Contributions à la théorie des positrons*, Bull. Soc. Roum. Phys., *41*, 47—68 (1940) ; ibid. *42*, 3—8 (1941).

La profondeur de son esprit, le talent avec lequel il exposait la physique, la netteté de ses leçons, ses „trucs“ lors des démonstrations difficiles et enfin son exigence ont fait de Şerban Ţiţeica le professeur le plus admiré et aimé de nombreuses promotions de physiciens.

Les travaux scientifiques bien connus de cette période ont des sujets très variés : ils traitent des problèmes concernant le troisième principe de la thermodynamique, la propagation de la chaleur, la théorie du rayonnement électromagnétique multipolaire, les ensembles statistiques en rélativité restreinte et générale, l'analyse théorique de la désintégration $\pi \rightarrow \mu + \nu$, la représentation des algèbres de Lie des groupes unitaires par des transformations canoniques infinitésimales. Ami du professeur Costin Neniţescu, Şerban Ţiţeica fut sollicité par celui-ci de participer à l'élucidation du mécanisme et de la cinétique de certaines réactions d'alcoylation du noyau aromatique. Le résultat de cette collaboration a été une série de travaux remarquables de cinétique chimique organique.

Auprès du professeur Horia Hulubei, Şerban Ţiţeica aida à l'organisation et au développement de la recherche de physique dans les instituts créés après 1948. Il fut successivement chef de la Section de Physique théorique de l'Institut de Physique de l'Académie (1949—1956), directeur adjoint scientifique de l'Institut de Physique Atomique (1956—1971) et directeur adjoint de l'Institut Central de Physique (1974—1977). Dès 1956, jusqu'en 1985 il fut rédacteur en chef adjoint et ensuite rédacteur en chef des revues „Studii și Cercetări de Fizică“ et „Revue Roumaine de Physique“.

Il a conduit un grand nombre de thèses de doctorat et de séminaires de physique théorique· stimulant sans cesse l'enseignement et la recherche scientifique de réel mérite dans ce domaine. Ainsi, le professeur Şerban Ţiţeica a fondé l'école roumaine de physique théorique qui a déjà obtenu des réussites notables, étant appréciée dans notre pays et à l'étranger.

Şerban Ţiţeica a promu avec fermeté les collaborations internationales des physiciens roumains. Il a été membre du Conseil scientifique de l'Institut Unifié de Recherches Nucléaires de Dubna (1956—1981), où il a travaillé aussi comme directeur adjoint scientifique (1962—1964). De 1970 à 1975 il fut membre du Conseil de la Société Européenne de Physique. Son autorité et sa culture scientifique extraordinaire lui ont permis d'avoir des rapports étroits avec beaucoup de physiciens étrangers illustres, au profit de la coopération scientifique internationale de la Roumanie.

Les travaux scientifiques brillants, son activité au service de l'enseignement et la science roumaine ont valu à Şerban Ţiţeica des distinctions académiques. Membre titulaire (depuis 1955) et vice-président de l'Académie Roumaine (depuis 1963), il consacra à cette dernière fonction vingt-deux ans de travail quotidien. Il a été aussi élu membre correspondant de l'Académie Saxonne de Leipzig, R.D.A. (en 1967) et de l'Académie des Sciences de l'U.R.S.S. (en 1969).

Şerban Ţiţeica a été député dans la Grande Assemblée Nationale de la République Socialiste de Roumanie pendant plusieurs législatures.

Après 1977, comme professeur en retraite, il a fait trois ans encore le cours général de mécanique quantique. De même il donna jusqu'en 1981 des cours spéciaux au sujet de la théorie des groupes de Lie et de compléments de mécanique quantique. Pourtant la tâche à laquelle il dévoua la plus grande partie de son temps fut d'achever son traité sur la mécanique quantique.

C'est le moment de dire que Ţiţeica a écrit peu de livres ou mieux que ses connaissances dépassaient de beaucoup ce qu'il a publié. Mais ce qu'il a écrit émerge d'une longue expérience, l'exposition est claire et naturelle, produisant au lecteur une vive satisfaction intellectuelle. Ceci s'applique à ses cours universitaires, „La radiation thermique — Mécanique statistique — Ancienne Théorie des Quanta" (1951) et „Mécanique analytique" (1978), aussi bien qu'à ses livres [6, 7, 8]. La dernière oeuvre „Mecanica cuantică" est le résultat de nombreuses années de réflexion et illustre l'une des idées fondamentales de Ţiţeica, celle que la physique expérimentale et la physique théorique ne peuvent pas être séparées. Par conséquent, c'est un livre qui s'adresse à toutes les catégories de physiciens, peut-être le meilleur livre de physique écrit chez nous.

Afin que l'image de l'homme Şerban Ţiţeica soit plus juste, il faut ajouter sa connaissance profonde de la langue et de la culture hellénique, du latin et l'aisance avec laquelle il parlait plusieurs langues modernes. Jeune homme, il escaladait dans les vacances les vallées et les crêtes des monts Bucegi et Piatra Craiului, Il fut toujours passionné par la littérature et surtout par la musique ; il jouait souvent du piano dans le cercle de la famille.

La fin. inattendue et rapide, a été provoquée par une maladie incurable. A soixante-dix-sept ans, il a opposé au mal la même force morale qui l'a caractérisé toute la vie. Lucide, il voulait vivre et avait pour quoi vivre. Pourtant il a du abandonner ses projets et se résigner devant le destin implacable. Jusque dans la dernière semaine, l'affection de ceux qu'il aimait, les souvenirs et la musique lui ont apaisé la souffrance.

De même que nos collègues du Centre National de Physique, nous garderons un vif souvenir de Şerban Ţiţeica, celui qui a été pour nous tous le modèle du professeur et du savant.

Le Comité de rédaction

---

[6] Ş. Ţiţeica, *Elemente de Mecanică statică*, Ed. Tehnică, Bucureşti, 1956.
[7] Ş. Ţiţeica *Termodinamica*, Ed. Academiei R.S.R., Bucureşti, 1982.
[8] Ş. Ţiţeica, *Mecanica cuantică*, Ed. Academiei R.S.R., Bucureşti, 1984.

Abonamentele în țară se pot contracta la oficiile P.T.T.R., agenții poștali și factorii poștali.

Cititorii din străinătate se pot abona prin ROMPRESFILATELIA — Sectorul export-import presă, P.O. Box 12—201, telex 10376 prsfir, București, Calea Griviței, nr. 64—66.

Lei 35